

DISSERTATION

FROM MENISCUS TO BONE: STRUCTURE AND FUNCTION OF HUMAN MENISCAL
ENTHESES AND DELETERIOUS EFFECTS OF OSTEOARTHRITIS

Submitted by

Adam Christopher Abraham

Department of Mechanical Engineering

In partial fulfillment of the requirements

For the Degree of Doctor of Philosophy

Colorado State University

Fort Collins, Colorado

Spring 2013

Doctoral Committee:

Advisor: Tammy L. Haut Donahue

Kenton R. Kaufman

Christian M. Puttlitz

Ketul C. Popat

Laurie R. Goodrich

Copyright by Adam Abraham 2013

All Rights Reserved

ABSTRACT

FROM MENISCUS TO BONE: STRUCTURE AND FUNCTION OF HUMAN MENISCAL ENTHESES AND DELETERIOUS EFFECTS OF OSTEOARTHRITIS

Knee osteoarthritis plagues millions of people in the U.S. alone, yet the mechanisms of initialization are not well understood. Recent work suggests that there are a myriad of potential disease inducing routes that may give rise to this debilitating condition. Understanding and elucidating the potential pathways leading to osteoarthritis may result in novel methods of prevention and/or treatment.

Human meniscus are C-shaped fibrocartilaginous structures contained within the diarthroidal knee joint, the primary function of which are to provide support and lubrication between the femur and the tibia. Each knee incorporates two menisci, lateral and medial, affixed at the anterior and posterior attachment sites to the tibial plateau. Meniscal attachments, or entheses, are unique graded tissue interfaces comprised of four distinct zones that diffuse longitudinal loads transmitted via hoop stresses of collagen fibrils in the meniscal body. The attachments must remain firmly rooted to the tibial plateau to effectively attenuate joint loads. If the attachments become structurally compromised, either through direct or indirect means, excessive transverse meniscal translation results. Such joint extrusion of the meniscal body is a known precursor to developing osteoarthritis. To date there have been no investigations of integrity of meniscal attachments in the aged arthritic knee.

A proposed treatment modality for meniscus degeneration is engineered replacements which focus solely on the meniscal body, disregarding the specialized tissue interface. However, the efficacy of these replacements likely remains dependent on restoring the meniscus to bone transition. Previous literature has shown that each meniscal attachment is biochemically and mechanically unique and thus should be independently examined. Therefore, the overall goal of this work is to examine the loading environment of each attachment in both a healthy and injured knee, as well as characterize the structure-function relationship. This knowledge can then be utilized to develop novel preventative strategies in order to deter the onset of osteoarthritis, thereby reducing the burden on individuals as they age.

Therefore, the goal of this work was to:

- Determine the transverse mechanical properties of the attachment sites and couple with current literature to aid in numerical modeling
- Determine the native loading environment for each attachment under physiological and pathological loading conditions
- Examine the structure and function of the native attachment sites
- Examine the deleterious effects of osteoarthritis on the attachment sites.

ACKNOWLEDGEMENTS

This work was supported by the National Institutes of Health, the National Institute for Arthritis and Skin Diseases, the National Institute for Child Health and Human Development, and the National Institute on Aging (R15 AR051906, R01 HD31476, and F31 AG038875). I would like to thank Dr. Julian Wegrzyn, Mayo Clinic, for assistance in preparing cadaver samples and assessment of knee tissue, and Dr. Stavros Thomopoulos, Washington University, for providing custom MATLAB processing software to determine collagen fiber orientation angles. Lastly, I would like to thank all my co-authors and collaborators for various aspects of this work.

TABLE OF CONTENTS

CHAPTER 1: INTRODUCTION.....	1
1.1 The Meniscus.....	1
1.1.1 Physiology.....	2
1.1.2 Pathology.....	3
1.2 Meniscal Enteses.....	4
1.2.1 Physiology.....	5
1.2.2 Pathology.....	8
1.3 Specific Aims.....	10
1.4 References.....	14
CHAPTER 2: HYPERELASTIC PROPERTIES OF HUMAN MENISCAL ATTACHMENTS	18
2.1 Summary.....	18
2.2 Introduction.....	19
2.3 Materials and Methods.....	21
2.3.1 Transverse specimen preparation.....	21
2.3.2 Transverse test setup.....	22
2.3.3 Transverse testing analysis.....	23
2.3.4 Longitudinal analysis:.....	24
2.3.5 Statistical analysis.....	26
2.4 Results.....	26
2.5 Discussion.....	31
2.6 References.....	35
CHAPTER 3: INTERNAL PRESSURE OF THE HUMAN MENISCAL ATTACHMENTS DURING PHYSIOLOGICAL AND PATHOLOGICAL LOADING.....	39
3.1 Summary.....	39
3.2 Introduction.....	40
3.3 Materials and Methods.....	42
3.4 Results.....	44
3.5 Discussion.....	46

3.6	References.....	52
CHAPTER 4: FROM MENISCUS TO BONE: A QUANTITATIVE EVALUATION OF STRUCTURE AND FUNCTION OF THE HUMAN MENISCAL ATTACHMENTS		
4.1	Summary	56
4.2	Introduction.....	57
4.3	Materials and Methods.....	59
4.3.1	Sample Preparation	59
4.3.2	Histology.....	60
4.3.3	Collagen Fiber Orientation	61
4.3.4	Interdigitation Analysis.....	62
4.3.5	Nano-indentation.....	64
4.4	Results.....	66
4.4.1	Collagen Fiber Orientation	66
4.4.2	Interdigitation Analysis.....	68
4.4.3	Nano-Indentation	69
4.5	Discussion.....	72
4.6	References.....	77
CHAPTER 5: DELETERIOUS EFFECTS OF OSTEOARTHRITIS ON THE STRUCTURE AND FUNCTION OF THE HUMAN MENISCAL ENTHESES		
5.1	Introduction.....	81
5.2	Methods.....	83
5.2.1	Sample preparation	83
5.2.2	Histomorphometry	84
5.2.3	μ CT	85
5.2.4	Indentation	86
5.3	Results.....	88
5.3.1	Histomorphometry	88
5.3.2	μ CT	90
5.3.3	Indentation	92
5.4	Discussion.....	94
5.5	References.....	99

CHAPTER 6: CONCLUSIONS AND FUTURE WORK.....	103
Appendix A: GOODNESS OF FIT FOR CONSTITUTIVE MODELS.....	106
Appendix B: VISCOELASTIC FRAMEWORK FOR INDENTATION	108
Appendix C: VISCOELASTIC TIME CONSTANTS	111

CHAPTER 1: INTRODUCTION

This overview will provide a brief explanation of the meniscus structure and function within a healthy joint as well as pathological changes that can lead to the development of osteoarthritis. This leads into a discussion on the importance of the meniscal entheses, their unique structure and function, and their considerable influence on meniscus mechanics thereby bringing about the specific aims of this work.

1.1 The Meniscus

Until the latter half of the 20th century the knee menisci were believed to be little more than functionless remnants of developing leg muscle¹. This presumption led to the complete removal of the menisci when faced with symptomatic tearing. However, it soon became apparent that these structures were, in fact, crucial for maintaining joint health and preventing the development of osteoarthritis (OA)². Laboratory investigations of the precise structure and functional roles of the menisci began in earnest in the 1970's and 80's leading to a paradigm shift in clinical care by placing an emphasis on maintaining the meniscus³. Since that time, however, the overarching goal of “preservation” remains the status quo of patient care. Ongoing investigations of meniscus biomechanics and molecular pathways, including response to injury, give rise to the hope that future treatment modalities, including targeted drug delivery and tissue engineered replacements, will greatly improve clinical outcomes and the quality of life in an aging population.

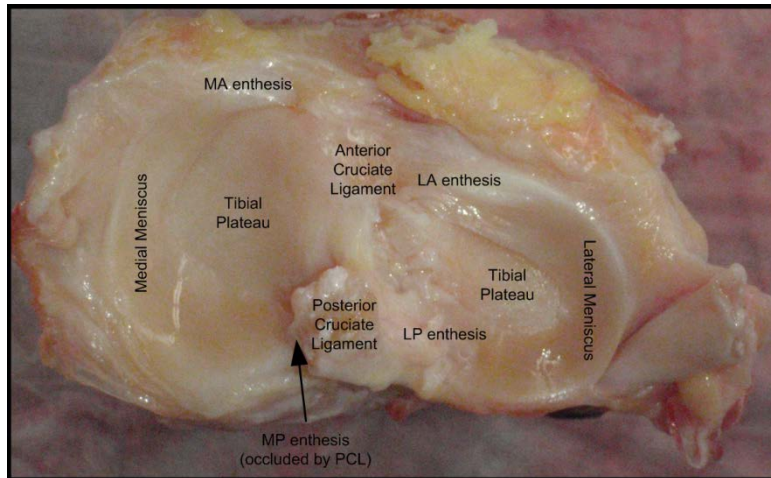


Figure 1-1: Anatomy of knee meniscus and its entheses. MA – Medial Anterior, LA – Lateral Anterior, MP – Medial Posterior, LP – Lateral Posterior.

1.1.1 Physiology

The menisci are fibrocartilaginous structures within the knee joint that aid in stability, lubrication, and load distribution³. Within each diarthrodial joint there are two menisci; the medial and lateral (Figure 1)⁴. Both are crescent shaped along the transverse plane and triangular in cross-section (Figures 1 & 2)⁴. Structurally, the menisci are comprised of inhomogeneous collagen fiber layers⁵. Beginning at the articular surfaces, the fibers form a woven mesh that gradually becomes circumferentially aligned with sparse radial tie fibers that stem from the periphery^{5,6} (Figure 2). This hierarchical morphology sustains and transduces applied compression and shear at the articulating surfaces into tensile hoop stresses. Additionally, the menisci are reinforced with water affine sulfated glycosaminoglycans (GAGs). This extraordinary amalgamation is able to endure 45%-99% of the knee joint loads⁷⁻⁹. In day to day activity compressive knee forces can be as high as three times body weight while walking and between ten and thirty-three times body weight while running¹⁰⁻¹³. The functional role of the

meniscus is crucial in maintaining joint health as disruption results in increased cartilage contact pressure, a known harbinger of osteoarthritis^{14,15}.

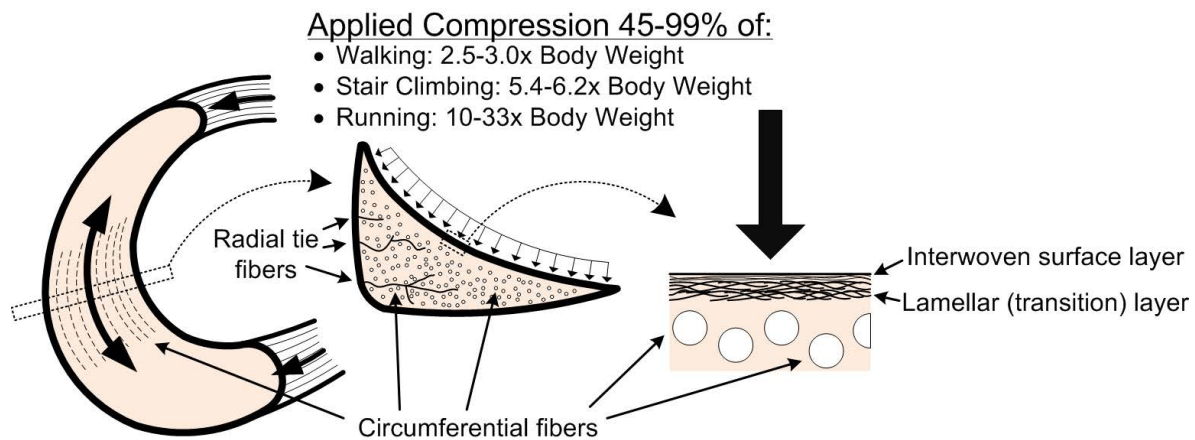


Figure 1-2: Schematic of loading mechanisms within the meniscus. Compression is applied to the femoral and tibial articulating surfaces, comprised of a tightly interwoven surface layer of collagen fibrils. Loading is transduced to hoop stresses and transmitted by circumferentially aligned deep zone of collagen fibrils. These stresses are attenuated at the tibial plateau via the entheses. Note: fiber sizes are not to scale.

Non-loading bearing structures within the meniscus include a limited amount of vasculature and innervation^{16,17}. These constituents branch from the periphery and are present in the outer 10-30% of the menisci, known as the “red zone.” This staggeringly limits the healing capacity of the meniscus to only peripheral damage¹⁸. Numerous attempts at promoting vascular and avascular repair in the inner two-thirds are reported in the literature with only limited success³. This makes ongoing investigations of the various structure-function relationships within the meniscus and their changes due to injury and degeneration imperative.

1.1.2 Pathology

The field of osteoarthritis research has transcended the notion that it is solely a disease of the cartilage and has acknowledged that excision of a damaged meniscus substantially increases the risk of joint degeneration. In many instances, even if reparative attempts are made, meniscus functionality is compromised and long-term outcomes remain bleak¹⁹. While in these instances

the source of OA initiation is easily derived, primary development (in the absence of trauma) mechanisms remain elusive²⁰. An often cited metric of OA progression is joint space narrowing, initially believed to be a product of thinning of the articular cartilage. However, radiographic evidence implicates that initial narrowing is a direct result of the meniscus being extruded radially out towards the joint margins²¹. Furthermore, this phenomenon has been shown to predate cartilage thinning²¹. Once the meniscus has been dislodged it becomes feasible to postulate that the standard primary OA pathogenesis; synovitis, cartilage thinning, abnormal ligament stress, and subchondral bone oedema, occurs²⁰. This gives rise to the supposition that one source of secondary OA may inherently be meniscogenically-derived.

One extrinsic structural retainer for the medial meniscus is the medial collateral ligament (MCL). Various MCL abnormalities have been exhibited in patients with and without meniscal extrusion²². However, it apparent this is not the sole source of meniscal extrusion. Therefore, there is a demand to explore additional tissues that dictate meniscus mechanics, including the entheses.

1.2 Meniscal Entheses

Various studies have shown that meniscus performance is substantially dictated by enthesis mechanics. In pioneering work by Haut Donahue et al., finite element modeling of the knee joint determined that modification of meniscal attachment stiffness had a significant effect on articular cartilage contact pressure distribution²³. Yao et al. expounded on these data by modeling meniscus motion and deformation and found that attachment stiffness had profound effects on meniscus translations²⁴. As pressure distribution and meniscal translation are critical for

preventing joint degeneration these important findings should drive rigorous investigations, however, there are only trace amounts of data regarding the native mechanical environment the entheses must bear. While many investigators have explored other interfacial tissues within and around the knee *ad nauseum*, such as the cruciate and collateral ligaments and articular cartilage, the meniscal attachments are often ignored. This is in part due to demand by clinicians for understanding of, and treatment options for, ligament and cartilage trauma; obvious sources of secondary osteoarthritis. Also, implementation of traditional mechanical evaluation tools (strain gages, optical strain, load cells, etc.), is made complicated by joint space limitations and complex tissue morphology and translations during loading. Encouragingly, however, several recent studies have begun to examine the attachment sites.

1.2.1 Physiology

Based on displacements and forces during loading, material properties, and geometry, it is deduced that the meniscal entheses must each endure a unique environment. Translation of the meniscal entheses during physiological loading has been explored using MRI^{25,26}. In these studies the investigators track the motion of the meniscal “horns,” a somewhat ambiguous term as there is no distinction between the pointed crescents of the meniscus and the fibrous portion of the enthesis. However, from their work it is known that the lateral meniscus is more mobile than the medial during flexion, and the lateral anterior and medial posterior horns are the most and least mobile, respectively. The forces generated during loading, however, remain poorly defined due to the aforementioned issue of instrumentation of the entheses. Only two investigators have been able to ascertain forces of anterior entheses in porcine and human joints. Stärke et al. coupled a uniaxial force transducer with a bone plug connected to the medial anterior meniscal

entheses in a porcine joint²⁷. Applying tibiofemoral compression generated tensile forces at the attachment dependent on the amount of loading. However, changes in flexion angle did not have an effect on the amount of force²⁷. Seitz et al., using strains measured during various joint loading scenarios and recursive force determination showed both medial and lateral anterior attachments were subjected to low amounts (peak 25N) of tensile force²⁸.

Ultimately, however, much of our understanding of insertion mechanics still relies on inferring from morphological studies and material properties. The meniscal entheses, similar to other fibrocartilaginous entheses, benefit from a stratified anatomy that brings together various constituents forming a highly effective stress transmitter with a low rate of failure^{29,30}. Extending from the main body of the meniscus, crimped type I collagen fibrils form the ligamentous (LI)

zone that carries tensile loads generated by compression on the meniscus³¹⁻³³ (Figure 1-3 & 4). The LI zone continues until it interfaces with uncalcified fibrocartilage (UFC) which is comprised of interwoven type II collagen and glycosaminoglycans (Figure 1-3), components linked with tissues primarily subjected to compression and shearing mechanisms³¹. The collagen fibers in the region span across a tidemark, and thereafter possess concomitant bioapatite, thus creating the calcified fibrocartilage (CFC) region³⁴ (Figure 1-3). In the unmineralized

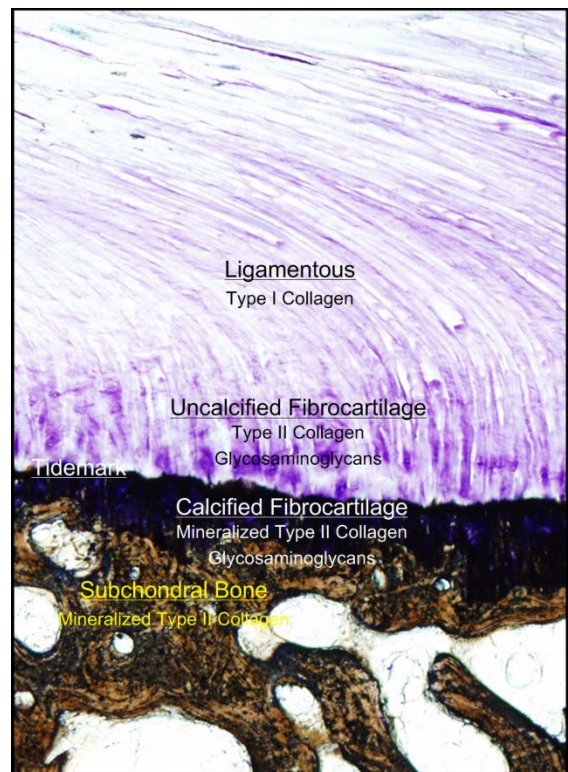


Figure 1-3: Stratified anatomy of the meniscal enthesis is comprised of ligamentous, uncalcified fibrocartilage, calcified fibrocartilage, and subchondral bone regions.

fibrocartilage the mechanical performance is primarily dictated by the organization and orientation of the collagen fibers whereas in the mineralized tissue the amount of mineral density dominates^{35,36}. Aside from the constituents themselves being indicative of the loading environment, it is hypothesized these regions are subjected to compression due to resisting Poisson's effect and changes in fiber angle which is directly correlated to the amount of fibrocartilage present³⁷ (Figure 1-4).

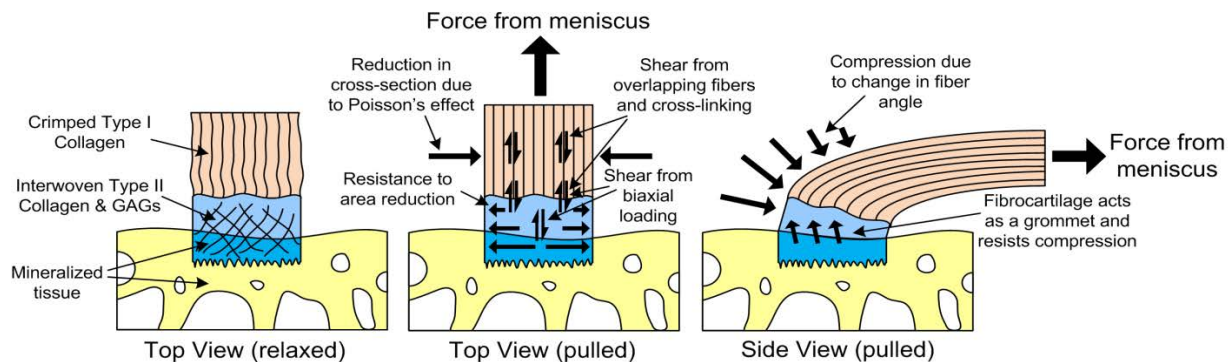


Figure 1-4: Schematic of the various loading mechanisms within the meniscal enthesis

In this way the fibrocartilaginous entheses are thought to behave as 1) a “stretching-brake” that limits the shape change due to loading and 2) a grommet, similar to that on an electrical cord^{29,34}. These properties bestow the abilities to sustain high loads with low risk for bone avulsion failure and changes in insertion angle with loading. Lastly, the enthesis forms an interdigitated cement line between the CFC region and terminates in the surrounding subchondral bone (SB)^{38,39} (Figure 1-3). These four regions; LI, UFC, CFC, and SB then comprise the entire enthesis organ³⁴.

Determining the mechanical properties for each meniscal enthesis is, currently, the only modality to make relative comparisons between them as each is, presumably, shaped by its unique environment. Maes & Haut Donahue were the first to investigate time-dependent material

performance in three entheses of a bovine stifle joint (the lateral posterior is attached to the femur and was not examined)⁴⁰. They found a significantly lower rate of creep displacement for the lateral anterior than the medial posterior, however no differences between entheses for relaxation. Expanding on these findings Villegas et al. additionally examined the failure properties and strain distribution⁴¹. In this instance the medial anterior enthesis had a significantly lower linear modulus and ultimate strain than the medial posterior or lateral anterior. Lastly, Hauch et al. investigated both time-dependent and failure properties of the human meniscal entheses. Different from the findings in bovine tissue, they found the medial posterior to possess the lowest linear modulus and ultimate strain. There were no differences in creep displacement and the medial posterior stress relaxed significantly slower than the medial anterior. Aggregating these findings and framing in the context of the meniscal horn trajectory MRI data it becomes apparent that the entheses are shaped by their environment²⁶. The medial posterior is the least mobile during deep knee flexion and hence possesses the lowest ultimate strain. Furthermore, the anterior entheses undergo larger posterior translations and have adapted by being endowed with a higher ultimate strain and linear modulus (Table 1.1).

Table 1.1: Summary of comparative material testing between meniscal entheses. Relationships shown are significantly different. LA – Lateral Anterior, MA – Medial Anterior, LP – Lateral Posterior, MP – Medial Posterior. No s.d. – no significant differences identified between entheses.

Authors	Tissue	Linear Modulus	Ultimate Strain	Creep Displacement Rate	Stress Relaxation Rate
Maes & Donahue 2006	Bovine	-	-	LA < MP	No s.d.
Villegas et al. 2007	Bovine	MA < MP, LA	MA < MP, LA	-	-
Hauch et al. 2010	Human	MP < MA, LA	MP < MA, LA	No s.d.	MP < MA

1.2.2 Pathology

The entheses themselves can succumb to their own pathologies which can affect the meniscus and joint integrity. The first amongst these is tearing of the soft-tissue within the ligamentous

zone and horn of the meniscus^{30,42} (Figure 1-5). This is similar to a radial tear of the meniscus main body in that it can represent a severe disruption of the functional load bearing capacity^{42,43}. Another type of failure is avulsion of the bony root wherein the bone surrounding the enthesis foot print breaks from the tibial plateau (Figure 1-5). The result is similar to a severe

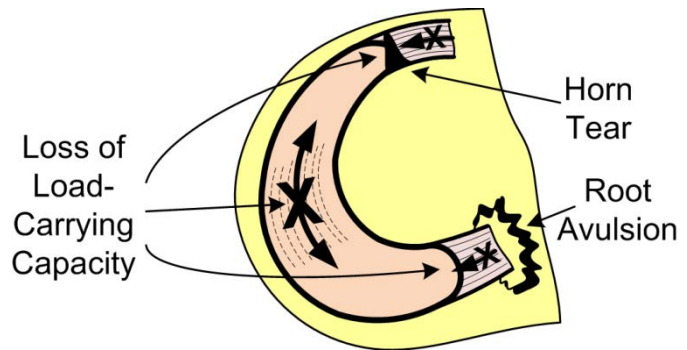


Figure 1-5: Schematic of meniscal horn radial tearing and posterior root avulsion. Both injuries disrupt the functional capacity of the meniscus and can result in primary osteoarthritis.

radial tear in functional significance⁴⁴. Most common is a medial posterior root injury due to the increased physical demands and limited mobility²⁵. Furthermore, posterior cruciate ligament injury can increase occurrence due to the proximity to the medial posterior enthesis footprint⁴⁴.

In the absence of trauma there is a current lack of data specific to the meniscal entheses. Even so, other fibrocartilaginous entheses are known to exhibit a multitude of pathologies that may arise at the meniscal entheses^{29,34}. Meknas et al. documented an aggregation of glycosaminoglycan content and calcium deposits in the internal obturator tendon of patients with hip arthritis⁴⁵. Both of these phenomena disrupt the extracellular matrix, although it remains unknown if these contributed to or are a result from OA pathogenesis. In mineralized tissue there appears to be a significant amount of activity manifested by a breakdown of the tidemark and micro fissures believed to result in osteophyte formation²⁹. Assimilating these findings gives rise to the supposition that the meniscus to bone interface is a potential disease forming pathway, possibly preceding or catalyzing other harbingers of degradation.

1.3 Specific Aims

In summary, meniscal entheses are unique graded tissue interfaces that diffuse longitudinal loads transmitted via hoop stresses of collagen fibrils in the meniscal body. The entheses must remain firmly rooted to the tibial plateau to effectively attenuate joint loads. Identified enthesopathic alterations at other tissue interfaces have shown, amongst additional changes, an increase in water affine proteoglycan content, potentially resulting in extracellular matrix swelling and disruption of the fiber network. If the entheses become structurally compromised, excessive transverse meniscal extrusion results and is a known precursor to developing osteoarthritis. Previous examination of the osteochondral interface reveals demonstrable changes in the mineralization state, a known indicator of bone integrity, dependent upon disease progression. Coupling this information with noted catabolic activity within the arthritic joint gives rise to the supposition that the meniscus to bone interface is a potential disease forming pathway, possibly predating other harbingers of degradation. To date there have been no investigations on the integrity of meniscal entheses in the aged arthritic knee.

Previous literature has shown that each enthesis is biochemically and mechanically unique, therefore, the overall goal of this work is to examine the loading environment of each enthesis in both a healthy and diseased knee (as a function of age), as well as characterize their structure-function relationship. This knowledge can then be utilized to develop novel preventative strategies and validate multi-scale material models in order to deter the onset of osteoarthritis, thereby reducing the burden on individuals as they age.

Specific Aim 1: Determine the transverse hyperelastic parameters of the meniscal entheses for a multitude of material models and select the most accurate. It is hypothesized that 1a) the posterior meniscal entheses have a higher transverse elastic modulus than the anterior due to their hypothesized in vivo loading conditions. Additionally, it is hypothesized that 1b) higher parameter continuum based material models will better encapsulate the transverse hyperelastic material behavior. **Approach 1:** Meniscal attachments will be excised from cadaver donor tissue, sectioned, and loaded in tension. Stress/strain data will be fit to several continuum-based material models. After determining the most accurate model, the data will be coupled with previous longitudinal testing to fit a hyperelastic, transversely isotropic material model which can be utilized to describe the material behavior for each human meniscal enthesis.

Specific Aim 2: Determine the internal fluid pressures in meniscal entheses during physiological and pathological loading of healthy, ACL transected/partially menisectomized. It is hypothesized that local fluid pressures are 2a) larger in the posterior entheses during physiological loading. Additionally, it is hypothesized that local fluid pressure 2b) is increased at the posterior enthesis in injured knees. **Approach 2:** Knee joints will be compressed up to 2X body weight at physiologically relevant flexion angles, while measuring fluid pressures in the entheses *in situ*. A material test stand and additional external actuator will apply joint load via the quadriceps muscle group. Fibre-optic pressure micro-sensors placed within the tissue will track changes in fluid pressure throughout the loading cycle.

Specific Aim 3: Quantify the collagen fiber orientation/organization, interdigitation architecture, and material properties at the transition zone. It is hypothesized that 3a) the anterior collagen

fiber insertion angles would be shallower, relative to the tidemark, and more organized, resulting in superior mechanical performance. Additionally, it is hypothesized that 3b) the instantaneous and infinite time elastic modulus in the transition zones of the meniscal entheses will vary between and within the attachments **Approach 3:** Meniscal entheses will be excised from the physiologically tested knee joints. Attachment sites will be bi-sected and adaxial sections will be histologically prepared and collagen fiber orientation/organization will be determined using polarized light microscopy. The viscoelastic material properties will be determined for the transition zones from the remaining abaxial sections using a nanoindenter.

Specific Aim 4: Determine quantitative changes in the material properties, mineralization, and histomorphometry at the transition zone in osteoarthritic entheses. It is hypothesized that 4a) there will be increased mineralized tissue, however it will be less mature resulting in 4b) increased mechanical compliance. Additionally, it is hypothesized that 4c) enthesopathic changes identified at other tissue interfaces including proteoglycan aggregation, osteophyte formation, and tidemark disruption, will be present in the osteoarthritic meniscal entheses. **Approach 4:** Meniscal entheses will be excised from tibial plateaus removed during total knee replacement surgery. Osteoarthritic entheses will be bi-sected and adaxial sections will be histologically prepared and enthesopathic changes will be quantified. Mineral state at the enthesis will be quantified using micro-computed tomography using the abaxial section. Furthermore, the viscoelastic material properties will be determined across the enthesis using a nanoindenter. These data will be statistically compared to healthy entheses to elucidate differences.

Results from this work will be applicable for understanding osteoarthritis propagation, developing disease preventative measures for at-risk patients, tissue engineered replacement strategies, and the continued development of multi-scale models.

1.4 References

1. Sutton, J. B. *Ligaments: their nature and physiology*. (MK Lewis & Co: London, 1897).
2. Fairbank, J. Knee joint changes after meniscectomy. *The journal of bone and joint surgery* **30-B**, 664–670 (1948).
3. Mow, V. C., Arnoczky, S. P. & Jackson, D. W. *Knee Meniscus: Basic and Clinical Foundations*. 208 (Raven Press: New York, 1992).
4. Standring, S. *Gray's Anatomy*. 1576 (Churchill Livingstone: 2008).
5. Petersen, W. & Tillmann, B. Collagenous fibril texture of the human knee joint menisci. *Anatomy and embryology* **197**, 317–24 (1998).
6. Skaggs, D. L., Warden, W. H. & Mow, V. C. Radial tie fibers influence the tensile properties of the bovine medial meniscus. *Journal of orthopaedic research : official publication of the Orthopaedic Research Society* **12**, 176–85 (1994).
7. Seedhom, B. B. Transmission of the load in the knee joint with special reference to the role of the menisci Part I: anatomy, analysis and apparatus. *ARCHIVE: Engineering in Medicine 1971-1988 (vols 1-17)* **8**, 207–219 (1979).
8. Shrive, N. G., O'Connor, J. J. & Goodfellow, J. W. Load-bearing in the knee joint. *Clinical orthopaedics and related research* 279–87
9. Messner, K. & Gao, J. The menisci of the knee joint. Anatomical and functional characteristics, and a rationale for clinical treatment. *Journal of anatomy* **193 (Pt 2)**, 161–78 (1998).
10. Scott, S. H. & Winter, D. A. Internal forces of chronic running injury sites. *Medicine and science in sports and exercise* **22**, 357–69 (1990).
11. Harrison, R. N., Lees, A., McCullagh, P. J. & Rowe, W. B. A bioengineering analysis of human muscle and joint forces in the lower limbs during running. *Journal of sports sciences* **4**, 201–18 (1986).
12. Taylor, W. R., Heller, M. O., Bergmann, G. & Duda, G. N. Tibio-femoral loading during human gait and stair climbing. *Journal of orthopaedic research : official publication of the Orthopaedic Research Society* **22**, 625–32 (2004).
13. Morrison, J. B. The mechanics of the knee joint in relation to normal walking. *Journal of biomechanics* **3**, 51–61 (1970).
14. Wu, J. Z., Herzog, W. & Epstein, M. Joint contact mechanics in the early stages of osteoarthritis. *Medical engineering & physics* **22**, 1–12 (2000).
15. Walker, P. S. & Erkman, M. J. The role of the menisci in force transmission across the knee. *Clinical orthopaedics and related research* 184–92 (1975).

16. Day, B., Mackenzie, W. G., Shim, S. S. & Leung, G. The vascular and nerve supply of the human meniscus. *Arthroscopy : the journal of arthroscopic & related surgery : official publication of the Arthroscopy Association of North America and the International Arthroscopy Association* **1**, 58–62 (1985).
17. Arnoczky, S. P. & Warren, R. F. Microvasculature of the human meniscus. *The American journal of sports medicine* **10**, 90–5
18. Arnoczky, S. P. & Warren, R. F. The microvasculature of the meniscus and its response to injury. An experimental study in the dog. *The American journal of sports medicine* **11**, 131–41
19. Lohmander, L. S., Englund, P. M., Dahl, L. L. & Roos, E. M. The long-term consequence of anterior cruciate ligament and meniscus injuries: osteoarthritis. *The American journal of sports medicine* **35**, 1756–69 (2007).
20. McGonagle, D., Tan, A. L., Carey, J. & Benjamin, M. The anatomical basis for a novel classification of osteoarthritis and allied disorders. *Journal of anatomy* **216**, 279–91 (2010).
21. Adams, J., McAlindon, T., Dimasi, M., Carey, J. & Eustace, S. Contribution of meniscal extrusion and cartilage loss to joint space narrowing in osteoarthritis. *Clinical Radiology* **54**, 502–506 (1999).
22. Blankenbaker, D. G., De Smet, A. A. & Fine, J. P. Is intra-articular pathology associated with MCL edema on MR imaging of the non-traumatic knee? *Skeletal radiology* **34**, 462–7 (2005).
23. Haut Donahue, T. L., Hull, M. L., Rashid, M. M. & Jacobs, C. R. How the stiffness of meniscal attachments and meniscal material properties affect tibio-femoral contact pressure computed using a validated finite element model of the human knee joint. *Journal of Biomechanics* **36**, 19–34 (2003).
24. Yao, J., Funkenbusch, P. D., Snibbe, J., Maloney, M. & Lerner, A. L. Sensitivities of medial meniscal motion and deformation to material properties of articular cartilage, meniscus and meniscal attachments using design of experiments methods. *Journal of biomechanical engineering* **128**, 399–408 (2006).
25. Vedi, V. *et al.* Meniscal movement. An in-vivo study using dynamic MRI. *The Journal of bone and joint surgery. British volume* **81**, 37–41 (1999).
26. Yao, J., Lancianese, S. L., Hovinga, K. R., Lee, J. & Lerner, A. L. Magnetic resonance image analysis of meniscal translation and tibio-menisco-femoral contact in deep knee flexion. *Journal of orthopaedic research : official publication of the Orthopaedic Research Society* **26**, 673–84 (2008).
27. Stärke, C., Kopf, S., Gröbel, K.-H. & Becker, R. Tensile forces at the porcine anterior meniscal horn attachment. *Journal of orthopaedic research : official publication of the Orthopaedic Research Society* **27**, 1619–24 (2009).

28. Seitz, A., Kasisari, R., Claes, L., Ignatius, A. & Dürselen, L. Forces acting on the anterior meniscotibial ligaments. *Knee surgery, sports traumatology, arthroscopy : official journal of the ESSKA* **20**, 1488–95 (2012).
29. Shaw, H. M. & Benjamin, M. Structure-function relationships of entheses in relation to mechanical load and exercise. *Scandinavian journal of medicine & science in sports* **17**, 303–15 (2007).
30. Gao, J., Rasanen, T., Persliden, J. & Messner, K. The morphology of ligament insertions after failure at low strain velocity: an evaluation of ligament entheses in the rabbit knee. *Journal of anatomy* **189**, 127–133 (1996).
31. Gao, J., Oqvist, G. & Messner, K. The attachments of the rabbit medial meniscus. A morphological investigation using image analysis and immunohistochemistry. *Journal of Anatomy* **185**, 663–667 (1994).
32. Setton, L. a, Guilak, F., Hsu, E. W. & Vail, T. P. Biomechanical factors in tissue engineered meniscal repair. *Clinical orthopaedics and related research* S254–72 (1999).
33. Villegas, D. F. & Donahue, T. L. H. Collagen morphology in human meniscal attachments: a SEM study. *Connective tissue research* **51**, 327–36 (2010).
34. Benjamin, M. *et al.* Where tendons and ligaments meet bone: attachment sites ('entheses') in relation to exercise and/or mechanical load. *Journal of anatomy* **208**, 471–90 (2006).
35. Thomopoulos, S., Marquez, J. P., Weinberger, B., Birman, V. & Genin, G. M. Collagen fiber orientation at the tendon to bone insertion and its influence on stress concentrations. *Journal of biomechanics* **39**, 1842–51 (2006).
36. Genin, G. M. *et al.* Functional grading of mineral and collagen in the attachment of tendon to bone. *Biophysical journal* **97**, 976–85 (2009).
37. Benjamin, M. & Ralphs, J. R. Fibrocartilage in tendons and ligaments--an adaptation to compressive load. *Journal of anatomy* **193** (Pt 4, 481–94 (1998).
38. Benjamin, M., Evans, E., Rao, R. & Findlay, J. Quantitative differences in the histology of the attachment zones of the meniscal horns in the knee joint of man. *Journal of Anatomy* **177**, 127–134 (1991).
39. Villegas, D. F., Hansen, T. A., Liu, D. F. & Donahue, T. L. H. A quantitative study of the microstructure and biochemistry of the medial meniscal horn attachments. *Annals of biomedical engineering* **36**, 123–31 (2008).
40. Maes, J. A. & Haut Donahue, T. L. Time dependent properties of bovine meniscal attachments: stress relaxation and creep. *Journal of biomechanics* **39**, 3055–61 (2006).
41. Villegas, D. F., Maes, J. A., Magee, S. D. & Donahue, T. L. H. Failure properties and strain distribution analysis of meniscal attachments. *Journal of biomechanics* **40**, 2655–62 (2007).

42. Bin, S.-I., Kim, J.-M. & Shin, S.-J. Radial tears of the posterior horn of the medial meniscus. *Arthroscopy : the journal of arthroscopic & related surgery : official publication of the Arthroscopy Association of North America and the International Arthroscopy Association* **20**, 373–8 (2004).
43. Bedi, A. *et al.* Dynamic contact mechanics of the medial meniscus as a function of radial tear, repair, and partial meniscectomy. *The Journal of bone and joint surgery. American volume* **92**, 1398–408 (2010).
44. Jones, A. O., Houang, M. T. W., Low, R. S. & Wood, D. G. Medial meniscus posterior root attachment injury and degeneration: MRI findings. *Australasian radiology* **50**, 306–13 (2006).
45. Meknas, K. *et al.* Could tendinosis be involved in osteoarthritis? *Scandinavian journal of medicine & science in sports* (2011).

CHAPTER 2: HYPERELASTIC PROPERTIES OF HUMAN MENISCAL ATTACHMENTS

2.1 Summary

Meniscal attachments are ligamentous tissues anchoring the menisci to the underlying subchondral bone. Currently little is known about the behavior of meniscal attachments, with only a few studies quantitatively documenting their properties. The objective of this study was to quantify and compare the tensile mechanical properties of human meniscal attachments in the transverse direction, curve fit experimental Cauchy stress-stretch data to evaluate the hyperelastic behavior, and couple those results with previously obtained longitudinal data to generate a more complete constitutive model. Meniscal attachment specimens were tested using a uniaxial tension test with the collagen fibers oriented perpendicular to the loading axis. Tests were run until failure and load-optical displacement data was recorded for each test. The medial posterior attachment was shown to have a significantly greater elastic modulus (5.38 ± 0.77 MPa) and ultimate stress (1.73 ± 0.32 MPa) when compared to the other three attachments. The Mooney-Rivlin material model was selected as the best fit for the transverse data and used in conjunction with the longitudinal data. A novel computational approach to determining the transition point between the toe and linear regions is presented for the hyperelastic stress stretch curves. Results from piece-wise non-linear longitudinal curve fitting correlate well with previous linear elastic and SEM findings. These data can be used to advance the design of meniscal replacements and improve knee joint finite element models.

2.2 Introduction

The menisci provide fundamental support in the human knee and encompass an array of functions, essentially regulating the load transmission across the knee joint (Walker and Erkman 1975; Shrive, O'Connor et al. 1978; Messner and Gao 1998). Menisci contain collagen fibers that are circumferentially aligned to distribute loading on the tibial plateau, intrinsically facilitating articular cartilage fortification and osteoarthritis prevention (Messner and Gao 1998). The menisci are joined to the tibia by means of ligamentous structures known as meniscal attachments (Messner and Gao 1998). With a ground substance matrix comprised of proteoglycans, elastin, glycolipids, fibroblasts and ~60-70% water (Woo 1982; Villegas, Maes et al. 2007) and collagen fibers as reinforcement; meniscal attachments serve as transitions from meniscal body fibrocartilage into the underlying subcondral bone (Villegas, Hansen et al. 2008). Loads sustained by the meniscus are diffused into these insertion sites, which reduce the stress concentrations by gradually transitioning soft tissue into the bone and increasing interface contact area (Messner and Gao 1998). Previous research has shown that meniscal attachments are important for retaining joint functionality (Haut Donahue, Hull et al. 2003) and their mechanical behavior directly affects stability of the knee (Chen, Branch et al. 1996; Goertzen, Gillquist et al. 1996; Alhalki, Howell et al. 1999; Haut Donahue, Hull et al. 2003), however, limited research has been conducted on this unique biological structure to date.

Previous mechanical testing has only been performed in the longitudinal direction of the collagen fibers in the attachments (Villegas, Hansen et al. 2008; Hauch, Villegas et al. 2010), despite implications that the anterior attachment is primarily in tension, while the posterior attachment is thought to be subjected to both tension and compression (Benjamin, Evans et al. 1991; Gao,

Oqvist et al. 1994). Furthermore, the presence of aggrecan in the attachment suggests that the attachments are likely subjected to compression (Benjamin and Ralphs 1998; Villegas, Hansen et al. 2008). Since ligamentous material is known to be mechanosensitive, the strength of each attachment may vary based on the external loading environment (de Boer, Selby et al. 2007; Provenzano, Alejandro-Osorio et al. 2007). Thus, understanding the transverse mechanical properties of the meniscal attachments is imperative for further elucidating the load distribution of the human meniscus. Previous studies of time-dependent and failure properties of meniscal attachments in the longitudinal direction (Villegas, Hansen et al. 2008; Hauch, Villegas et al. 2010) coupled with these transverse properties will enable tissue engineering replacement design and aid in three-dimensional modeling of the human knee joint (Haut Donahue, Hull et al. 2003). Furthermore, developed constitutive models from this data will aid in a greater understanding of the human meniscus during common injury loading scenarios (Gardiner and Weiss 2003). Thus, the first objective of this study was to measure the tensile mechanical properties of the human meniscal attachments along the transverse direction. Posterior meniscal attachments are hypothesized to have higher transverse moduli than the anterior attachments due to their hypothesized in vivo loading conditions.

A hyperelastic material model can be used to represent the attachments' non-linear tendencies in the transverse direction (Quapp and Weiss 1998; Gardiner and Weiss 2003). The second objective of this study was to characterize the constitutive behavior of the meniscal attachments using three independent hyperelastic models evaluated against the experimental data. Given previous studies (Quapp and Weiss 1998), it is hypothesized that the higher parameter models will better describe the hyperelastic transverse material properties of the specimens.

Additionally, previous longitudinal stress-strain data obtained by our laboratory has examined the linear elastic and time-dependent properties along this axis; however, due to the organization of the tissue, both matrix and fibers were examined simultaneously. By isolating the matrix via transverse testing, its contribution alone can be accounted for and a hyperelastic, transversely isotropic material model can be utilized to describe the material performance for each human meniscal attachment in the longitudinal direction.

2.3 Materials and Methods

2.3.1 Transverse specimen preparation

Five healthy human knees (males, ages 50-65, avg. age 58) (NDRI, Philadelphia, PA) were procured, wrapped in saline soaked gauze and frozen at -20°C until the time of dissection. All surrounding tissue was cut away from each knee until the tibial plateau and meniscal bodies were exposed (Figure 2-1).

The medial anterior (MA), medial posterior (MP), lateral anterior (LA), and lateral posterior (LP) attachments were extracted and stored in 0.9% saline solution at 4°C . A custom drop-cutter was used for preparing the individual specimens by slicing 1 or 2 mm thick sections of the meniscal attachment, depending on attachment size (Figure 2-1). Sections were cut perpendicular to the

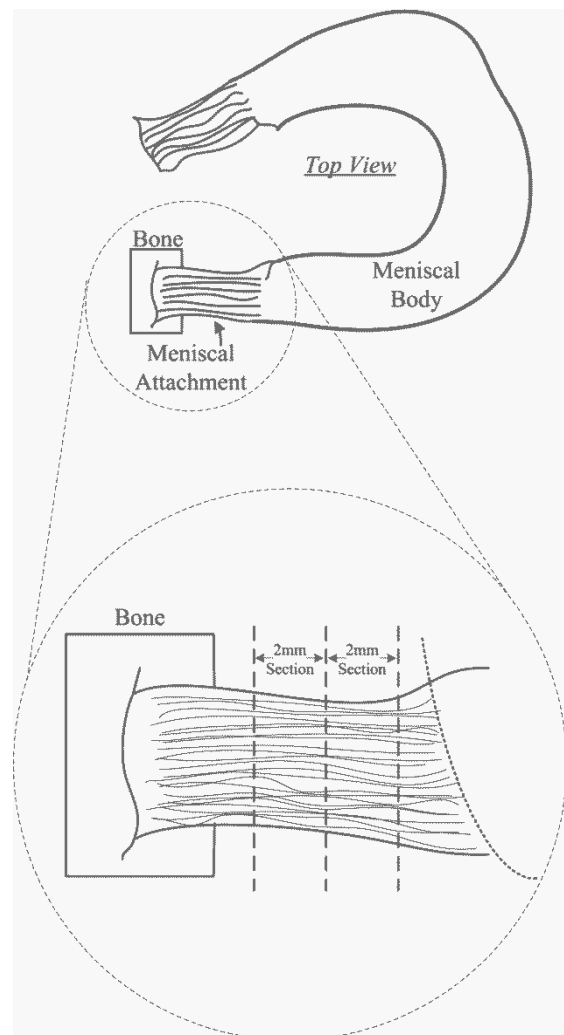


Figure 2-1: Schematic showing where specimens were excised from between the tibial plateau and meniscal body (Villegas, Hansen et al. 2008). 1-2mm sections were removed based on tissue availability.

orientation of collagen fibers. Specimens were then blotted dry and four parallel ink lines were applied, for optical tracking purposes and slip detection, such that there would be a line located below each grip face and 1mm interiorly. Specimens were rehydrated and stored in saline prior to testing.

2.3.2 Transverse test setup

Specimens were loaded into modified thin-film grips (Imada, Northbrook, IL) with the collagen fibers oriented perpendicular to the direction of load (Figure 2-2A). A scale was etched on the outer surface of each grip for dimensioning. Each grip face was serrated and roughened to eliminate slippage. Specimens were loaded such that the aspect ratio was maximized, while providing ample material to secure each specimen; approximately 3 mm of each specimen was inside the grip faces (Figure 2-2).

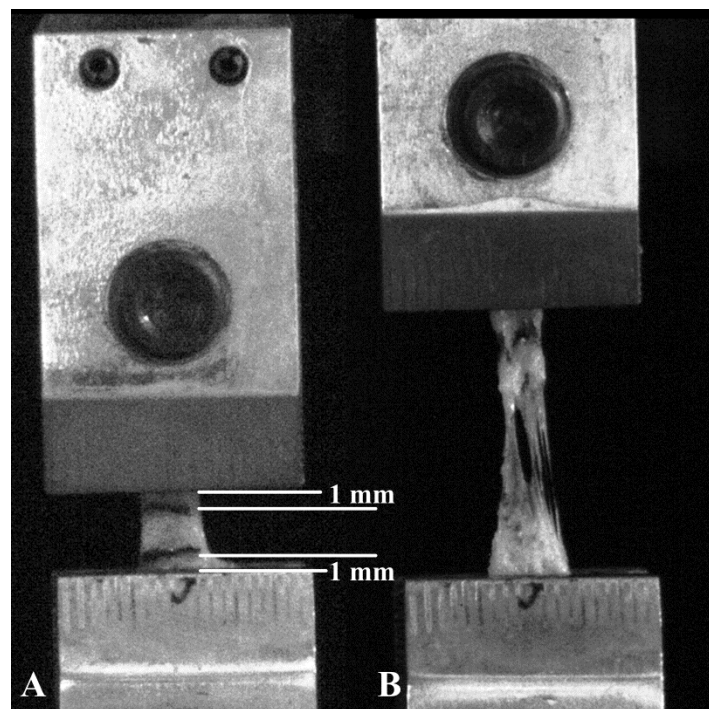


Figure 2-2: Representative meniscal attachment A) prior to initiation of test, and B) immediately following mid-substance failure of specimen. White lines indicate where ink lines were placed to track strain. Failure of specimen can be seen tearing midsubstance with no appearance of lines placed just below the grip face, indicating no slippage during testing.

Grips were attached to a 44.5 N S-beam load cell (Futek, Irvine, CA) and stationary base holding block. The load cell was attached to a servo-hydraulic uniaxial materials testing machine (Model 8872, Instron Corp, Canton, MA). A pre-load of approximately 0.025 N was applied to the specimen and initial gauge length between the ink lines and width were measured using a scale. Previous studies have shown that strain rate in the transverse direction does not affect mechanical properties of tendons, so a constant strain rate of 10 mm/min was set for all testing (Lynch, Johannessen et al. 2003). No preconditioning was performed on the specimens due to the load being perpendicular to the fiber orientation (Lynch, Johannessen et al. 2003). A charge-couple video camera (Model MicroPix M-1024 CCD camera, Ann Arbor, MI) was utilized to track the motion of the ink lines through testing.

2.3.3 Transverse testing analysis

Load and optical displacement data was recorded for each specimen and processed using a custom MATLAB program (MATLAB R2008a, Natick, MA). Given initial gauge width, thickness, and length, mechanical properties were calculated from user-selected points on the load-displacement curve. Elastic modulus was calculated from the linear region of the stress-strain curve using Hooke's Law. The ultimate stress and strain were measured at failure (Figure 3) using machine displacement as the tracking lines became marred during failure, optical data was crosschecked against machine data to ensure good correlation.

In addition to linear elastic properties, the stress-strain data was analyzed to determine hyperelastic behavior of the meniscal attachments in the transverse direction. The experimentally-measured stress, 2nd Piola-Kirchhoff stress (S_{11}), was converted to Cauchy

stress (T_{11}) using Equation 1 for a uniaxial test. The 1-direction is defined as the direction of the tensile tests, that is, in the transverse direction of the attachments. The uniaxial strain in the testing direction (ϵ) was converted to stretch (λ) using Equation 2. Datasets were then compiled into a single set for each attachment site, four in total. The Neo-Hookean (Equation 3), Mooney-Rivlin (Equation 4), and Ogden (Equation 5) hyperelastic models were fit to the attachment site specific datasets using the MATLAB Optimization Toolbox.

$$T_{11} = S_{11}\lambda^2 \quad (1)$$

$$\lambda = 1 + \epsilon \quad (2)$$

Neo-Hookean (Weiss, Maker et al. 1996; Quapp and Weiss 1998; Holzapfel 2000):

$$T_{11} = 2C_1(\lambda^2 - \frac{1}{\lambda}) \quad (3)$$

Mooney-Rivlin (Weiss, Maker et al. 1996; Quapp and Weiss 1998; Holzapfel 2000):

$$T_{11} = (2C_1 + \frac{2C_2}{\lambda})(\lambda^2 - \frac{1}{\lambda}) \quad (4)$$

Ogden (Holzapfel 2000; Ogden R. W. 2004):

$$T_{11} = \sum_{p=1}^N (\mu_p \lambda^{\alpha_p} - \mu_p \lambda^{-\frac{1}{2}\alpha_p}) \quad (5)$$

The MATLAB program utilized the experimental Cauchy stress and stretch data to produce hyperelastic curves that fit the test data. The unknown coefficients C_1 , C_2 , μ_p and α_p were calculated for each respective model.

2.3.4 Longitudinal analysis:

Longitudinal data was procured by means of a pull to failure test. In brief, 6 healthy human knees were potted and aligned in a fixture that mimicked *in situ* loading conditions. A custom-made freeze clamp gripped the meniscus at the transition line between meniscal tissue and attachment. Each attachment was preconditioned for 10 cycles at 10 mm/min between 0% and

3% of the gauge length. Pull to failure was then performed using displacement control at a rate of $2\% \text{sec}^{-1}$. We previously reported local elastic and failure properties of these attachments (Hauch, Villegas et al. 2010). In this study, Weiss' ligament model for an incompressible, hyperelastic, transversely isotropic biological composite was used to describe to behavior of the meniscal attachments (Weiss, Maker, et al., 1996)

$$\Psi = \Psi(I_1, I_2, I_4) = \Psi_m(I_1, I_2) + \Psi_f(I_4) + \Psi_{m-f}(I_1, I_4) \quad (6)$$

Where Ψ_m and Ψ_f represent the matrix and fiber contributions, respectively, and Ψ_{m-f} embodies the matrix-fiber interaction. This last term is ignored as it pertains to shearing effects and its contribution can be considered relatively insignificant for the attachments. Rewriting in terms of principal stretch the matrix portion is obtained by means of the aforementioned transverse testing and analysis. A piece-wise function is required for the fiber contribution in order to encapsulate the non-linear phase, when uncrimping of the collagen fibers occurs, and linear phase such that

$$\lambda \frac{\partial \Psi_f}{\partial \lambda} = \begin{cases} 0 & \lambda < 1 \\ C_3(e^{C_4(\lambda-1)} - 1) & \lambda < \lambda^* \\ C_5\lambda + C_6 & \lambda \geq \lambda^* \end{cases} \quad (7)$$

Where λ^* represents the stretch at the point the collagen fibers become taut. Curve fitting was performed on longitudinal data for all samples at a given attachment site. Determination of λ^* was achieved by minimizing the objective function

$$\min_{\lambda} \left[\frac{\partial}{\partial \lambda} (C_3(e^{C_4(\lambda-1)} - 1)) - C_5 \right] \quad (8)$$

where, the first two experimental points are fit to the exponential equation and the remaining points with the linear function. The process is then iterated upon by removing the first point from the linear portion and appending it to exponential set. The lowest resultant for all iterations using (8) identifies the value of λ^* .

2.3.5 Statistical analysis

One way Analysis of Variance (ANOVA) was performed to determine differences between each anatomical meniscal attachment for mechanical properties. When significant results were identified by ANOVA, a post-hoc Student's two-tailed *t*-test was performed to compare individual meniscal attachment region variances to one another. The goodness-of-fit of the evaluated hyperelastic material models was determined using a Student's *t*-test to evaluate the null hypothesis that the mean of the standardized variance is zero; a higher p-value represents a better model fit for the data set (Morrow, Haut Donahue et al. 2010).

2.4 Results

Specimen failure occurred mid-substance (Figure 2-2B) and no slippage in the grips was observed during the testing procedure, as evidenced by no ink line excursion from the grip face. Stress-strain curves were typical of ligamentous-type tissues with a characteristic toe-region (Figure 2-3) preceding an elastic region until failure. There were no significant differences in gauge length and cross-sectional area between different specimens. The average gauge length and cross-sectional area (mean \pm standard error) for all specimens tested (n=20) were 6.1 ± 0.4 mm and 3.7 ± 0.4 mm², respectively. The anterior attachments of both the medial and lateral menisci exhibited similar behavior during testing (Table 2.1). The MP attachment was approximately five times stiffer than the other attachment sites (Table 2.1). Failure strains for all attachments coincided with one another; however ultimate stresses were found to be significantly different, with the MP ultimate stress being approximately five times greater than the MA and LP attachments (Table 2.1).

Table 2.1: Experimental transverse tensile properties of human meniscal attachments. Elastic modulus is derived from optically tracked strain data, ultimate stress and failure strain are determined using test machine strain data. MA=medial anterior, MP=medial posterior, LA=lateral anterior, LP=lateral posterior. Mean +/- Standard error

	Elastic Modulus (MPa)	Ultimate Stress (MPa)	Failure Strain (mm/mm)
MA	1.35±0.76 *	0.34±0.12 *	0.82±0.13
MP	6.42±0.78	1.73±0.32	0.49±0.06
LA	1.21±0.48 *	0.56±0.04 *^	0.81±0.17
LP	1.21±0.56 *	0.33±0.06 *	0.94±0.11

* = significantly different than MP
 ^ = significantly different than LP
 P < 0.05

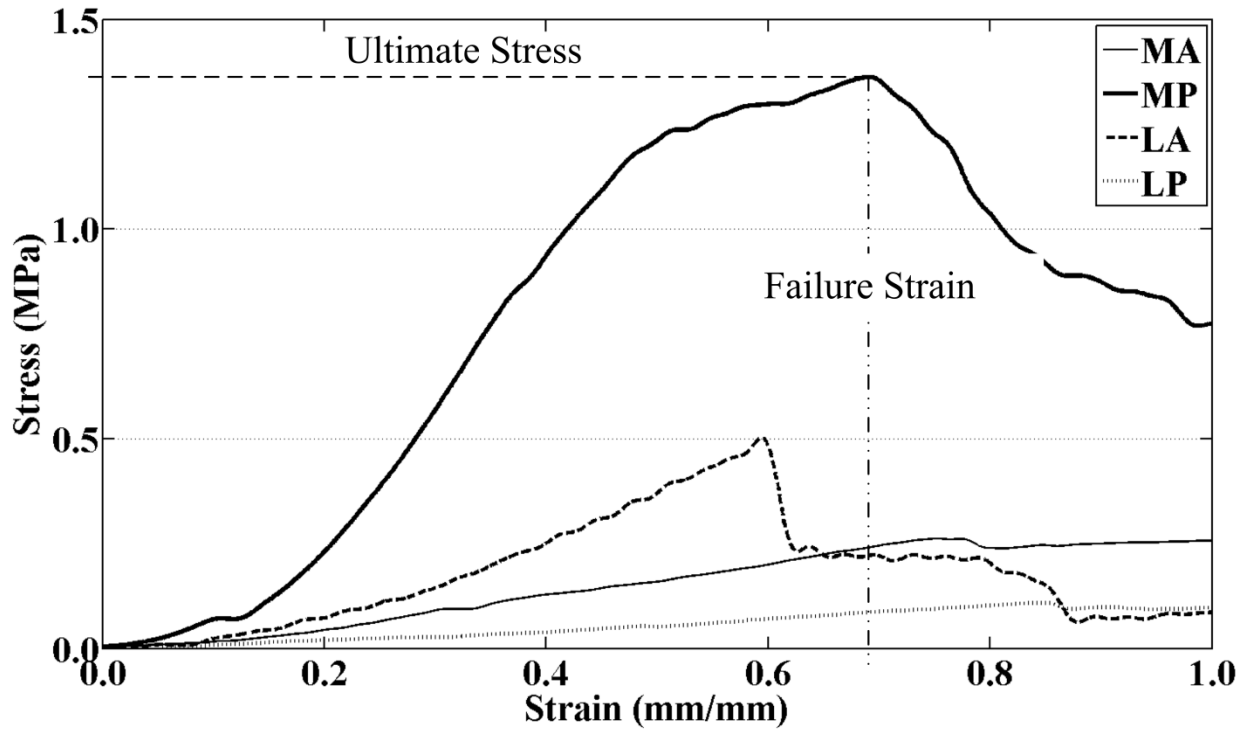


Figure 2-3: Representative tensile stress-strain curves in the transverse direction for human meniscal attachments using machine displacement to obtain ultimate stress and failure strain. Elastic moduli were computed from optical data (not shown) that was comparable to machine displacement. On average, the medial and lateral posterior attachments exhibited the greatest ultimate stress and failure strain, respectively.

A non-linear toe region for Cauchy stress-stretch data was seen in the transversely stretched meniscal attachments (Figure 2-4). The Neo-Hookean (NH), Mooney-Rivlin (MR) and Ogden (OG) hyperelastic material models were optimized for each sample tested (Figure 2-4). The material parameters of each hyperelastic model varied between the attachment zones (Table 2.2). The NH model resulted in the lowest p-value for all attachment sites while OG and MR produced comparable p-values (see Appendix A for additional goodness of fit metrics). Since MR quantitatively outperformed OG, transverse MR parameters were used in conjunction with longitudinal data (Figure 2-5).

Table 2.2: Calculated coefficient parameters and p-value for each evaluated hyperelastic material model. MA=medial anterior, MP=medial posterior, LA=lateral anterior, LP=lateral posterior. Mooney-Rivlin model consistently resulted in a better fit, as indicated by a higher p-value. (see Appendix A for additional goodness of fit metrics)

	Ogden			Mooney-Rivlin			Neo-Hookean	
	μ_1	α_1	p-value	C_1	C_2	p-value	C_1	p-value
MA	0.1081	3.1915	0.8741	0.1904	-0.1227	0.9275	0.1003	0.7933
MP	0.4360	4.9310	0.9432	2.2485	-1.9525	0.9941	0.8621	0.6334
LA	0.1114	6.1978	0.8604	1.1192	-1.0787	0.9790	0.3171	0.3593
LP	0.0982	4.3606	0.5486	0.3808	-0.3136	0.7542	0.1389	0.2809

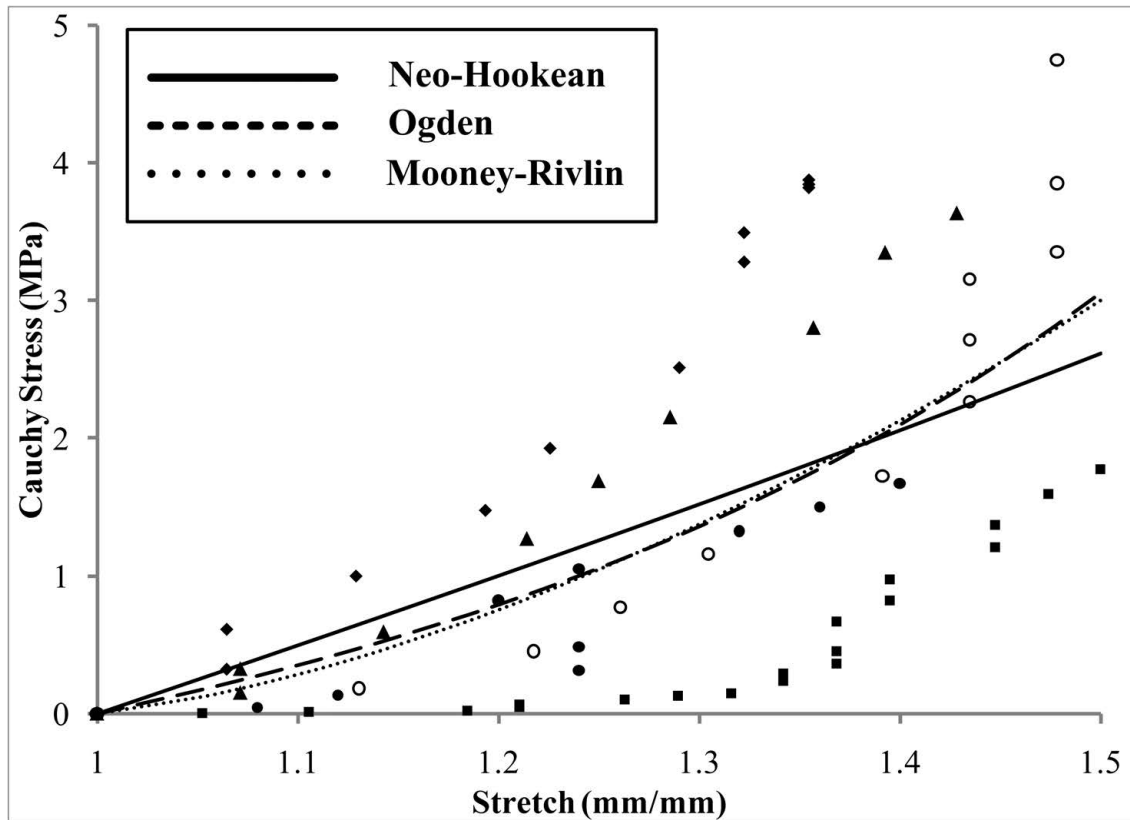


Figure 2-4: Cauchy stress-stretch curve showing hyperelastic curve fits to the experimental data for the medial posterior attachment site. Solid line = Neo-Hookean, dashed line= Ogden, dotted line = Mooney-Rivlin, symbols = testing data points for each specimen. The latter two models fit the trend of the data well. Mooney-Rivlin tends to describe samples with a large toe region better than Ogden, which favors specimens that have less compliant linear regions.

All longitudinal datasets analyzed using the piece-wise material model were optimized to meet the statistical evaluation criteria during the fitting process (Figure 2-5). The transition point, λ^* , was the highest for the anterior attachment sites with the MA reaching over 10% strain. The non-linear scaling coefficient, C_3 , was also greatest for the MA and lowest for both the posterior attachments. The rate of collagen uncrimping, C_4 , was higher for the lateral attachments. Anterior attachment sites possessed a linear elastic constant, C_5 , at least double that of the posterior (Table 2-3). C_6 is an offset factor to ensure continuity at λ^* and thus bears no physiological relevance.

Table 2.3: Calculated coefficient parameters (C_3 - C_6) and transition point (λ^*) from non-linear (toe) to linear regions using Mooney-Rivlin material model for matrix performance (C_1 , C_2). MA=medial anterior, MP=medial posterior, LA=lateral anterior, LP=lateral posterior.

	λ^*	Toe Region		Linear Region	
		C_3	C_4	C_5	C_6
MA	1.1088	8.7418	9.7111	246.3200	-256.3306
MP	1.0579	2.7881	7.0331	29.2884	-29.5832
LA	1.0797	5.6253	13.0889	210.9640	-217.4616
LP	1.0427	2.4003	17.7646	90.4355	-90.2595

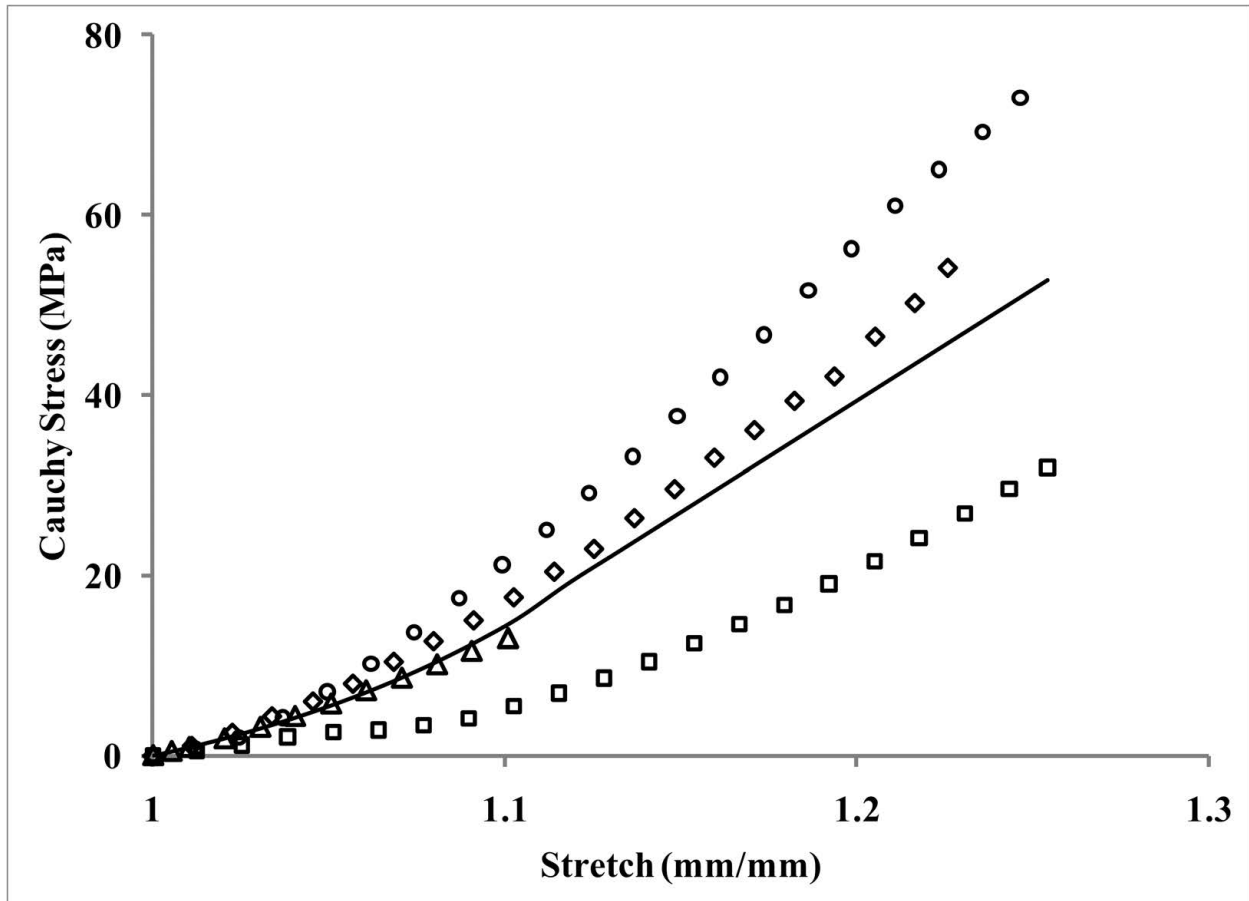


Figure 2-5: Cauchy stress-stretch curve showing hyperelastic curve fits for the longitudinal data for the medial anterior attachment site. Symbols = test data, solid line = curve fit. The piece-wise function used to fit the data performs a good fit for all data sets considered.

2.5 Discussion

The results of this study show significant differences in the transverse mechanical properties between meniscal attachments. Namely, the elastic modulus and ultimate stress in MP attachments were significantly greater than all other attachments, which may support theories that this region endures larger compressive loads during dynamic activity compared to others (Benjamin, Evans et al. 1991; Gao, Oqvist et al. 1994). Additionally, failure strains and elastic moduli for both anterior attachments were approximately equal in this study, supporting previous findings of comparable GAG content between anterior attachments (Benjamin, Evans et al. 1991; Villegas, Hansen et al. 2008). However, these conclusions are based on a material which demonstrates compressive-tensile non-linearity, and these cues may not be directly translatable. Additionally, on average the MP attachment reported the lowest failure strains. This may explain why previous clinical studies show more posterior meniscal root tears compared to anterior in humans (Brody, Lin et al. 2006; Jones, Houang et al. 2006; Choi, Son et al. 2008; Lee, Jee et al. 2008; Ahn, Lee et al. 2009; De Smet, Blankenbaker et al. 2009). Scanning electron microscopy of transverse sections of the meniscal attachments has revealed a network of large planar collagen fibers sheathed in loose membrane septae comprised of thinner, randomly oriented, and interwoven fibrils (Villegas, Haut Donahue 2010). While most collagen fibers are aligned with the longitudinal axis, some can be seen diverging in the transverse direction, however, no quantitative analysis has been performed comparing the prevalence of these deviated fibers in the different attachment sites. Future studies should investigate this to elucidate the differences found here.

Mechanical properties obtained from this study agree with previous studies of other ligamentous materials tested in the transverse direction. Human interosseous ligament and medial collateral ligament (MCL) exhibited elastic moduli of 11.02 ± 3.57 MPa and 1.82 ± 2.93 MPa, respectively (Quapp and Weiss 1998; Stabile, Pfaeffle et al. 2004). These moduli values are comparable to those of the attachments tested in this study. Another study conducted on lapine patellar tendons in the transverse directions gave an elastic moduli and ultimate stress value of 1.27 MPa and 0.37 MPa, respectively (Yamamoto, Hayashi et al. 2000). Additionally, ultimate stresses from the transversely strained MCL were 1.69 ± 0.53 MPa (Quapp and Weiss 1998), which is comparable to that of the MP attachment. The failure strain of lapine patellar tendon (0.41 mm/mm) (Yamamoto, Hayashi et al. 2000) was comparable to that of the MP attachment (0.49 mm/mm).

The meniscal attachments exhibited hyperelastic behavior when strained in the transverse direction. Of the three evaluated hyperelastic material models, the OG model can have the highest number of material parameters, and thus has the potential to describe the most complex material behavior. For this study, the OG material model was evaluated with $p=1, 2$ and 3 to compare the relative accuracy. Increasing the number of material parameters in the OG model did not increase the goodness-of-fit. Therefore, the two-coefficient model only was reported and analyzed. The NH material model did not fit the convex hyperelastic nature of the experimental data, resulting instead in a more linear shape. The MR model involved two unknown coefficients for the hyperelastic curve-fitting and consistently reported the highest resulting p -value for each attachment site. Qualitatively, by comparison, there was little difference between the two complex material models, MR and OG, with the former being more adept at assessing the low stretch ($\lambda < 1.2$) phase and the latter more accurately encapsulating the tail end of the

stretch-stress curve. Due to better quantitative results and superior computational efficiency the MR model was used in conjunction with the longitudinal data.

Traditionally, determining λ^* is performed qualitatively and consistency is dependent on the person assessing the data (Quapp and Weiss 1998). Here, a novel approach to determining λ^* has been employed which entails an exhaustive computational method, providing a more robust, user independent evaluation of λ^* . The results of this study show that the anterior attachments exhibited the greatest amount of non-linear stretch during longitudinal testing. Imaging techniques have shown that these locations exhibit more mobility during loading, potentially due to a more compliant microstructure (Thompson, et al. 1991; Vedi, et al. 1999).

Additionally, the higher rate of uncrimping exhibited by the lateral attachments correlates with SEM findings that the collagen crimp length is longest at these locations, hence the response time required before the collagen fibers become taut is decreased (Villegas, Haut Donahue 2010). Lastly, the initial study conducted on the failure properties of meniscal attachments in the longitudinal direction (Hauch, Villegas et al. 2010) reported elastic moduli values of 169 ± 130 MPa and 91 ± 67 MPa for the anterior and posterior attachments, respectively. The more complex assessment performed here found similar results with the LA and MA attachments possessing the highest longitudinal linear elastic moduli (C5). The anterior and posterior attachments moduli were well within their respective standard deviations from the previous study; evidence that the piece-wise material model corresponds well with commonplace linear elastic evaluation.

This is the first study to examine the mechanical properties of meniscal attachments in the transverse direction. Results suggest that there are significant mechanical differences between attachments. While it is not believed that the attachments are loaded in pure tension in the transverse direction, this transverse mechanical data, coupled with longitudinal data, was used to improve upon previous constitutive modeling of the mechanical behavior of meniscal attachments. Future studies are needed to determine if the different transverse properties of the MP attachment translates into clinically meaningful effects. These data are vital to engineer meniscal replacements, as the apparent anisotropic nature of the meniscal attachments is an important feature that likely needs to be replicated during meniscal tissue engineering.

2.6 References

- Ahn, J. H., Y. S. Lee, et al. (2009). "Arthroscopic all inside repair of the lateral meniscus root tear." Knee 16(1): 77-80.
- Alhalki, M. M., S. M. Howell, et al. (1999). "How three methods for fixing a medial meniscal autograft affect tibial contact mechanics." Am J Sports Med 27(3): 320-8.
- Benjamin, M., E. J. Evans, et al. (1991). "Quantitative differences in the histology of the attachment zones of the meniscal horns in the knee joint of man." J Anat 177: 127-34.
- Benjamin, M. and J. R. Ralphs (1998). "Fibrocartilage in tendons and ligaments--an adaptation to compressive load." J Anat 193 (Pt 4): 481-94.
- Brody, J. M., H. M. Lin, et al. (2006). "Lateral meniscus root tear and meniscus extrusion with anterior cruciate ligament tear." Radiology 239(3): 805-10.
- Chen, M. I., T. P. Branch, et al. (1996). "Is it important to secure the horns during lateral meniscal transplantation? A cadaveric study." Arthroscopy 12(2): 174-81.
- Choi, N. H., K. M. Son, et al. (2008). "Arthroscopic all-inside repair for a tear of posterior root of the medial meniscus: a technical note." Knee Surg Sports Traumatol Arthrosc 16(9): 891-3.
- de Boer, M. D., A. Selby, et al. (2007). "The temporal responses of protein synthesis, gene expression and cell signalling in human quadriceps muscle and patellar tendon to disuse." J Physiol 585(Pt 1): 241-51.

- De Smet, A. A., D. G. Blankenbaker, et al. (2009). "MR diagnosis of posterior root tears of the lateral meniscus using arthroscopy as the reference standard." AJR Am J Roentgenol 192(2): 480-6.
- Gao, J., G. Oqvist, et al. (1994). "The attachments of the rabbit medial meniscus. A morphological investigation using image analysis and immunohistochemistry." J Anat 185 (Pt 3): 663-7.
- Gardiner, J. C. and J. A. Weiss (2003). "Subject-specific finite element analysis of the human medial collateral ligament during valgus knee loading." J Orthop Res 21(6): 1098-106.
- Goertzen, D., J. Gillquist, et al. (1996). "Tensile strength of the tibial meniscal attachments in the rabbit." J Biomed Mater Res 30(1): 125-8.
- Hauch, K. N., D. F. Villegas, et al. (2010). "Geometry, time-dependent and failure properties of human meniscal attachments." J Biomech 43(3): 463-8.
- Haut Donahue, T. L., M. L. Hull, et al. (2003). "How the stiffness of meniscal attachments and meniscal material properties affect tibio-femoral contact pressure computed using a validated finite element model of the human knee joint." J Biomech 36(1): 19-34.
- Holzappel, G. A. (2000). Nonlinear solid mechanics : a continuum approach for engineering. Chichester ; New York, Wiley.
- Jones, A. O., M. T. Houang, et al. (2006). "Medial meniscus posterior root attachment injury and degeneration: MRI findings." Australas Radiol 50(4): 306-13.
- Lee, S. Y., W. H. Jee, et al. (2008). "Radial tear of the medial meniscal root: reliability and accuracy of MRI for diagnosis." AJR Am J Roentgenol 191(1): 81-5.

- Lynch, H. A., W. Johannessen, et al. (2003). "Effect of fiber orientation and strain rate on the nonlinear uniaxial tensile material properties of tendon." J Biomech Eng 125(5): 726-31.
- Messner, K. and J. Gao (1998). "The menisci of the knee joint. Anatomical and functional characteristics, and a rationale for clinical treatment." J Anat 193 (Pt 2): 161-78.
- Morrow, D. A., T. Haut Donahue, G.Odegard, K. Kaufman (2010). "A method for assessing the fit of a constitutive material model to experimental stress-strain data." Comput Methods Biomech Biomed Engin: 1.
- Ogden R. W., S. G., Sgura I. (2004). "Fitting hyperelastic models to experimental data." Computational Mechanics 34(6): 18.
- Provenzano, P. P., A. L. Alejandro-Osorio, et al. (2007). "Systemic administration of IGF-I enhances healing in collagenous extracellular matrices: evaluation of loaded and unloaded ligaments." BMC Physiol 7: 2.
- Quapp, K. M. and J. A. Weiss (1998). "Material characterization of human medial collateral ligament." J Biomech Eng 120(6): 757-63.
- Shrive, N. G., J. J. O'Connor, et al. (1978). "Load-bearing in the knee joint." Clin Orthop Relat Res(131): 279-87.
- Stabile, K. J., J. Pfaeffle, et al. (2004). "Bi-directional mechanical properties of the human forearm interosseous ligament." J Orthop Res 22(3): 607-12.
- Thompson, W. O., F. L. Thaete, et al. (1991). "Tibial meniscal dynamics using three-dimensional reconstruction of magnetic resonance images." American Journal of Sports Medicine 19(3): 210-5.

- Villegas, D. F., T. A. Hansen, et al. (2008). "A quantitative study of the microstructure and biochemistry of the medial meniscal horn attachments." Ann Biomed Eng 36(1): 123-31.
- Villegas, D. F., J. A. Maes, et al. (2007). "Failure properties and strain distribution analysis of meniscal attachments." J Biomech 40(12): 2655-62.
- Villegas, D. F. and T. L. Haut Donahue (2010). "Collagen Morphology in human meniscal attachments: a SEM study." Connective Tissue Research. *In Press*
- Walker, P. S. and M. J. Erkman (1975). "The role of the menisci in force transmission across the knee." Clin Orthop Relat Res(109): 184-92.
- Weiss, J. A., B. N. Maker, et al. (1996). "Finite element implementation of incompressible, transversely isotropic hyperelasticity." Comput methods in applied mechanics and engineering 135(1-2): 21.
- Woo, S. L. (1982). "Mechanical properties of tendons and ligaments. I. Quasi-static and nonlinear viscoelastic properties." Biorheology 19(3): 385-96.
- Vedi, V., A. Williams, et al. (1999). "Meniscal movement: An in-vivo study using dynamic mri." The Journal of Bone & Joint Surgery 81(1): 37-41.
- Yamamoto, E., K. Hayashi, et al. (2000). "Effects of stress shielding on the transverse mechanical properties of rabbit patellar tendons." J Biomech Eng 122(6): 608-14.

CHAPTER 3: INTERNAL PRESSURE OF THE HUMAN MENISCAL ATTACHMENTS DURING PHYSIOLOGICAL AND PATHOLOGICAL LOADING

3.1 Summary

Knee menisci bear up to 85% of intra-articular compressive loads. Mechanical functionality is dictated primarily by attachment sites that interface with bone. Disruption of attachment integrity represents a significant clinical dilemma, leading to meniscal extrusion. However, little is known of the mechanical environment or changes due to joint injury of the attachments. Cadaver knees were loaded at a range of flexion angles with a novel pressure micro sensor within each attachment site. Results were compared at ramp pressure, upon achieving two times body weight, and at equilibrium, after twenty minutes. The anterior cruciate ligament was transected then the knee was re-tested, followed by a longitudinal incision in the lateral posterior horn, and re-testing. For intact knees, medial attachments typically increased in pressure over time while lateral decreased. Ramp and equilibrium pressure was greatest at 0° of flexion. The medial posterior attachment pressure was greater than the medial anterior at ramp and all other attachments at equilibrium. Following ACL transection ramp pressure was significantly lower in the lateral posterior attachment and greater for the equilibrium pressure in the medial posterior attachment and at 0° of flexion. These data provide new insight into the mechanical environment of the meniscal attachments during loading.

3.2 Introduction

Knee menisci are semi-lunar, fibrocartilaginous structures that transduce applied compressive loads to circumferential hoop stresses which are attenuated at the tibial plateau via the meniscal attachments¹. These specialized interfaces, located at the lateral anterior (LA), lateral posterior (LP), medial anterior (MA), and medial posterior (MP) horns, are crucial to maintaining mechanical functionality of menisci, thereby preventing osteoarthritis (OA)¹⁻⁶. Similar to other insertion tissue, the ligament-like attachments link the meniscus main body to the subchondral bone utilizing a blend of collagen fibers and proteoglycans which assuage complex stress concentrations due to proposed tensile, compressive, and shear loading⁷. Mechanical evaluation of the attachments elucidates distinct differences in their material properties⁸, with the anterior being significantly stiffer than the posterior along the main fiber axis⁹. This is a presumed adaptation to the distinct mechanical environment that each attachment site must endure. Magnetic resonance imaging (MRI) of meniscal translation and articular surface contact supports this hypothesis as the anterior attachment sites demonstrate greater mobility and the posterior compartment exhibiting direct contact during deep knee flexion¹⁰. Histological investigation reveals significant differences in the amount of fibrocartilage at the attachment sites, a constituent directly linked to the amount of compression applied to insertion tissues^{11,12}. Additionally, the proteoglycans present at the meniscus to bone interface aid in resisting the applied stresses by retaining interstitial fluid¹². Seitz et al. have recursively determined the forces acting on the anterior attachment sites during loading revealing very low loads for physiological trajectories¹³. The posterior attachment sites, however, are more clinically relevant as they are believed to endure higher forces and are known to be less mobile^{10,14}. Specifically, medial posterior horn tears and root avulsion are most often reported in the literature and are believed to

be of greater functional significance¹⁵. Thus, it is imperative to determine the mechanical environment of all attachment sites and how they work in conjunction with the meniscus to support load bearing activities.

In addition to ascertaining the native mechanics, changes in joint biomechanics due to injury, including anterior cruciate ligament (ACL) and meniscal tearing, are of particular interest. Risk of OA is significantly increased following traumatic injury and is due in part to changes in joint mechanics^{16,17}. Specifically, ACL rupture results in posterolateral shifts in tibiofemoral contact points, increased contact area, and decreased pressure¹⁷⁻¹⁹. Conversely, meniscal lesions have resulted in a significant decrease in tibiofemoral contact area and increase in peak pressure²⁰. Clinical treatment of acute meniscal tearing often involves partial meniscectomy to prevent damage propagation; however, this procedure can result in pathological contact pressures and fail to stave off OA progression^{20,21}. Restoration of meniscus mechanics can be infeasible as tears often occur in the mostly avascular inner two thirds of the meniscus and attempted repair is not necessarily better than partial meniscectomy²². Tissue engineered replacements present a possible solution to this orthopaedic challenge, however fully realized constructs remain unproven *in vivo* and long-term success will depend on fixation that recreates the native tissue mechanics, including the attachment sites^{4,23}.

Determining physiological attachment mechanics is complicated due to tight spatial constraints when considering transducer fixation, particularly in the posterior compartments¹³. Recent development of a novel, minimally invasive, pressure micro-sensor (250 μ m in diameter) facilitates direct observation of fluid pressure within biological tissues, with implications for the

surrounding stress environment²⁴⁻²⁶. These sensors are implanted using a 21-ga syringe needle and remain rooted to the tissue via a small barb on the outer surface. After insertion the needle is then retracted from the tissue. The latest iteration of these sensors exhibits relative immunity to temperature, electromagnetic-interference, and corrosive environments. Their dynamic operating range is in excess of 250mmHg, sampled at 960Hz, with accuracy of 2% of full-scale output and repeatability and hysteresis better than 1%²⁷⁻²⁹. Leveraging this technology provides an unprecedented examination of the internal mechanical environment within the attachment sites.

Based on clinical and laboratory evidence it is hypothesized that 1) the fluid pressure within the posterior attachment sites would be highest during physiological loading, 2) fluid pressure will decrease in the anterior and increase in posterior sites with greater flexion angles and 3) ACL rupture and disruption of meniscal integrity will decrease fluid pressure within the attachment sites as more tibiofemoral contact is transferred directly through the articular cartilage. As meniscus functionality is dependent on its fixation understanding meniscal attachment mechanics and changes due to injury is paramount when considering future reparative and replacement modalities.

3.3 Materials and Methods

Six human cadaver knees (ages: 41-61, average age 55) were acquired from the Mayo Clinic donor program with institutional review board approval. Knees selected had no history of joint surgery nor showed any apparent signs of articular cartilage thinning based on radiographic examination by an orthopaedic surgeon. Specimens were dissected such that the patellar tendon, patella, and a portion of the quadriceps as well as the structural ligaments and most of the

synovial sac were left intact. A threaded rod was bonded inside the medullary cavity of the femur and the tibia was potted using fiber strand compound (Bondo-Glass, 3M, St.Paul, MN). The joints were then mounted in a uni-axial material tester (Model 8872, Instron Corporation, Canton, MA) with custom made fixtures that fix the position of the tibia while allowing free rotation of the femur about all three axes. The pressure microsensors were then inserted into the meniscal attachments using a 21.5-ga needle. The sensors monitored the relative change in pressure during loading.

Knees were at five flexion angles (*15°, 0°, 15°, 30°, 45°). Three of the angles positioned the knee with the simulated ankle behind the hip (15°, 30°, 45°), one directly in line (0 – full extension), and one with the ankle in front of the hip (*15°) (Figure 3-1). An electric actuator (Model EC2, Danaher Motion, Radford, VA) applied a pre-load of 45 N to the

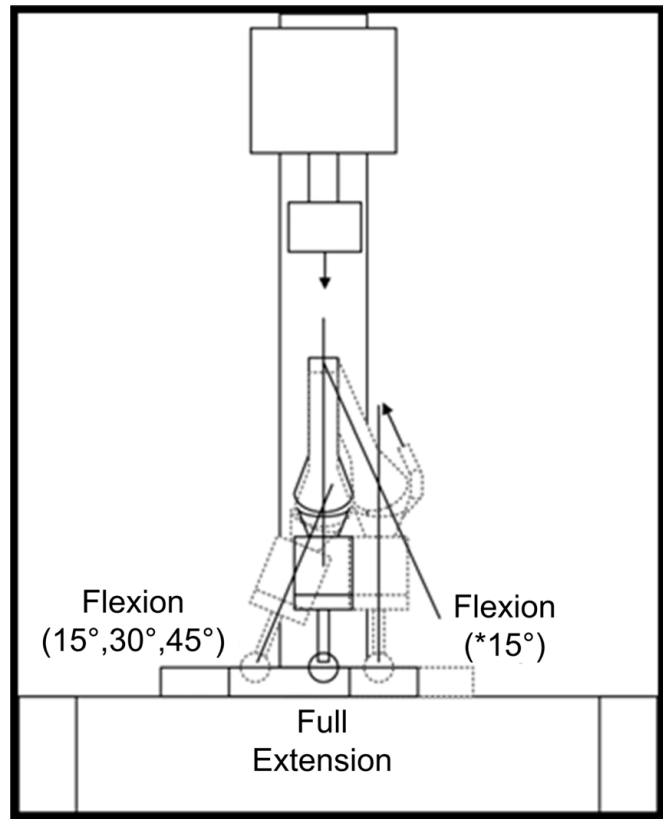


Figure 3-1: Schematic of joint loading apparatus and relative flexion angles used for testing.

quadriceps complex, followed by loading the joint to two times body weight. The

load was ramped up over 100 sec and then held constant for 20 minutes while pressure was recorded continuously throughout the entire loading history. After loading, the joint was unloaded for 20 minutes, and then tested under load at another flexion angle. Upon completion of all walking angle joint positions for the intact joint, the anterior cruciate ligament was

transected (ACLT) and the test cycle was repeated. Lastly, a circumferential lesion was cut into the lateral posterior meniscus and the test sequence was again repeated (ACLT+cut)³⁰. Knees were wrapped in saline soaked gauze to keep tissues moist during testing. Flexion angle was randomized to eliminate any potential test sequence effects.

In order to compare loading angles and conditions, specific points of interest were identified from the pressure-time histories: pressure at the start of holding cycle (“ramp”), after 20 minutes of constant load (“equilibrium”). Walking angle results were analyzed using a three-factor ANOVA with repeated measures (attachment site, physical condition, and flexion angle). Post-hoc analysis using Tukey’s method was used to identify explicit differences, $p < 0.05$ was considered statistically significant.

3.4 Results

The fiber optic micro-sensors were able to record changes in pressure over time in meniscal attachment tissue (Figure 3-2). Pressure-time series data demonstrated consistent, though uniquely different, patterns for the attachment sites. Medial anterior and posterior attachment sites exhibited little change or an increase in fluid pressure over time with one exception at 30deg (Figure 3-3). The LA attachment exhibited little change or decreased with time (Figure 3-3). The LP attachment consistently decreased in fluid pressure over time. These results suggest tissue creep in the medial compartment and relaxation in the lateral under sustained loading.

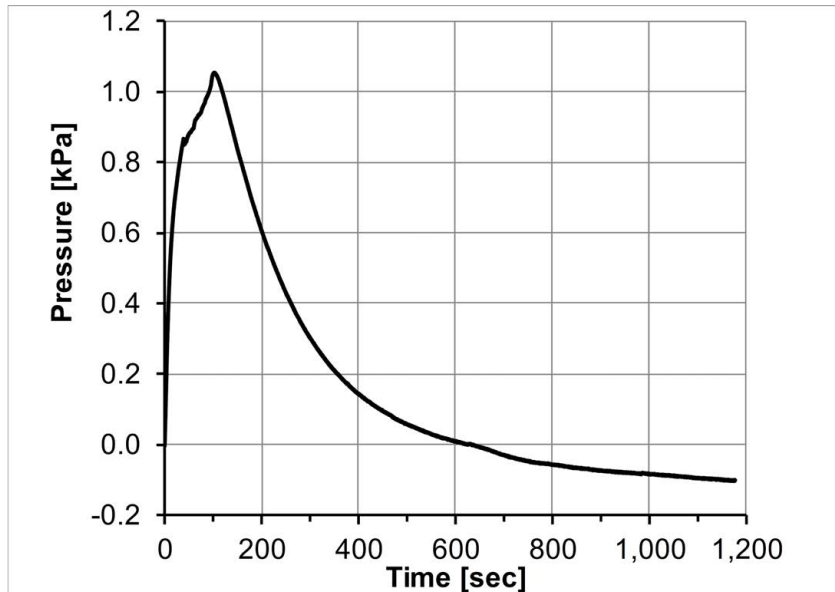


Figure 3-2: Representative pressure-time history for a healthy, lateral anterior attachment site at *15°. Pressure steadily decreases after achieving peak pressure at the end of the ramp loading phase.

Examining fluid pressure for each attachment site the MP was significantly greater than the MA at ramp pressure. At equilibrium, the MP attachment had significantly greater pressure than all other attachment sites. When considering joint flexion angle, the fluid ramp pressure at zero degrees of flexion was significantly greater than the *15°, 30°, and 45° angles. This effect is reduced at equilibrium as zero is only greater than 45° at this time point (Figure 3-4).

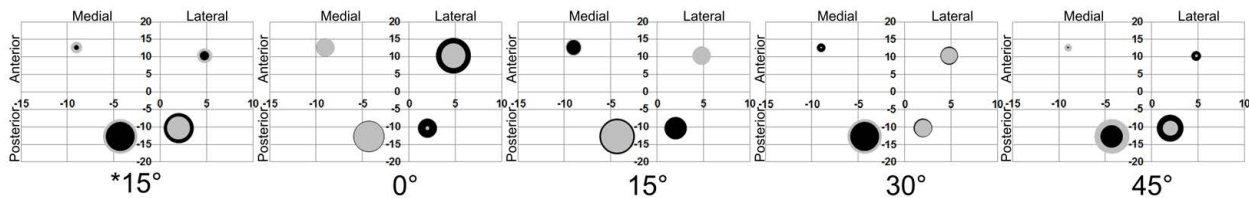


Figure 3-3: Bubble charts showing the relative amount and change in fluid pressure for each attachment site at each tested angle of flexion. Black circles are ramp pressure (when 2xBW has been achieved) and gray circles are equilibrium pressure (after 20 minutes of constant load). Bubble size is directly proportional to fluid pressure. Relative bubble locations are shown to correct anatomical scale in millimeters (mean data from 46). Medial attachment sites show little change or increase in fluid pressure over time. Lateral attachment sites show little change or decrease in fluid pressure over time. Note: if only gray circle can be seen then black is same size, indicating little to no change.

Ramp and equilibrium pressures are affected considerably following ACLT, specifically at 0 degrees flexion. Post-hoc analysis revealed a significant difference between the healthy and the

ACL and ACLT+cut in the LP attachment for ramp pressure and MP attachment for equilibrium (Figure 3-4).

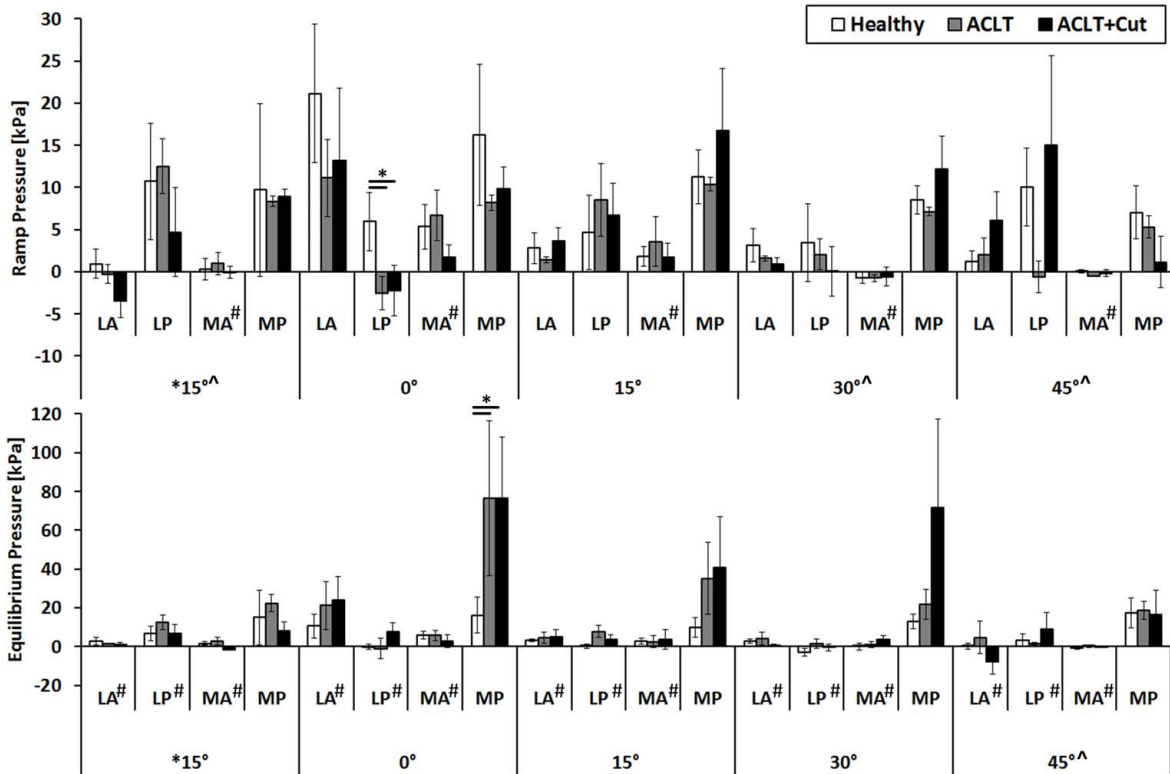


Figure 3-4: Relative change in pressure for each meniscal attachment site at various flexion angles and joint condition loaded to two times body weight (ramp) and after twenty minutes of constant load (equilibrium). Significant differences observed for average relative change in pressure at ramp and equilibrium time points for angle and attachment site. Loading at zero degrees of flexion resulted in significantly greater pressure at *15°, 30°, and 45° at the end of the ramp loading cycle (^ - sig. diff. than 0°). This effect was reduced following 20 minutes of steady-state loading as zero degrees was only significantly greater than 45° at this time point. The relative change in pressure for the medial posterior (MP) attachment site was significantly greater than medial anterior (MA) at ramp, however, after 20 minutes of loading the MP was significantly greater than MA, lateral anterior (LA), and lateral posterior (LP) attachments (# - sig. diff. than MP). Post-hoc analysis revealed significant changes in ramp and equilibrium pressure at 0 degrees of flexion following transection of the ACL for the LP and MP, respectively (* - p < 0.05).

3.5 Discussion

This work reports direct measurement of internal pressures in human meniscal attachments for the first time. Unique changes in fluid pressure over time were observed between menisci. The medial compartment attachment site pressures often increased over time, implicating that the medial meniscus crept under constant body force. It has been shown that the medial meniscus must sustain higher forces and is less mobile than the lateral^{10,14}. Additionally, Hosseini et al. showed that in 300 seconds of single leg body weight loading *in vivo* the medial cartilage contact

area was greater than the lateral and increased over time³¹. Furthermore, coronal tibial slope is predominately oriented downward from lateral to medial compartments³². Thus, with limited translational capability the medial meniscus may be forced to sustain constant loading whereas the increased mobility of the lateral meniscus and relative contact of the femur and tibia facilitates minimal changes, even potential relaxation, in load bearing over time. However, there is limited data pertaining to equilibrium tissue behavior over long loading cycles *in vivo* or *in situ*.

As expected the fluid pressure in the medial posterior attachment site was greatest. This again correlates well with findings that the medial meniscus body and horn are subjected to greater forces during loading^{10,14}. Seitz et al. demonstrated that the anterior sites are subjected to very low forces, approximately 10-15N¹³; accordingly our data also show relatively small changes in fluid pressure for these sites. In their study the posterior sites were not examined due to occlusion by the posterior cruciate ligament preventing sensor placement; however they acknowledge the need for data on the posterior sites. With the micro-sensor employed here we were able to directly monitor and compare the pressure between all attachment sites and affirm that while the anterior sites develop relatively low internal pressure the medial posterior site is subjected to significantly greater pressure. Hauch et al. determined the human medial posterior to possess significantly lower failure properties and linear modulus⁹. Coupling these findings with our results corresponds with clinical findings that medial posterior root injuries are most common and represent a major disruption in effective knee biomechanics¹⁵.

Unexpectedly, the pressure was often highest at 0 degrees of flexion. This may be due to the load concentrated at the cartilage-cartilage contact area forcing interstitial fluid radially outwards, consolidating in the attachment site compartments. Alternatively or additionally, at 0 degrees flexion, the attachments may be loaded the most to keep the joint load transferred through the meniscus and off the underlying articular cartilage³³. Large tensile loads in conjunction with Poisson's effect could in turn reduce cross sectional area and increase fluid pressure. In contrast, Seitz et al. showed no difference in anterior forces with changes in flexion angle¹³. Additionally, Stärke et al. used a load cell in line with a bone tunnel of the medial anterior site in porcine knees to determine attachment force and found no change in force with a change in flexion angle³⁴. Neither study, however, accounted for changes in the posterior compartments. Tibiofemoral contact begins approximately central between the root attachment sites and translates posteriorly during deep knee flexion¹⁰, therefore the posterior sites may be subjected to higher contact stresses in addition to hoop stresses developed in the meniscus main body. It should be noted that Seitz et al. removed all surrounding soft tissue from the anterior portion of the joint capsule, which may have significantly influenced their findings as the patella and adjacent fat pad are in close proximity, if not directly contacting the anterior sites.

While it is known that joint mechanics and pressure distribution are altered due to ACL and meniscal tears^{17,19-21,35-38}, how these conditions effect the mechanical environment of all the meniscal attachments at the time of injury is not understood³⁵. Data presented here showed significant differences in average meniscal attachment ramp pressure when the ACL was transected. Explicitly, the lateral posterior attachment exhibited a large decrease in ramp pressure at zero degrees of flexion. This suggests that the meniscus may become less supportive post-

injury as more load is transferred directly to the cartilage. Corroborating this idea is the documented increase in tibiofemoral cartilage-cartilage deformation for both medial and lateral compartments following ACL injury, when compared to healthy contralateral limbs³⁹. In addition to an increase in cartilage deformation, average tibiofemoral contact location shifts in both the anteroposterior and mediolateral directions in ACL deficient joints^{19,39}. The tibia moves anteriorly and medially, relative to the femur, resulting in average contact occurring more posterior-laterally. In the medial compartment this would drive the femoral condyle away from the meniscus, but towards the MP attachment site, potentially increasing the pressure at this site over time as is seen at 0° of flexion (Figure 4). In the lateral compartment, however, this shift should result in greater lateral meniscus translation. Our data shows a decrease in lateral posterior ramp pressure following transection. This may be due to joint incongruity that arises following loss of ACL functionality, resulting in cartilage-cartilage impingement thereby reducing the load on the lateral meniscus at zero degrees of flexion. Our findings do differ slightly from Markolf et al. who showed that while forces of the medial posterior horn increase following ACL transection with an applied 500N joint load, this was only for flexion angles greater than 15°³⁵. Although trends in our data do suggest a general increase in pressure following ACLT this was only significant at 0° and only after achieving steady-state behavior.

A longitudinal lateral posterior incision was used in this study as a previously developed closed joint injury model in our laboratory frequently yielded this result³⁰. This type of injury is mimetic of knee injuries initiated in jump-landing sports impacts. Assessment of skiers with combined ACL and meniscus tears shows an increased prevalence for the lateral compartment^{40,41}. Medial meniscus injuries are more common, however, it is believed the lateral meniscus plays a more

important role in dictating knee biomechanics, especially in the ACL deficient joint⁴². There were no additional significant differences in attachment pressure after cutting the lateral posterior horn of the meniscus. This is most likely due to the incision being along the main fiber axis of the meniscal body, this would not necessarily disrupt the longitudinal fibers from bearing the applied static loading. While attachment site mechanics appeared unchanged with the additional lesion this does not suggest that this sort of tear can be considered inconsequential. The initial longitudinal tear may propagate, leading to a necessary meniscectomy, and ultimately precipitating OA development.

While this study aimed at recreating conditions that are physiologically relevant, static loading conditions were examined rather than dynamic cycling. Many dynamic systems have proven vital in studying changes in joint kinematics; however, few achieve physiologically relevant joint loads as ensuring accurate loads and displacements in a relevant time frame is a non-trivial and an expensive challenge. However, we choose to focus on achieving loads that approached physiological levels to obtain truly mimetic conditions within the attachment sites, particularly considering the low loads for the anterior sites as determined by Seitz et al.¹³. Additionally, ramp loading speeds were kept relatively slow to prevent dislodging the sensors from the tissue. The relatively stiff/tough collagen fibrils of the meniscal attachments do not provide as secure fixation as muscle tissue, for which these sensors were originally developed. Work continues to refine these sensors for a wide array of laboratory and clinical applications²⁸. Another limitation is the implementation of only a single muscle group, the quadriceps. Clearly, inclusion of additional muscle groups can alter the contact mechanics; however, we opted to include the quadriceps as it is tied to the patella and patellar tendon which are instrumental in closing the

joint and can potentially influence the mechanics of the anterior sites due to their anatomical location. Lastly, changes due to ACL transection and meniscal cutting are more replicative of immediate changes in joint mechanics. Plainly, chronic factors such as inflammation, limping, occult damage, etc. would alter results here. Also, muscle adaptation does set in during recovery and alter mechanics, thus this is not directly comparable to the complex clinical case. It is understood that OA is a complex disease with multiple pathways involving non-biomechanical elements, however, the meniscal attachments may play an important role in degeneration and should be considered in future attempts to stave off propagation.

In summary, this study has demonstrated for the first time that the mechanical environment, as indicated by fluid pressure, of the meniscal attachments during loading are unique between sites and can change significantly with flexion angle and loss of ACL integrity. This information can be used as means to validate whole joint mechanical models, improving understanding of the anatomical role of each attachment site, and changes within each that occur with injury.

3.6 References

1. Mow, V. C., Arnoczky, S. P. & Jackson, D. W. 1992. *Knee Meniscus: Basic and Clinical Foundations*. New York: Raven Press; 208 p.
2. Yao, J., Funkenbusch, P. D., Snibbe, J., et al. 2006. Sensitivities of medial meniscal motion and deformation to material properties of articular cartilage, meniscus and meniscal attachments using design of experiments methods. *J Biomech Eng* 128: 399–408.
3. Arnoczky, S. 1999. Building a meniscus. Biologic considerations. *Clin Orthop* 367: S244–S253.
4. AufderHeide, A. C. & Athanasiou, K. A. 2004. Mechanical Stimulation Toward Tissue Engineering of the Knee Meniscus. *Ann Biomed Eng* 32: 1163–1176.
5. Setton, L. A., Guilak, F., Hsu, E. W. & Vail, T. P. 1999. Biomechanical factors in tissue engineered meniscal repair. *Clin Orthop* 367: S254–72.
6. Haut Donahue, T. L., Hull, M. L., Rashid, M. M. & Jacobs, C. R. 2003. How the stiffness of meniscal attachments and meniscal material properties affect tibio-femoral contact pressure computed using a validated finite element model of the human knee joint. *J Biomech* 36: 19–34.
7. Shaw, H. M. & Benjamin, M. 2007. Structure-function relationships of entheses in relation to mechanical load and exercise. *Scand J Med Sci Sports* 17: 303–315.
8. Abraham, A. C., Moyer, J. T., Villegas, D. F., et al. 2011. Hyperelastic properties of human meniscal attachments. *J Biomech* 44: 413–418.
9. Hauch, K. N., Villegas, D. F. & Haut Donahue, T. L. 2010. Geometry, time-dependent and failure properties of human meniscal attachments. *J Biomech* 43: 463–468.
10. Yao, J., Lancianese, S. L., Hovinga, K. R., et al. 2008. Magnetic resonance image analysis of meniscal translation and tibio-menisco-femoral contact in deep knee flexion. *J Orthop Res* 26: 673–684.
11. Benjamin, M. & Ralphs, J. R. 1998. Fibrocartilage in tendons and ligaments--an adaptation to compressive load. *J Anat* 193: 481–494.
12. Benjamin, M., Evans, E., Rao, R., Findlay, J. 1991. Quantitative differences in the histology of the attachment zones of the meniscal horns in the knee joint of man. *J Anat* 177: 127–134.
13. Seitz, A., Kasisari, R., Claes, L., et al. 2012. Forces acting on the anterior meniscotibial ligaments. *Knee Surg Sports Traumatol Arthrosc* 20: 1488–1495.

14. Vedi, V., Williams, A., Tennant, S. et al. 1999. Meniscal movement. An in-vivo study using dynamic MRI. *J Bone Joint Surg Br* 81: 37–41.
15. Jones, A. O., Houang, M. T. W., Low, R. S., Wood, D. G. 2006 Medial meniscus posterior root attachment injury and degeneration: MRI findings. *Australas Radiol* 50: 306–313.
16. Anderson, D. D., Chubinskaya, S., Guilak, F., et al. 2011. Post-traumatic osteoarthritis: improved understanding and opportunities for early intervention. *J Orthop Res* 29: 802–809.
17. Andriacchi, T. P., Dyrby, C. O. 2005. Interactions between kinematics and loading during walking for the normal and ACL deficient knee. *J Biomech* 38: 293–298.
18. Wu, J. Z., Herzog, W., Epstein, M. 2000. Joint contact mechanics in the early stages of osteoarthritis. *Med Eng Phys* 22: 1–12.
19. Li, G., Moses, J., Papannangari, R., 2006. Anterior cruciate ligament deficiency alters the in vivo motion of the tibiofemoral cartilage contact points in both the anteroposterior and mediolateral directions. *J Bone Joint Surg Am* 88: 1826–1834.
20. Lohmander, L. S., Englund, P. M., Dahl, L. L., Roos, E. M. 2007. The long-term consequence of anterior cruciate ligament and meniscus injuries: osteoarthritis. *The Am J Sports Med* 35: 1756–1769.
21. Bedi, A., Kelly, N., Baad, M. 2010. Dynamic contact mechanics of the medial meniscus as a function of radial tear, repair, and partial meniscectomy. *J Bone Joint Surg Am* 92: 1398–1408.
22. Messner, K., Gao, J. 1998. The menisci of the knee joint. Anatomical and functional characteristics, and a rationale for clinical treatment. *J Anat* 193: 161–78.
23. Makris, E. A., Hadidi, P., Athanasiou, K. A. 2011. The knee meniscus: structure-function, pathophysiology, current repair techniques, and prospects for regeneration. *Biomaterials* 32: 7411–7431.
24. Winters, T., Takahashi, M., Lieber, R. 2009. Correlation between isometric force and intramuscular pressure in rabbit tibialis anterior muscle with an intact anterior compartment. *Muscle Nerve* 40: 79–85.
25. Ward, S. R., Davis, J., Kaufman, K. R., Lieber, R. L. 2007. Relationship between muscle stress and intramuscular pressure during dynamic muscle contractions. *Muscle Nerve* 36: 313–319.
26. Davis, J., Kaufman, K. R., Lieber, R. L. 2003. Correlation between active and passive isometric force and intramuscular pressure in the isolated rabbit tibialis anterior muscle. *J Biomech* 36: 505–512.

27. Chen, S., Pislaru, C., Kinnick, R. 2005. Evaluating the dynamic performance of a fibre optic pressure microsensor. *Physiol Meas* 26: N13–19.
28. Cottler, P. S., Karpen, W. R., Morrow, D. A., Kaufman, K. R. 2009. Performance characteristics of a new generation pressure microsensor for physiologic applications. *Ann Biomed Eng* 37: 1638–1645.
29. Kaufman, K. R., Wavering, T., Morrow, D. A., et al. 2003. Performance characteristics of a pressure microsensor. *J Biomech* 36: 283–287.
30. Killian, M. L., Isaac, D., Haut, R. 2010. Traumatic anterior cruciate ligament tear and its implications on meniscal degradation: a preliminary novel lapine osteoarthritis model. *J Surg Res* 164: 234–241.
31. Hosseini, A., Van de Velde, S., Kozanek, M., et al. 2010. In-vivo time-dependent articular cartilage contact behavior of the tibiofemoral joint. *Osteoarthritis Cartilage* 18: 909–916.
32. Hashemi, J., Chandrashekar, N., Gill, B., et al. 2008. The geometry of the tibial plateau and its influence on the biomechanics of the tibiofemoral joint. *J Bone Joint Surg Am* 90: 2724–2734.
33. Ahmed, A. M., Burke, D. L. 1983. In-vitro measurement of static pressure distribution in synovial joints—part 1: Tibial surface of the knee. *J Biomech Eng* 105: 216–225.
34. Stärke, C., Kopf, S., Gröbel, K.-H., Becker, R. 2009. Tensile forces at the porcine anterior meniscal horn attachment. *J Orthop Res* 27: 1619–1624.
35. Markolf, K. L., Jackson, S. R., McAllister, D. R. 2012. Force measurements in the medial meniscus posterior horn attachment: effects of anterior cruciate ligament removal. *The Am J Sports Med* 40: 332–338.
36. Chaudhari, A. M. W., Briant, P. L., Bevill, S. L., et al. 2008. Knee Kinematics, Cartilage Morphology, and Osteoarthritis After ACL Surgery. *Med Sci Sports Exerc* 40: 215–222.
37. Magnussen, R. A., Mansour, A. A., Carey, J. L., Spindler, K. P. 2009. Meniscus status at anterior cruciate ligament reconstruction associated with radiographic signs of osteoarthritis at 5- to 10-year follow-up: a systematic review. *J Knee Surg* 22: 347–357.
38. Tengrootenhuysen, M., Meermans, G., Pittoors, K., et al. 2011. Long-term outcome after meniscal repair. *Knee Surg Sports Traumatol Arthrosc* 19: 236–241.
39. Van de Velde, S. K., Bingham, J., Hosseini, A., et al. 2009. Increased tibiofemoral cartilage contact deformation in patients with anterior cruciate ligament deficiency. *Arthritis Rheum* 60: 3693–3702.

40. Duncan, J. B., Hunter, R., Purnell, M., Freeman, J. 2005. Meniscal injuries associated with acute anterior cruciate ligament tears in alpine skiers. *The Am J Sports Med* 23: 170–172
41. Paletta, G. A., Levine, D. S., O'Brien, S. J., et al. 1992. Patterns of meniscal injury associated with acute anterior cruciate ligament injury in skiers. *The Am J Sports Med* 20: 542–547
42. Noyes, F., Bassett, R., Grood, E., Butler, D. 1980. Arthroscopy in acute traumatic hemarthrosis of the knee. Incidence of anterior cruciate tears and other injuries. *J Bone Joint Surg Am* 62: 687–695.
43. Urban, W., Nyland, J. 1999. The radiographic position of medial and lateral meniscal horns as a basis for meniscal reconstruction. *Arthroscopy* 15: 147–154.

CHAPTER 4: FROM MENISCUS TO BONE: A QUANTITATIVE EVALUATION OF STRUCTURE AND FUNCTION OF THE HUMAN MENISCAL ATTACHMENTS

4.1 Summary

Knee menisci are c-shaped, fibrocartilaginous structures comprised of a hierarchical collagen morphology that transmits applied intra-articular compressive and shear loads to longitudinal hoop stresses terminated at the tibial plateau via meniscal entheses. Meniscus efficacy at promoting joint congruity and preventing osteoarthritis hinges on entheses integrity. Despite this, little is known of the structure-function relationships within the native insertion sites. Gross-scale tensile testing and histomorphometry reveal significant differences between the four attachments, implicating that each must endure a unique mechanical environment thereby dictating their structure. Magnetic resonance imaging of meniscal horn translations during flexion indeed corroborate this point. However, little data exists to elucidate how these interfaces have adapted to their complex loading environment, particularly on a relevant scale as the entheses transition through several unique zones in less than a millimeter. In our study we leveraged nano-indentation to determine viscoelastic material properties through the transition zones. Additionally, we employed histological techniques to evaluate entheses structure including collagen organization and interdigitation morphometry. Mechanical evaluation revealed the medial posterior insertion site to be significantly more compliant than others. Collagen fiber orientation and dispersion as well as interdigitation morphometry was significantly different between attachment sites. These findings are clinically relevant as a disproportionate amount of entheses failure occurs in the medial posterior attachment. Also, meniscal entheses structure and

function will need to be considered in future reparative and replacement strategies in order to recreate native meniscus mechanics and prevent osteoarthritis propagation.

4.2 Introduction

Classically defined by the thinning of articular cartilage, knee osteoarthritis (OA) entails a complex series of events attributed to either trauma or progressive degeneration. Increasing evidence has identified various joint structures as potential disease-initiating pathways, including cartilage, bone, ligaments, synovial fluid, and the meniscus [1]. The latter, which has historically been surgically triaged post-injury, is now known to be crucial in maintaining joint health and preventing OA [2]. Currently, treatment of menisci-derived OA using surgical intervention via repair, meniscectomy, or allograft replacement can be implemented; however, this can fail to halt OA progression [3, 4]. While diagnosis of meniscal injury and subsequent treatment are significantly more successful in younger patients [5], patients with identifiable meniscal damage increases with age, posing a serious physical and monetary burden [6]. One hope is that tissue engineered replacements will provide an alternative modality for individuals with severe meniscal degeneration and decrease the onset and progression of OA. In both donor and engineered replacements, particular attention is paid to the meniscal body itself. However, several studies have stressed the importance of meniscal attachments [7–9]. These studies have encouraged natural reconstruction of the meniscus to bone interface in order to prevent pathological contact pressures, load transmission, and excessive meniscal translation, a known indicator of OA [10]. While soft-tissue to bone tissue engineering is a thriving field of research, little attention has been paid to the meniscus to bone interface.

The main bodies of the menisci consist of fibrocartilaginous semi-lunar structures that are triangular in cross-section. This shape aids in joint alignment and cushioning by transducing applied compression to hoop stresses which are attenuated at the tibial plateau via fibrocartilaginous (FC) entheses [11–13]. These sites are located at the medial anterior (MA), lateral anterior (LA), medial posterior (MP), and lateral posterior (LP) portions of the menisci. As the main body of the meniscus transitions to bone, the superficial, randomly oriented and radial tie collagen fibers of the meniscal body diminish, leaving primarily ligament-like aligned type I collagen fibers [14]. These fibers demonstrate a crimped patterning and are responsible for bearing tensile loads developed from hoop stresses [8]. The ligamentous region (LI) extends from the body of the meniscus and transitions into the tibial plateau via uncalcified fibrocartilage (UFC) and calcified fibrocartilage (CFC). The UFC region contains primarily types I and II collagen fibers that are continuous across a calcification front known as the tidemark (TM) and transition into the CFC [15]. Changes in the depth and thickness of the TM can be indicative of pathophysiology, although little is known of its definitive purpose [16, 17]. Lastly, the CFC meets subchondral bone [SB] at an interdigitated cement line (Figure 4-1) [18, 19]. Developmental studies demonstrate that type I collagen fibers must be continuous through the enthesis at least until this junction [20]. Other forms of collagen are found in FC insertions, but in much smaller quantities, and the mechanical behavior of this transitional tissue is mostly dependent on contributions of type I and II collagens [21].

The presence and amount of FC at insertion sites can be attributed to compressive and shear loads as well as insertion angle changes during joint movement [18, 22, 23]. Specifically, the UFC region is considered analogous to a rubber grommet on an electrical plug, shielding the

insertion site from compression, while the CFC region protects the bone from shear loads [23].

In the context of the meniscal attachments, the femoral condyles may also be applying direct compressive and shear forces to some or all the insertion sites throughout the gait cycle.

Magnetic resonance imaging (MRI) evaluation of meniscal translation, mechanical testing, and histological evaluation of the attachments has revealed significant differences between the sites, elucidating that each are dependent on the loading environment unique to their location [9, 18, 19, 24]. In particular the anterior sites possess significantly greater failure properties than the posterior insertion sites.

In this study we aim to quantitatively define the structure and mechanical function of the human meniscal attachments using nanomechanical and histomorphological techniques. Based on previous research, we hypothesized that the anterior collagen fiber insertion angles would be shallower, relative to the tidemark, and more organized, resulting in superior mechanical performance.

4.3 Materials and Methods

4.3.1 Sample Preparation

Eight cadaver knees (ages 41-61, average age: 55) were obtained from the Mayo Clinic tissue donor program with institutional review board approval. X-ray evaluation prior to dissection as well as gross evaluation of soft-tissue prior to testing/embedding was performed by an orthopaedic surgeon to ensure healthy samples. Bone blocks were excised to include meniscal attachment sites from the tibial plateau and bisected along the axis of collagen fiber insertion. Regular wetting using phosphate buffered saline (PBS) was used to keep tissue moist during

processing. Each half of the attachment sites were wrapped in PBS soaked gauze and stored sealed at -20°C until further processing for either structural evaluation or mechanical testing.

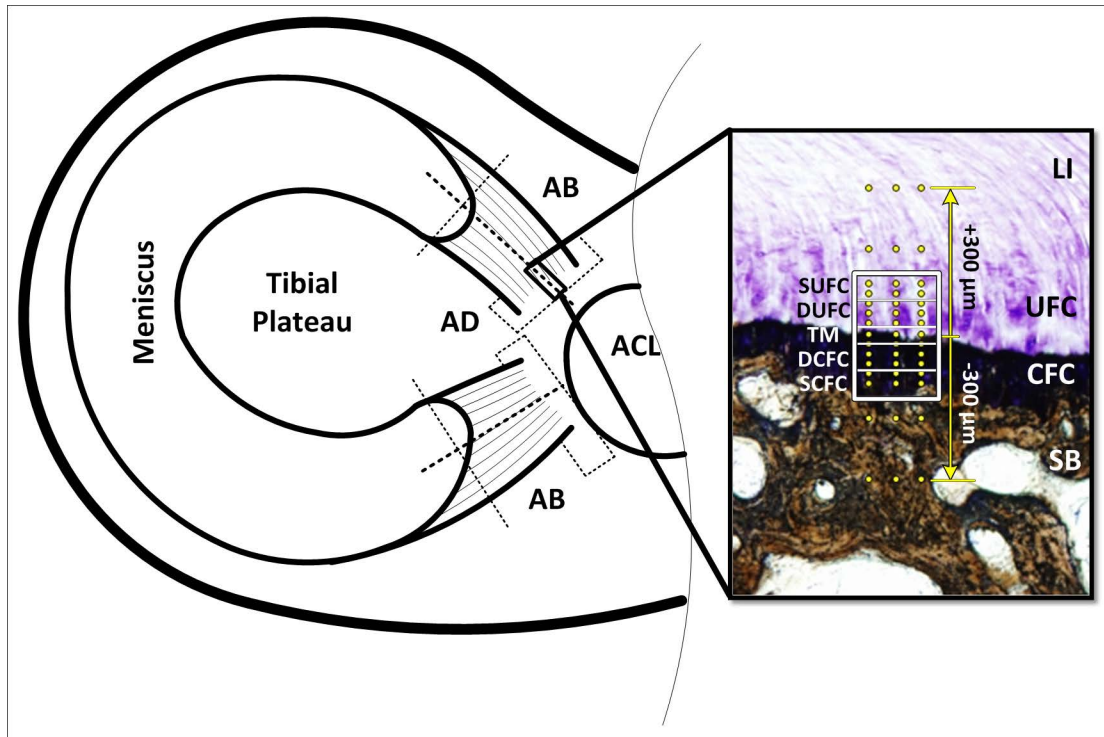


Figure 4-1: Schematic of sample extraction and analysis regions. Dotted lines represent cut surfaces. Adaxial (AD) sections were used for collagen fiber orientation and interdigitation analyses, abaxial (AB) sections were used for mechanical evaluation. Inset shows the unique zones of the meniscal attachments: Ligamentous (LI), Uncalcified Fibrocartilage (UFC), Calcified Fibrocartilage (CFC), and Subchondral Bone (SB). The regions of fibrocartilage are separated by the tidemark (TM). Boxed region represents areas used for polarized light analysis (SUFC – Superior UFC, DUFC – Deep UFC, DCFC – Deep CFC, S – Superior CFC). Dots represent location of mechanical evaluation using nanoindentation. Indentation was performed in a region 300µm above and below the TM. Section is stained using toluidine blue and counter stained using Von Kossa technique.

4.3.2 Histology

Adaxial sections were utilized for histological analysis (Figure 4-1). Attachments were fixed in 10% neutral buffered formalin for 48 hours, serially dehydrated in ethanol, defatted in xylene and then embedded in methyl methacrylate (Technovit 9100 New, Heraeus Kulzer GmbH, Wehrheim, Germany). Sections were made (30µm thick) using standard cutting and grinding techniques. Collagen fiber orientation sections were decalcified and stained with 0.1% picrosirius red. Interdigitation sections were stained using von Kossa and counterstained with toluidine blue.

4.3.3 Collagen Fiber Orientation

Exploiting the enhancement of collagen fiber birefringence by sirius red allowed for determination of collagen fiber angles by utilizing polarized light analysis [25]. Stained sections were imaged using a microscope (Olympus BX51P) equipped with rotating polarizer and analyzer, a quarter wavelength compensator, and digital camera (DP70). The slides were placed between the polarizer and analyzer and aligned with the TM horizontal (along the 0-180° plane) so that all angular measurements were in reference to the TM. Images were obtained at 10° increments between 45 ° and 135 ° with and without the compensator in place.

A custom Matlab graphical user interface [26], was used to determine the fiber extinction angle based on the minimum light intensity as a function of section orientation relative to the crossed polarizers. To characterize the fiber angle across the insertion site, the Matlab interface was used to select the tidemark and build a grid of measurement points above and below this feature. This grid was then further subdivided into 5 sub-regions, described by their proximity to the tidemark: superior uncalcified fibrocartilage (SUFC), deep uncalcified fibrocartilage (DUFC), tidemark (TM), deep calcified fibrocartilage (DCFC), superior calcified fibrocartilage (SCFC) (Figure 4-1). Angular mean and variance for each sub-region were calculated using the Matlab circular statistics toolbox [27]. For examining fiber dispersion/organization, angular deviation was inclusive of all fiber angles. Individual attachment sites in each sub-region were compared using a Watson-Williams test ($p < 0.01$).

4.3.4 Interdigitation Analysis

To analyze the interdigitated joining of fibrocartilage to bone the CFC region is first isolated using the ImageJ color deconvolution tool [28]. The resultant 8-bit single color image is then thresholded and all extraneous points are removed. The resultant binary pixels are then stored as discrete X & Y locations. A function defining the interface is generated by taking the minimum y-pixel value at each unique x-location. To simplify the analytical process the “drift” that is due to the anatomical shape of the insertion must be removed. This is accomplished by applying a coarse Savitzky-Golay smoothing function [29] to the interdigitation function and subtracting it from the original function (Figure 4-2).

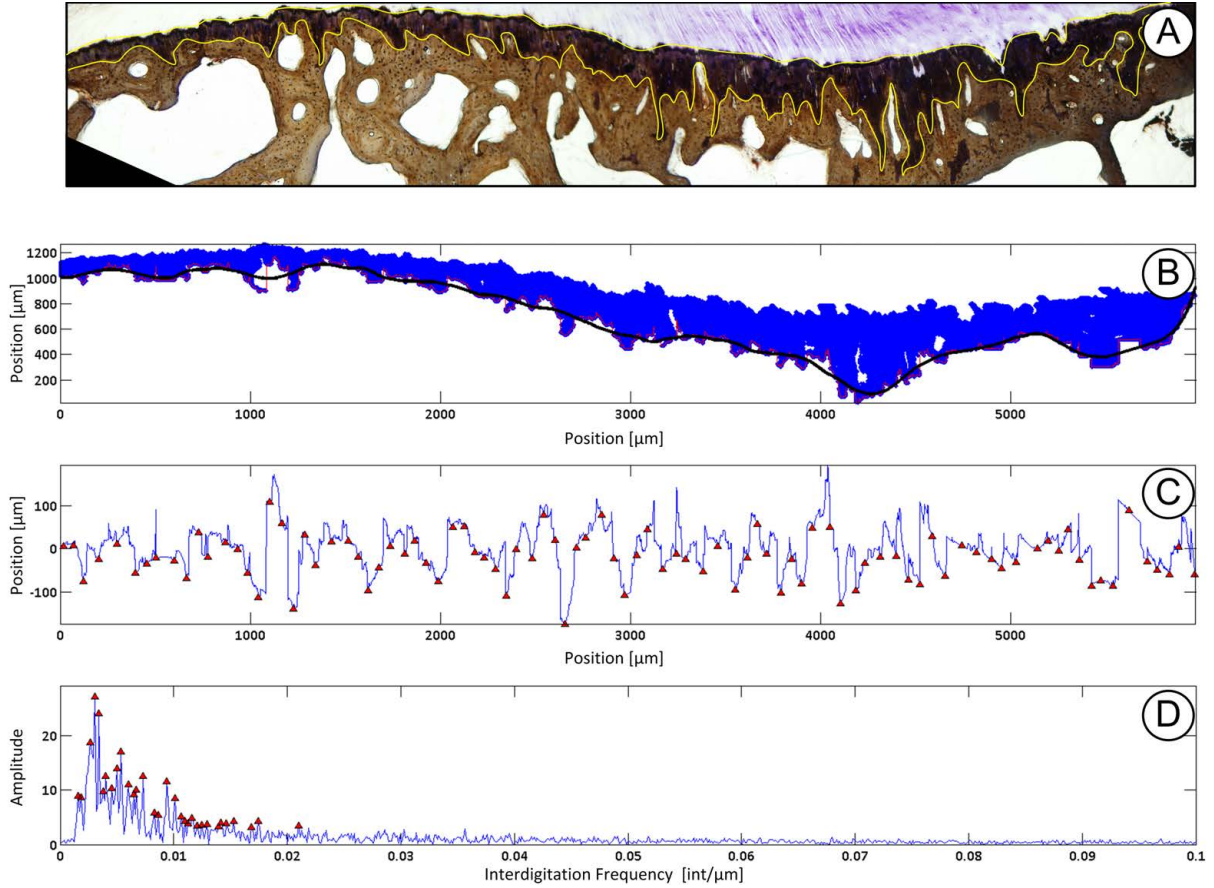


Figure 4-2: Example of interdigitation analysis performed. A) To identify the calcified fibrocartilage (CFC) region the insertion site was stained with toluidine blue and counter stained using Von Kossa technique. The CFC region (outlined in yellow) was isolated using the ImageJ color deconvolution tool. B) Pixel locations were loaded into Matlab and a coarse Savitzky-Golay smoothing function is overlaid (black line) at the cement line between CFC and subchondral bone. C) The smoothing function was then subtracted from the pixels at the cement line yielding unique x,y coordinates representing the interdigitations. Interdigitation size and average frequency was then computed using custom written scripts determine the nearest neighbor peak/valley pairs. Size is the height difference between pairs. Average frequency is the total number of interdigitations determined along the insertion site. D) A fast Fourier transform was then applied to the data to determine the peak and high frequency of interdigitation.

The complex interdigitations were defined using the average size, average-, most dominant-, and highest- frequency. A Matlab built-in function (`findpeaks()`) was used to identify the peaks/valleys of the interdigitation function. The average size of the interdigitations were ascertained by first determining the closest peak/valley pairs, with a pre-determined spacing and height threshold to remove any data “jitter”. An assessment algorithm sought through all valleys and peaks and determined the nearest neighbor. The difference in height between the two points

was then computed. For a given sample the mean amplitude was then computed across the whole insertion site. Average frequency was determined from the number of peak/valley pairs over the length of the whole insertion site. As the interdigitations are inhomogeneous across the site, it is an oversimplification to define only a single frequency value, so more spectral data was required to fully define the interface. The interdigitation function was transformed to the frequency domain using a Fast Fourier Transform to identify the most dominant and highest frequency components. Results were compared using a student's t-test ($p < 0.05$).

4.3.5 Nano-indentation

4.3.5.1 *Testing*

Abaxial sections were prepared for mechanical evaluation. Samples were thawed, rinsed in PBS, and placed cut surface up in mounting molds to allow for the insertion to be properly indented. A high viscosity acrylic resin that did not penetrate the specimen (ClaroCit, Struers Inc., Cleveland, OH) was then poured into the mold, without touching the cut surface, and allowed to fully cure. The exposed indentation surface was then series ground flat along the insertion fiber axis, so as to prevent fraying of soft-tissue, using 600- and 1200-grit silicon carbide paper with constant distilled water lubrication [30].

Embedded specimens were indented using a 300 μ m spherical ruby tip (Agilent Technologies, Inc., Santa Clara, CA) at 45 discrete locations (3 columns x 15 rows aligned from the TM). It should be noted that while the tip is relatively large compared to the insertion constituents, actual penetration depth resulted in a contact radius of less than 50 μ m. Indentation locations were chosen by first locating the apparent TM separating the calcified and uncalcified fibrocartilage

then mapping 7 indents above and below the tidemark at varying distances (Figure 4-1 inset). Selection was based upon previous histological data as discerning the four unique zones is not possible using the basic light microscope installed on the nano-indentation test machine. The primary region of interest was at the immediate proximity to TM, and indent spacing was finer closer to and sparser further away from the TM. Three adjacent columns, separated by 50 μ m, were indented so as to capture the variability in material properties due to the highly interdigitated calcified fibrocartilage to subchondral bone interface [18, 19]. Indentation location order was randomized and specimens were kept moist with 0.9% saline during testing.

A variable maximum load of either 10-, 5-, or 1-mN was applied, depending if the presumed indentation location was subchondral bone, calcified fibrocartilage, or uncalcified fibrocartilage/ligamentous, respectively. The changing load is factored into the analytical model used, as discussed in the following section, and is thus accounted for [31]. The load was held for 100 seconds in order to exhaust time dependent behavior as determined through pilot testing.

4.3.5.2 Processing

Displacement time histories for the load-hold period were fit to a viscoelastic indentation model [31, 32] using a constrained trust-region reflective optimization algorithm. Instantaneous and steady-state shear moduli were extracted from the fitting process. The robust model accounted for the effect of material creep during load ramping, indenter geometry, and the variable applied load. The model assumption of isotropy was corrected using $G^v = 2G^l(1 - \nu)$ assuming a Poisson's ratio of $\nu = 0.3$ [33, 34]. Lastly, shear moduli were converted to elastic moduli using $E = 2G(1 + \nu)$. Model fits were evaluated using a t-test to compare mean standardized variance

between the model and experimental data ($p < 0.01$) [35]. Indents that “failed,” either due to an optimization or testing anomaly, were rejected and replaced with a interpolated value based on one-dimensional piece-wise cubic interpolation. Material elastic fraction was evaluated using the ratio of steady-state and instantaneous moduli [36]. Modulus disparities due to the joining of the dissimilar mineralized and unmineralized zones were assessed using the slope of the elastic moduli across the tidemark. Due to the variability of zonal constituents and shortcoming of using a basic light microscope to select indentation points, a custom written MATLAB script determined the optimal points to include in slope determination. The processing algorithm optimized indentation locations to determine best linear fit for points within 100 μm of TM. Remaining points not included in the slope fitting process were grouped into hard tissue and soft tissue and averaged accordingly. Material parameters were compared using a two-factor ANOVA (attachment site, indent location). Explicit differences were elucidated post-hoc using Tukey’s method ($p < 0.01$). Modulus disparities were compared between the anterior and posterior for each meniscus using paired t-tests ($p < 0.05$).

4.4 Results

4.4.1 Collagen Fiber Orientation

Structural analysis revealed the presence of interwoven fibers throughout the insertion sites (Figure 3). These fibers, not atypical of FC entheses [17], were ignored by removing angles greater than 90° . This effectively removed skewing of the mean for the primary fiber direction due to the woven fibers. The angular cutoff was determined by examining the resultant histograms generated from this analysis. Removing these fibers and determining the primary mean fiber angle direction revealed significant differences between attachments. The collagen

fibers of the medial anterior attachment inserts into the bone at significantly shallower angles than the posterior, relative to the tidemark, throughout the entire interface (Figure 4-3). In the lateral attachment sites this was only true for the SUFC region. Fiber dispersion was significantly different within and between attachment sites. Specifically, the medial anterior attachment site significantly increased in dispersion between the SUFC and SCFC. Additionally, the medial anterior site was significantly more disperse than the posterior in the SCFC region (Figure 4-4).

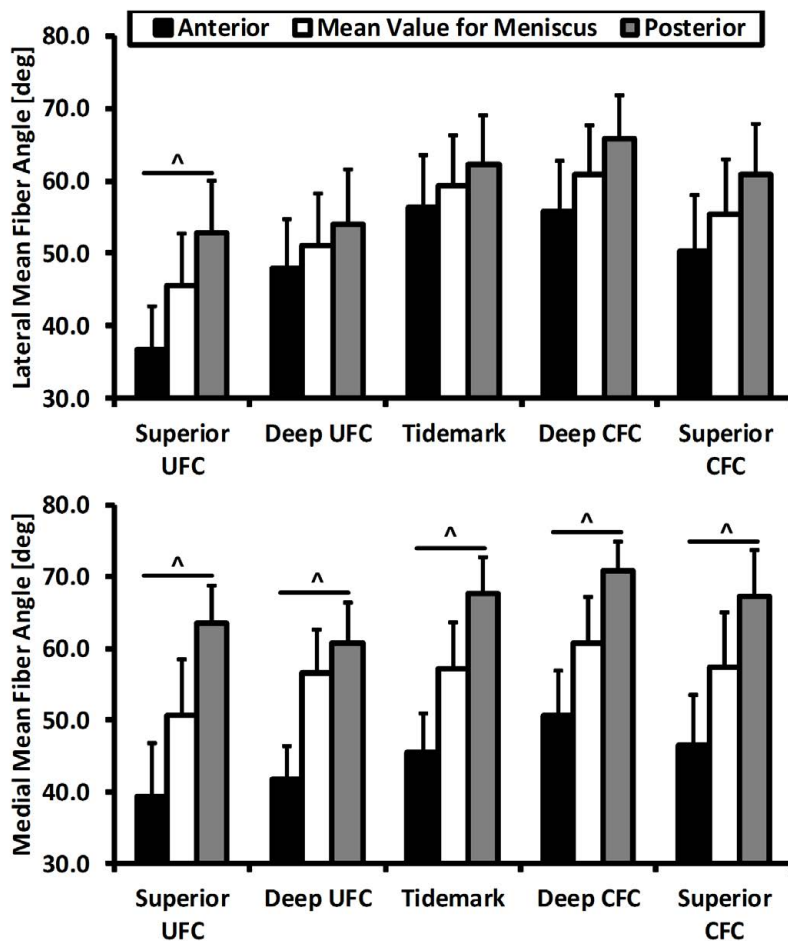


Figure 4-3: Mean collagen fiber orientation through the meniscal insertions. The medial attachment sites were significantly different from one another throughout the entire interface. The lateral attachment sites fiber angle was only significantly different in the superior uncalcified fibrocartilage zone. Mean \pm standard error. (^ - $p < 0.01$)

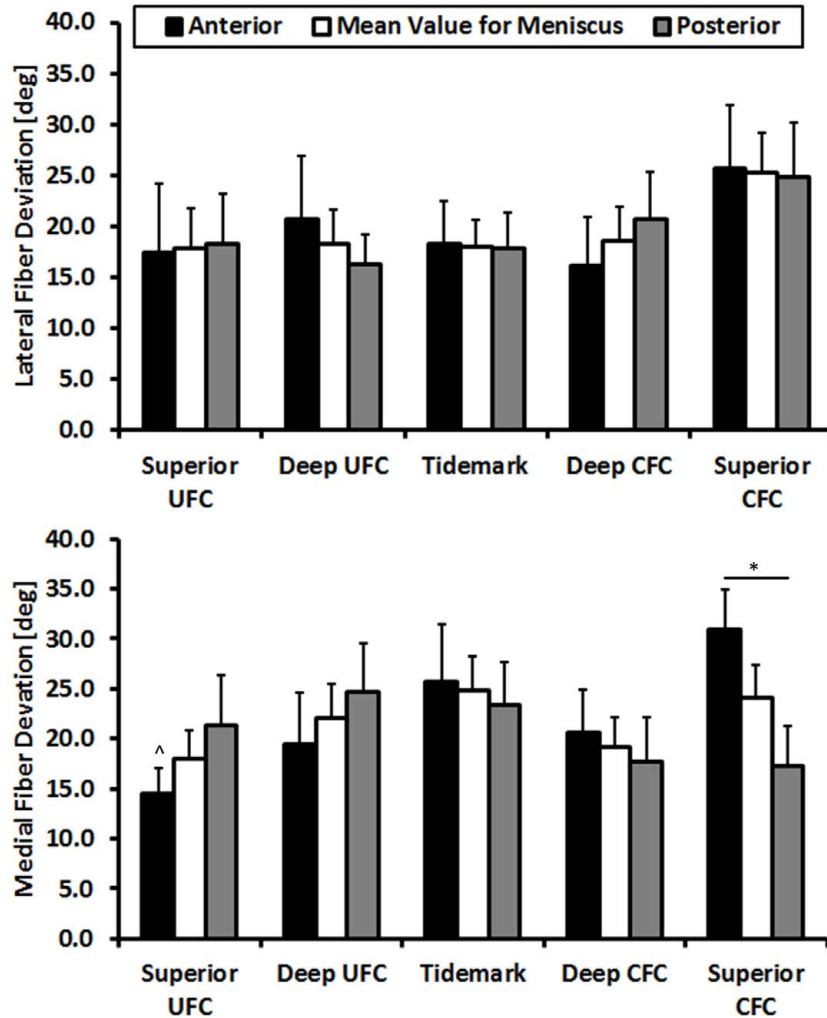


Figure 4-4: Collagen fiber deviation through the meniscal insertions. Medial anterior fiber dispersion significantly increased from the superior uncalcified fibrocartilage to the superior calcified fibrocartilage. Fiber dispersion was significantly greater in the medial anterior superior calcified fibrocartilage region than the medial posterior. Mean \pm standard error (^ - s.d. from medial anterior SCFC $p < 0.01$, * - $p < 0.05$)

4.4.2 Interdigitation Analysis

Interdigitation size was found to be significantly different in the medial compartment, with the posterior being significantly larger than the anterior (Figure 4-5). No significant differences were identified in the lateral compartment, or between compartments. The average frequency of interdigitations was found to be approximately 15.4 interdigitations per millimeter for both menisci. There was a significant difference between the anterior and posterior in the lateral compartment, however the medial appeared to be similar between attachment regions (Figure 4-

5). The most dominant frequency is a low interdigitation oscillation of approximately 3-3.5 interdigitations per millimeter (Figure 4-5). The highest frequency observed varied between sites, however there was no identified significant difference between attachment or meniscus ($p < 0.05$).

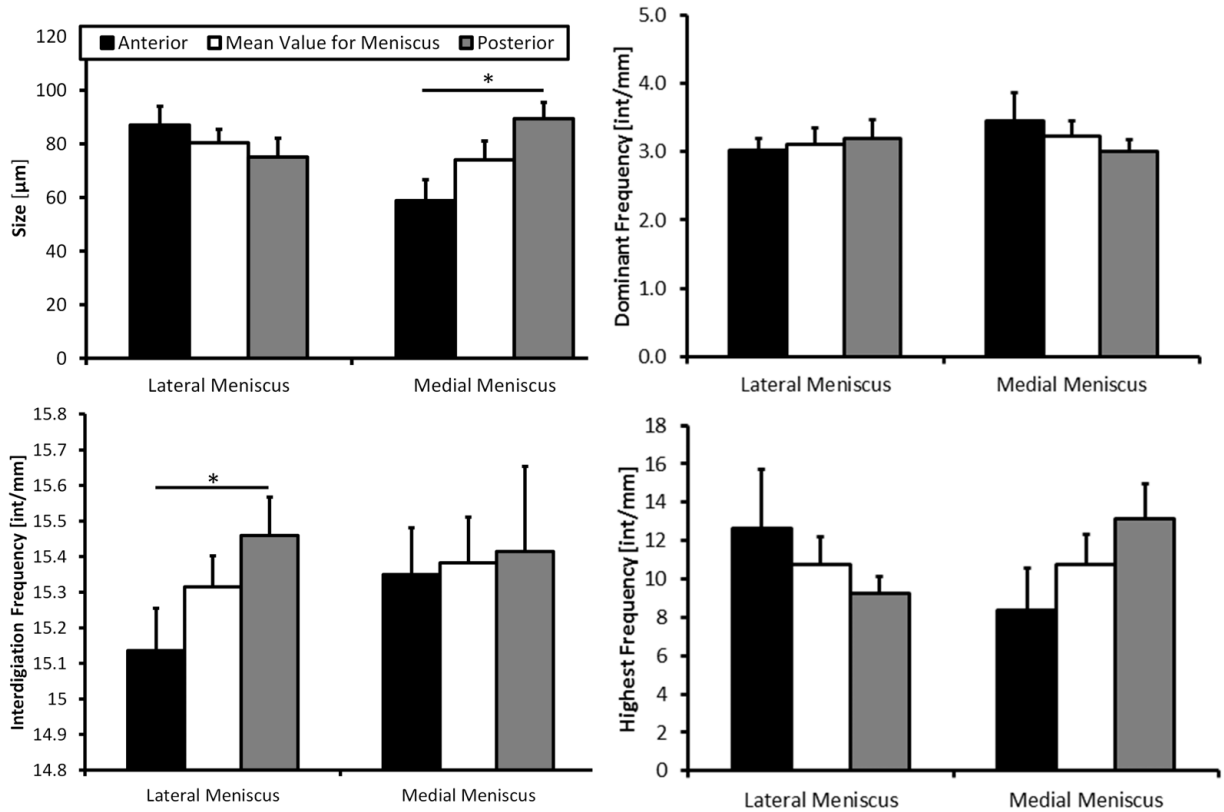


Figure 4-5: Interdigitation geometry. The medial posterior was significantly larger than the anterior. Average interdigitation frequency was significantly higher in the lateral posterior than the lateral anterior. Determination of most dominant and highest frequencies did not yield any significant differences between attachment sites. Mean \pm standard error. ($^{\wedge}$ - $p < 0.01$)

4.4.3 Nano-Indentation

Mechanical evaluation of the insertions using nano-indentation elucidated that the medial posterior attachment is significantly more compliant for both instantaneous and steady-state behavior (Figure 4-6A&B). While there was an apparent difference in elastic fraction between soft and hard tissue, particularly towards the LI portion of the insertion, this behavior was consistent among attachments (Figure 4-6C). Instantaneous elastic modulus disparities were

significantly different between the medial meniscus attachments, with the posterior having the lowest disparity between the soft and hard tissue (Figure 4-7). No significant differences were identified in the lateral meniscus. The mean fiber angle appeared to be inversely correlated with the slope of the instantaneous modulus ($R^2=0.9505$); however this was inferiorly correlated for steady-state behavior ($R^2=0.8569$) (Figure 4-8).

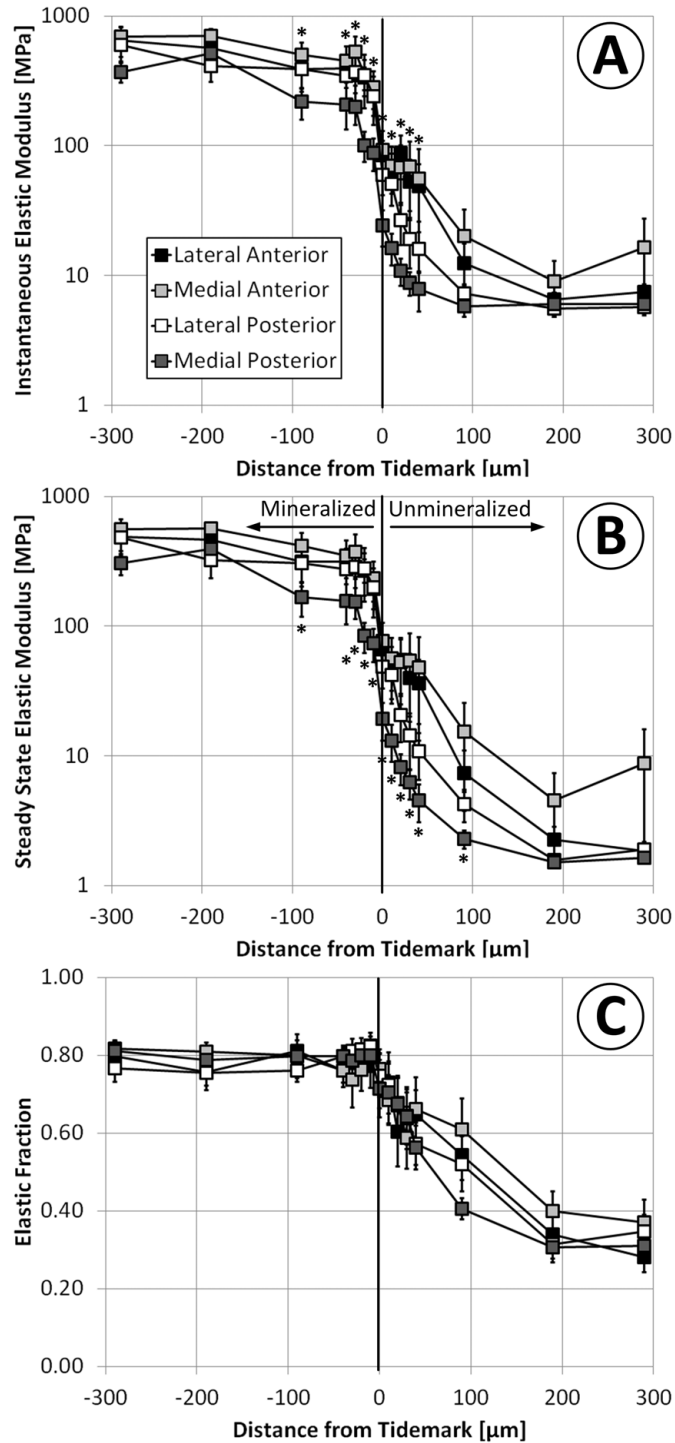


Figure 4-6: Mechanical properties of the meniscal insertions determined using nano-indentation. X-axis represents distance from the tidemark with positive values towards the ligamentous region and negative towards the subchondral bone. A) Instantaneous elastic modulus of the four attachment sites. Medial posterior was significantly more compliant than all other insertions, particularly in the fibrocartilage regions. B) Steady-state elastic modulus of the four attachment sites. Medial posterior was significantly more compliant than all other insertions, specifically in the fibrocartilage regions. C) Elastic fraction of the attachment sites. Mineralized regions were more elastic while unmineralized were more viscous. There were no significant differences for elastic fraction between insertions. Mean \pm standard error. (* - $p < 0.05$)

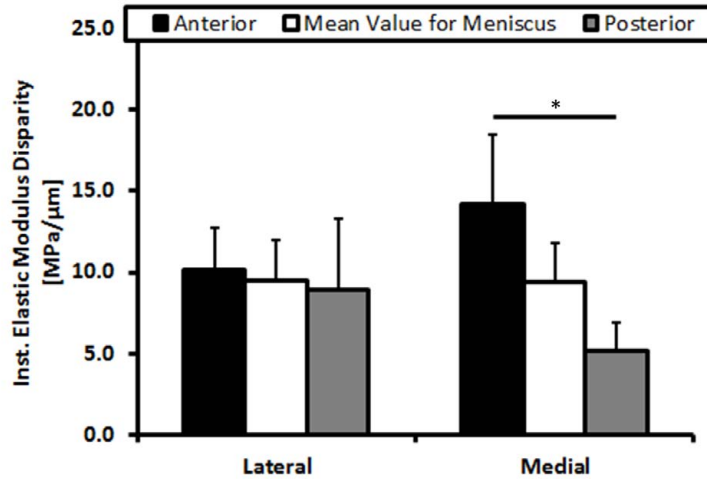


Figure 4-7: Modulus disparity at each meniscal attachment site as determined by the slope of the instantaneous elastic modulus. The medial anterior and posterior insertions were significantly different from one another. Mean \pm standard error. (* - $p < 0.05$)

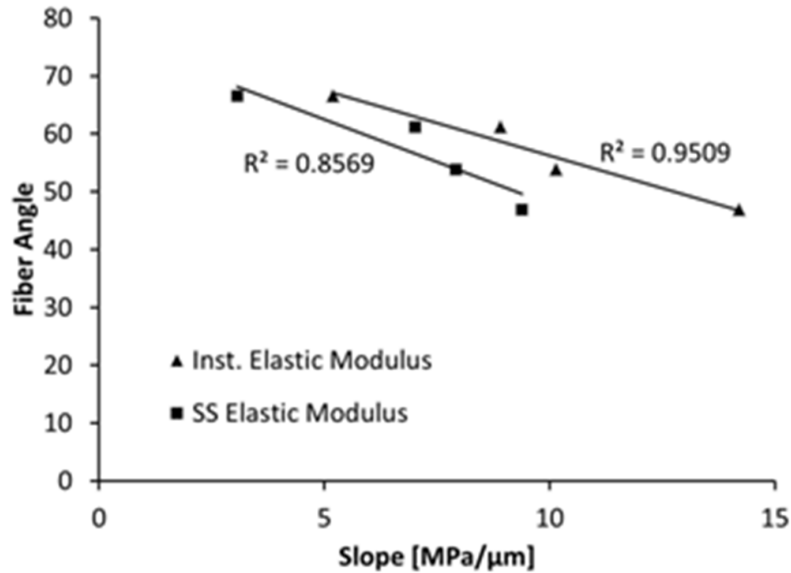


Figure 4-8: Linear correlation between the modulus disparity and the mean fiber angle across the tidemark.

4.5 Discussion

This research documents for the first time the quantitative differences in structure and function within and between the human meniscal attachment sites. Our results agreed with the hypothesis that the anterior attachment sites would have a more acute insertion angle and be mechanically superior to the posterior.

Meniscus mobility may shape fiber insertion angle as MRI investigation of meniscus translation during deep knee flexion has shown that the anterior horns undergo significantly greater translation than the posterior and remain flatter to the tibial plateau [37]. Accordingly, posterior fiber insertion angles were found to be more direct, with respect to the tidemark, potentially indicative of the limited displacement during knee flexion. Contrary to findings in tendon enthesis, fiber angle dispersion of the meniscal attachments was rarely significantly different between the zones examined here [26]. However, the regions examined here were smaller than that quantified in the aforementioned study which focused on the supraspinatus of a rat. Previous qualitative examination of the ligamentous region of the meniscal attachments does reveal a highly aligned network [14] which would suggest a similar transition from highly to a more disperse collagen fibril network. This structural organization is thought to be a mechanical adaptation to attenuating different modes of loading that the insertion site is subjected to [17, 21, 26, 38]. Notably, overall fiber deviation of the meniscal attachments appears more disperse than the tendon enthesis perhaps indicating different loading mechanisms between passive and active force transmitters.

To encapsulate the high degree of compositional variability at the interface, nano-indentation techniques were used to facilitate direct mechanical testing. Additionally, for data analysis the typical goodness of fit metric R^2 was not utilized as it can be misleading in the context of multi-parameter non-linear least squares optimization. Results here agreed with previous biomechanical evaluation on the macro- and nano-scale of meniscal attachments that the anterior attachment sites are significantly stronger than the posterior [24, 30]. This work expounded on

the previous nano-scale study by comparing each attachment site individually and identifying that the medial posterior is weakest. Comparing these results with tensile data that examined the strain distribution between the bone and meniscus shows a similar trend for data acquired at the middle of the bony insertion [24]. The anterior attachments appear to be stiffer than the posterior and explicitly the medial posterior, again, appears to be more compliant. Within the attachment sites nano-indentation demonstrated an increasing amount of material time-dependency when transition from the calcified regions to the uncalcified regions. This is to be expected as the response of the soft-tissue is heavily influenced by the presence hydrophilic proteoglycans [41].

As structure can directly, though not solely, influence function the relative fiber angle was shown to be inversely correlated with relative change in modulus across the TM. More direct insertion angles appear to result in lower stress concentrations, indicated by a lower elastic modulus slope. Additionally, increased fiber organization has been shown to improve tensile mechanics for various biological tissues [26, 42, 43]. Increased interwoven fibers may enhance the compressive mechanical properties for the meniscal attachments. This effect is analogous to woven fiber composites that are reduced in compressive strength when fibers are clustered together [44]. The high fiber dispersion in the anterior sites, particularly the medial anterior may be an adaptation to the high compressive forces generated during load due to the more acute insertion angle [16, 17]. This is similar to the randomly oriented network of collagen fibers at the surface of articular cartilage [45]. It must be recognized, however, that other constituents play an important role in dictating biomechanical performance of entheses aside from collagen fiber orientation, including but not limited to: fiber cross-linking, mineralization, and proteoglycans [38, 46]. Continued evaluation and comparison of various insertion tissue mechanics using nano- and micro-scale

testing would aid in elucidating how the various structural and compositional variants lend to specific enthesis efficacy.

Interdigitation size data trends closely resemble the findings of Benjamin et. al. when examining total cortical calcified tissue thickness (defined as the calcified fibrocartilage and lamellar bone layer until the trabeculae) [18]. Likely, cortical thickness has been dictated by the unique mechanical demands of each attachment site and, along with interdigitated interfacing with CFC, lends to overall enthesis functionality. Interdigitation size reported by Villegas et al., however, are much larger (up to an order of magnitude) than data presented here, however, investigation was performed on bovine tissue, which possess much larger menisci and attachment sites [19]. Interestingly, the medial posterior and lateral anterior appear to have the most “jagged” interdigitations, as exhibited by the high frequency. In the particular case of the medial posterior this may be an adaptation to increase adjoining surface area between the mineralized fibrocartilage and subchondral bone in order to sustain the potentially high degree of loading at this site.

These results are clinically relevant due to the higher prevalence of medial posterior horn and root injuries [39, 40, 47, 48], which coincides with the nano-indentation result indicating a more compliant attachment site. In radial tearing of the medial posterior horn it is hypothesized that deep flexion leads to compartmental impingement and subsequent tear initiation [37, 47], which may be exacerbated by the mobility of the attachment site. In traumatic tearing or root avulsion the insertion may fail to cope with pathological loading as readily as the remaining meniscal attachments.

Evaluation of the meniscal attachments provides the unique opportunity to examine four similar, yet distinct, entheses as compared to other soft tissue to bone insertions. The attachment sites were shown to be both structurally and functionally unique as well as heterogeneous when transitioning from the meniscal body into the subchondral bone. Their inherent differences are most likely attributed to the particular mechanical environment sustained during loading and will need to be considered when developing future repair and replacement strategies.

4.6 References

1. McGonagle D, Tan AL, Carey J, Benjamin M. The anatomical basis for a novel classification of osteoarthritis and allied disorders. *J Anat* 2010;216:279–291.
2. Fairbank J. Knee joint changes after meniscectomy. *J Bone Joint Surg Br* 1948;30-B:664–670.
3. Magnussen RA, Mansour AA, Carey JL, Spindler KP. Meniscus status at anterior cruciate ligament reconstruction associated with radiographic signs of osteoarthritis at 5- to 10-year follow-up: a systematic review. *J Knee Surg* 2009;22:347–357.
4. Brucker PU, von Campe A, Meyer DC, Arbab D, Stanek L, Koch PP. Clinical and radiological results 21 years following successful, isolated, open meniscal repair in stable knee joints. *Knee* 2011;18:396–401.
5. Tengrootenhuysen M, Meermans G, Pittoors K, van Riet R, Victor J. Long-term outcome after meniscal repair. *Knee Surg Sports Traumatol Arthrosc* 2011;19:236–241.
6. Englund M, Guermazi A, Lohmander LS. The meniscus in knee osteoarthritis. *Rheum Dis Clin North Am* 2009;35:579–590.
7. Haut Donahue TL, Hull ML, Rashid MM, Jacobs CR. How the stiffness of meniscal attachments and meniscal material properties affect tibio-femoral contact pressure computed using a validated finite element model of the human knee joint. *J Biomech* 2003;36:19–34.
8. Setton LA, Guilak F, Hsu EW, Vail TP. Biomechanical factors in tissue engineered meniscal repair. *Clin Orthop* 1999;367:S254–S272.
9. Yao J, Funkenbusch PD, Snibbe J, Maloney M, Lerner AL. Sensitivities of medial meniscal motion and deformation to material properties of articular cartilage, meniscus and meniscal attachments using design of experiments methods. *J Biomech Eng* 2006;128:399–408.
10. Stehling C, Souza RB, Hellio Le Graverand MP, Wyman BT, Li X, Majumdar S, Link TM. Loading of the knee during 3.0T MRI is associated with significantly increased medial meniscus extrusion in mild and moderate osteoarthritis. *Eur J Radiol* 2011;81:1839–1845.
11. Cameron HU, Macnab I. The structure of the meniscus of the human knee joint. *Clin Orthop* 1972;89:215–219.
12. Walker PS, Erkman MJ. The role of the menisci in force transmission across the knee. *Clin Orthop* 1975:184–192.

13. Petersen W, Tillmann B. Collagenous fibril texture of the human knee joint menisci. *Anat Embryol* 1998;197:317–324.
14. Villegas DF, Donahue TLH. Collagen morphology in human meniscal attachments: a SEM study. *Connect Tissue Res* 2010;51:327–336.
15. Gao J, Oqvist G, Messner K. The attachments of the rabbit medial meniscus. A morphological investigation using image analysis and immunohistochemistry. *J Anat* 1994;185:663–667.
16. Benjamin M, Toumi H, Ralphs JR, Bydder G, Best TM, Milz S. Where tendons and ligaments meet bone: attachment sites ('entheses') in relation to exercise and/or mechanical load. *J Anat* 2006;208:471–490.
17. Shaw HM, Benjamin M. Structure-function relationships of entheses in relation to mechanical load and exercise. *Scand J Med Sci Sports* 2007;17:303–315.
18. Benjamin M, Evans E, Rao R, Findlay J. Quantitative differences in the histology of the attachment zones of the meniscal horns in the knee joint of man. *J Anat* 1991;177:127–134.
19. Villegas DF, Hansen TA, Liu DF, Donahue TLH. A quantitative study of the microstructure and biochemistry of the medial meniscal horn attachments. *Ann Biomed Eng* 2008;36:123–131.
20. Gao J, Rasanen T, Persliden J, Messner K. The morphology of ligament insertions after failure at low strain velocity: an evaluation of ligament entheses in the rabbit knee. *J Anat* 1996;189:127–133.
21. Benjamin M, Ralphs JR. Fibrocartilage in tendons and ligaments--an adaptation to compressive load. *J Anat* 1998;193:481–494.
22. Evans EJ, Benjamin M, Pemberton DJ. Fibrocartilage in the attachment zones of the quadriceps tendon and patellar ligament of man. *J Anat* 1990;171:155–62.
23. Schenider H. Structure of tendon attachments. *Z Anat Entwicklungsgesch* 1956;119:431–456.
24. Hauch KN, Villegas DF, Haut Donahue TL. Geometry, time-dependent and failure properties of human meniscal attachments. *J Biomech* 2010;43:463–468.
25. Dickey JP. Measuring collagen fiber orientation: a two-dimensional quantitative macroscopic technique. *J Biomech Eng* 1998;120:537–540.

26. Thomopoulos S, Williams GR, Gimbel JA, Favata M, Soslowky LJ. Variation of biomechanical, structural, and compositional properties along the tendon to bone insertion site. *J Orthop Res* 2003;21:413–419.
27. Berens P. CircStat: a MATLAB toolbox for circular statistics. *J Stat Soft* 2009;31:1–21.
28. Ruifrok AC, Johnston DA. Quantification of histochemical staining by color deconvolution. *Anal Quant Cytol Histol* 2001;23:291–299.
29. Savitzky A, Golay MJE. Smoothing and Differentiation of Data by Simplified Least Squares Procedures. *Anal Chem* 1964;36:1627–1639.
30. Hauch KN, Oyen ML, Odegard GM, Haut Donahue TL. Nanoindentation of the insertional zones of human meniscal attachments into underlying bone. *J Mech Behav Biomed Mater* 2009;2:339–347.
31. Oyen ML. Spherical Indentation Creep Following Ramp Loading. *J Mat Res* 2005;20:2094–2100.
32. Oyen ML. Sensitivity of polymer nanoindentation creep measurements to experimental variables. *Acta Mater* 2007;55:3633–3639.
33. Rho J, Roy II M, Tsui T. Elastic properties of microstructural components of human bone tissue as measured by nanoindentation. *J Biomed Mater Res* 1999;45:48–54.
34. Hu K, Radhakrishnan P, Patel RV, Mao JJ. Regional structural and viscoelastic properties of fibrocartilage upon dynamic nanoindentation of the articular condyle. *J Struct Biol* 2001;136:46–52.
35. Morrow DA, Donahue TH, Odegard GM, Kaufman KR. A method for assessing the fit of a constitutive material model to experimental stress-strain data. *Comput Methods Biomech Biomed Eng* 2010;13:247–256.
36. Oyen ML. Nanoindentation of Biological and Biomimetic Materials. *Experimental Techniques* 2011; epub ahead of print
37. Yao J, Lancianese SL, Hovinga KR, Lee J, Lerner AL. Magnetic resonance image analysis of meniscal translation and tibio-menisco-femoral contact in deep knee flexion. *J Orthop Res* 2008;26:673–684.
38. Genin GM, Kent A, Birman V, Wopenka B, Pasteris JD, Marquez PJ, Thomopoulos S. Functional grading of mineral and collagen in the attachment of tendon to bone. *Biophys J* 2009;97:976–985.
39. Vedi V, Williams A, Tennant SJ, Spouse E, Hunt DM, Gedroyc WM. Meniscal movement. An in-vivo study using dynamic MRI. *J Bone Joint Surg Br* 1999;81:37–41.

40. Jones AO, Houang MTW, Low RS, Wood DG Medial meniscus posterior root attachment injury and degeneration: MRI findings. *Australas Radiol* 2006;50:306–313.
41. McDevitt CA. Biochemistry of articular cartilage. Nature of proteoglycans and collagen of articular cartilage and their role in ageing and in osteoarthritis. *Ann Rheum Dis* 1973;32:364–378.
42. Thomopoulos S, Marquez JP, Weinberger B, Birman V, Genin GM. Collagen fiber orientation at the tendon to bone insertion and its influence on stress concentrations. *J Biomech* 2006;39:1842–1851.
43. Lynch HA, Johannessen W, Wu JP, Jawa A, Elliott DM. Effect of Fiber Orientation and Strain Rate on the Nonlinear Uniaxial Tensile Material Properties of Tendon. *J Biomech Eng* 2003;125:726-731.
44. Basford D, Griffin P, Grove S. Relationship between mechanical performance and microstructure in composites fabricated with flow-enhancing fabrics. *Composites* 1995;26:675–679.
45. Aspden RM, Hukins DWL. Collagen Organization in Articular Cartilage, Determined by X-Ray Diffraction, and its Relationship to Tissue Function. *Proc R Soc Lond B Biol Sci* 1981;212:299–304.
46. Pins G, Christiansen D, Patel R. Self-assembly of collagen fibers. Influence of fibrillar alignment and decorin on mechanical properties. *Biophys J* 1997;73:2164–2172.
47. Bin S-I, Kim J-M, Shin S-J. Radial tears of the posterior horn of the medial meniscus. *Arthroscopy* 2004;20:373–378.
48. Costa C, Morrison W. Medial meniscus extrusion on knee MRI: is extent associated with severity of degeneration or type of tear? *Am J Radiol* 2004;183:17–23.

CHAPTER 5: DELETERIOUS EFFECTS OF OSTEOARTHRITIS ON THE STRUCTURE AND FUNCTION OF THE HUMAN MENISCAL ENTESIS

5.1 Introduction

Meniscal enteses are graded tissue interfaces that diffuse longitudinal loads transmitted via collagen fibrils which extend from the meniscus main body¹⁻⁷. The enteses must remain firmly rooted to the tibial plateau to effectively attenuate joint loads⁸⁻¹⁰. Identified enthesopathies at other tissue interfaces reveal an array of structurally degenerative mechanisms potentially jeopardizing functionality^{7,11,12}. Clinically, if a meniscal entesis is torn or avulsed excessive transverse meniscal extrusion results, thereby initiating or expediting secondary osteoarthritis development^{9,13,14}. Pathophysiology of individuals with primary osteoarthritis, however, is also inclusive of meniscal extrusion implicating progressive degeneration of intra-articular meniscus fixation¹⁴⁻¹⁶. To date there have been no investigations on the integrity of meniscal enteses in the arthritic knee.

Similar to other fibrocartilaginous enteses the meniscal enteses are compositionally graded to withstand a myriad of interfacial loading mechanisms. Primarily type I collagen fibrils, extending from the main body of the meniscus, form a ligamentous (LI) zone which sustains longitudinal tensile forces manifested by compression on the meniscus^{5,17}. These fibers then join with type II collagen fibers forming interwoven uncalcified and calcified fibrocartilage zones (UFC and CFC, respectively), separated by a tidemark (TM)^{1,6,18}. These proteoglycan rich zones withstand compression and shear generated by dynamic changes in fiber angle and avulsion

stress shielding⁷. Lastly, the CFC zone joins the subchondral bone (SB) at an interdigitated cement line^{1,6,18}. These four zones can vary in size at each meniscal enthesis site, presumably structurally adapting to their unique functional environment^{1,6,18}. Coupling mechanical and magnetic resonance imaging studies typifies this as the posterior sites, known to translate more during flexion, are significantly more compliant than the anterior sites¹⁹⁻²¹.

Examination of joint and enthesis degeneration identifies various stimuli that may influence insertion mechanics. Regulation of inflammatory and anabolic cytokines can have detrimental effects on ECM integrity. In the OA joint increased production of aggrecanase, resulting in proteoglycan cleavage, and matrix metalloproteinase-13, causing irreversible degeneration of type II collagen, erodes the structural and mechanical efficacy of articular cartilage. The osteochondral interface also exhibits demonstrable changes in mineralization state and integrity, dependent upon disease progression^{22,23}. Similarly, ligament and tendon pathophysiology at various insertion sites in the body exhibit ECM disruption, TM breakdown, micro fissures, and osteophyte formation which impact structural organization and functionality⁷. Assimilating these findings gives rise to the supposition that the meniscus to bone interface is a potential disease forming pathway, possibly preceding or catalyzing other harbingers of degradation.

In this study we examined each meniscal enthesis for changes in histomorphometry, mineralization, and mechanical properties. Our hypotheses were osteoarthritic entheses would exhibit similar deleterious effects that are observed in tissue interfaces in other articulating joints. These pathogeneses include breakdown of the TM, clefts and micro-fissures, osteophyte formation, calcium deposition and increased GAG content in the soft tissue, and changes in

mineralization. These changes would then result in degeneration of the viscoelastic properties of the entheses, thereby contributing to meniscal extrusion.

5.2 Methods

5.2.1 Sample preparation

Healthy tissue ($n=8$, ages 41-61, average: 55) was obtained from the Mayo Clinic tissue donor program. Selection was based on fluoroscopic evaluation and visual inspection by an orthopaedic surgeon for no apparent signs of degeneration. End-stage osteoarthritic tissue ($n=7$) was obtained from patients undergoing total knee arthroplasty. All samples were obtained with institutional review board approval. All meniscal entheses (medial anterior (MA), lateral anterior (LA), medial posterior (LP), and lateral posterior (LP)) were excised and bisected along the main fiber axis. Adaxial sections, used for histomorphometry, were fixed in 10% neutral buffered formalin, serially dehydrated in ethanol, defatted in xylene and then embedded in methyl methacrylate (Technovit 9100 New, Heraeus Kulzer GmbH, Wehrheim, Germany). Abaxial sections, used for micro-computed tomography (μ CT) and indentation, were embedded in a high viscosity acrylic resin (ClaroCit, Struers Inc., Cleveland, OH) that did not penetrate the specimen, wrapped in phosphate buffered saline soaked gauze and stored at -20°C .

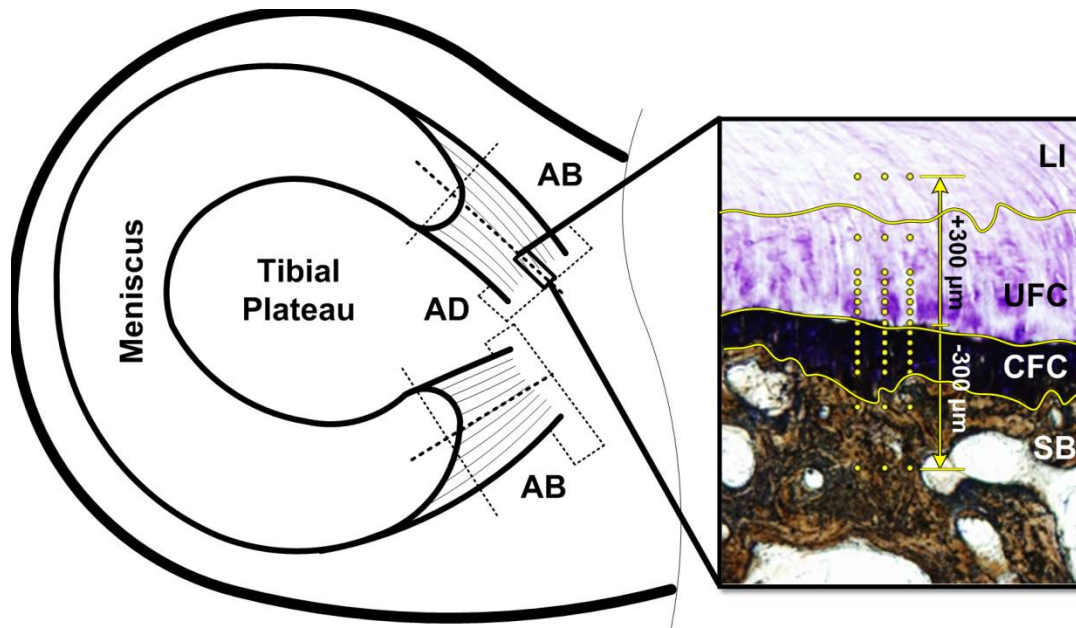


Figure 5-1: Schematic of sample location. Adaxial (AD) sections used for histomorphometry. Abxial (AB) sections used for indentation and μ CT. Inset – Meniscal enthesis stained with toluidine blue/Von Kossa to highlight the four unique regions: ligamentous (LI), uncalcified fibrocartilage (UFC), calcified fibrocartilage (CFC), and subchondral bone (SB). Yellow lines highlight the demarcations between zones. Yellow dots represent location of indentation test points.

5.2.2 Histomorphometry

Histological sections (30 μ m thick) were made using standard cutting and grinding techniques. Samples were stained with toluidine blue (TB) to identify GAGs and then counterstained using the Von Kossa (VK) technique for calcium. Changes in GAG presence in the insertion zones were quantified using Bioquant software (Bioquant Osteo 12.5, Bioquant Image Analysis Corporation, Nashville, TN) to identify the thickness of the TB stained and the TB+VK stained regions. Each region was outlined and measurements were performed at 20 μ m intervals. TM integrity was assessed quantitatively. First the TM was isolated using image processing software (Image J), converted to a binary image, and pixel locations were stored. A custom written Matlab script (version 7.14 (R2012a), Natick MA) then determined the variance of the first derivative and the mean amplitude of the peaks/valleys, estimating TM smoothness. Calcium deposition

was scored using a modified grading scale as described by Sun et al. 2010²⁴. Briefly, deposits were scored on a scale of 0-4 with 0 being no calcium and 4 being large deposits within and around the fibrous insertion. Two blind reviewers examined each section independently and results were averaged between them. A two-way ANOVA ($p < 0.05$) considering attachment health and location was used to examine differences in GAG thickness and TM smoothness. A Wilcoxon rank sum test ($p < 0.05$) was used to elucidate differences in calcium deposition between groups.

5.2.3 μ CT

The bisected insertions were scanned in saline via μ CT (Scanco μ CT 80, Scanco Medical AG, Brüttisellen, Switzerland) using the following parameters: voltage: 55 kVp, current: 114 μ A, integration time: 500 ms. A resolution of 18 μ m was obtained, yielding approximately 250 axial slices per specimen. The area of insertion was visually determined using the original specimen and multiple scanned views as reference. Tissue mineral density gradient measurements (mgHA/cm^3) across the TM were obtained using Image Processing Language (Scanco Medical AG, Brüttisellen, Switzerland). For each specimen density measurements were taken at the center of the insertion and 54 μ m above and below the center line (Figure 5-1). Three additional measurements were taken 54 μ m deeper into the initial reference plane, analogous to the tissue depth penetrated by the indenter tip (section 5.2.4). A custom Matlab script was used to identify the first peak value of density measurements which was considered to be indicative of mineralization at the TM and the values across the TM were averaged for each specimen. The thickness of the cortical shell of each insertion was determined by calculating the number of data points over which the initial density peak occurred. Multiple measurements were taken 28 μ m

apart extending up and down from the center of each insertion to avoid inadvertently taking measurements through only trabecular struts or voids. The number of measurements for each insertion varied from 6 to 18 depending on the size of the insertion. A custom Matlab script was used to average the lengths of the initial peak of density measurements to quantify the cortical thickness of each insertion. Student's t-tests ($p < 0.05$) were performed to make thickness and peak mineral density comparisons between healthy and osteoarthritic samples overall and at specific insertion sites. Additionally, the rate of increase in mineral density at the soft tissue to bone interface was examined. All data from initial until peak mineral density for each group was entered into a single sorted dataset and then fit to a sigmoidal Gompertz function such that

$$\text{Mineral Density}(x) = Ae^{Be^{Cx}}$$

where A is the upper asymptote (peak density), B is the shift along the x-axis, and C is the growth rate. This specific formulation of the generalized logistic function was selected as there is sharp increase in mineral content followed by a gradual maturation to peak mineralization.

Methodology outlined by Morrow et al. was used to check the goodness of fit wherein a student's t-test is performed with null hypothesis that the mean of the standardized variance is zero²⁵.

5.2.4 Indentation

Indentation was accomplished using a commercial nano-indenter (MTS Nanoindenter XP) with a 300 μm spherical ruby tip. Creep testing was performed using a trapezoidal loading profile with a max load of 1-, 5-, or 10-mN depending if the indentation location was in the LI, UFC or CFC, or SB zone, respectively. Each sample had forty-five test locations selected by establishing the

TM and creating three columns of fifteen rows. Column spacing was 50 μm and row spacing was 10-, 50, or 100- μm depending on the zone (Figure 5-1). Material properties were determined based on the viscoelastic analysis of Oyen^{26,27}. For the general case of creep displacement, when time t is greater than the rise time τ_R , is

$$h(t) = \left[\left(\frac{1}{a} \right) \left[C_0 \dot{P} \tau_R - \sum_{i=1}^n \left[C_i \tau_i \dot{P} e^{-t/\tau_i} \left(e^{\tau_R/\tau_i} - 1 \right) \right] \right] \right]^{\frac{1}{m}}, \text{ for } t \geq \tau_R$$

where C_i and τ_i are creep compliance coefficients and time constants, respectively. The variables a and m pertain to tip geometric factors, for the explicit case of spherical indentation with tip radius r , $a = 8\sqrt{r}/3$ and $m = 3/2$. Lastly, the term $\dot{P} = P_{max}/\tau_R$ refers to the rate of loading from the initial ramp phase. For all data $i = 2$ was found to provide a quality fit to displacement-time histories. The creep compliance coefficients were utilized to compute the instantaneous ($G_0 = 1/(2(C_0 - \sum_{i=1}^n C_i))$) and equilibrium ($G_\infty = 1/(2C_0)$) shear moduli. These properties, computed from an assumption of incompressibility were then converted to a shear modulus with a constant and compressible assumption for Poisson's ratio such that $G_{0,\infty}^v = 2G_{0,\infty}(1 - \nu)$ where $\nu = 0.3^{28-30}$. Lastly, shear modulus was converted to elastic modulus using $E_{0,\infty} = 2G_{0,\infty}^v(1 + \nu)$. All material properties were averaged across the test rows to create a mean value for each relative position. A two-way ANOVA ($p < 0.05$) considering attachment health and location was used to examine differences in moduli. Post-hoc analysis using a student's t-test determined explicit differences for each indentation location.

5.3 Results

Table 5.1: Histomorphometry results. There was a significant amount of calcium deposition in both anterior entheses. The tidemark was significantly less organized in the arthritic medial anterior enthesis. Glycosaminoglycan thickness was significantly greater in arthritic lateral anterior, medial anterior, and medial posterior entheses. * - represents significant difference ($p < 0.05$) between healthy and OA tissue for a specific enthesis. Mean ($\pm 95\%$ CI)

		Calcium Deposition	Tidemark Integrity		Glycosaminoglycan Thickness	
			Variance of 1st Derivate (μm^2)	Mean Peak Amplitude (μm)	Uncalcified Fibrocartilage (μm)	Calcified Fibrocartilage (μm)
LA	Healthy	1.03 (± 0.57)*	5.62 (± 5.46)	1.02 (± 0.28)	239.68 (± 52.44)	209.21 (± 45.16)*
	OA	2.94 (± 0.86)	14.74 (± 17.28)	1.63 (± 0.74)	577.26 (± 365.70)	371.91 (± 229.85)
LP	Healthy	0.97 (± 0.60)	8.95 (± 5.85)	1.33 (± 0.38)	745.72 (± 504.77)	182.89 (± 29.32)
	OA	2.50 (± 1.39)	20.74 (± 25.60)	1.85 (± 1.20)	809.65 (± 480.38)	264.04 (± 79.15)
MA	Healthy	1.06 (± 0.68)*	2.59 (± 1.65)*	0.88 (± 0.19)*	265.83 (± 281.53)	102.95 (± 55.25)*
	OA	2.63 (± 0.57)	17.15 (± 18.16)	1.85 (± 1.06)	1054.15 (± 755.42)	226.41 (± 69.63)
MP	Healthy	2.63 (± 0.93)	4.36 (± 2.58)	1.20 (± 0.25)	450.25 (± 417.36)	257.76 (± 61.57)*
	OA	1.63 (± 1.46)	75.09 (± 124.09)	3.19 (± 3.02)	658.87 (± 320.46)	591.12 (± 337.64)

5.3.1 Histomorphometry

GAG thickness in the UFC regions were not significantly different between healthy and OA tissue. However, there was an increase in GAG thickness in the CFC regions. Specifically, there was significantly more thickness in the LA ($p = 0.027$), MA ($p = 0.028$), and MP entheses ($p = 0.002$) (Table 5-1). TM organization was significantly reduced in osteoarthritic tissue, as evident from the appearance of repeated tidemarks, osteophytes, and micro-fissures (Figure 5-2D, E &

F). This was most apparent in MA entheses as indicated by the increase in the variance of the first derivative ($p = 0.028$) and mean peak amplitude ($p = 0.029$) (Table 5.1). Lastly, there was a significant amount of calcium deposition in both the medial ($p = 0.037$) and lateral ($p = 0.002$) anterior entheses (Table 5.1, Figure 5-2).

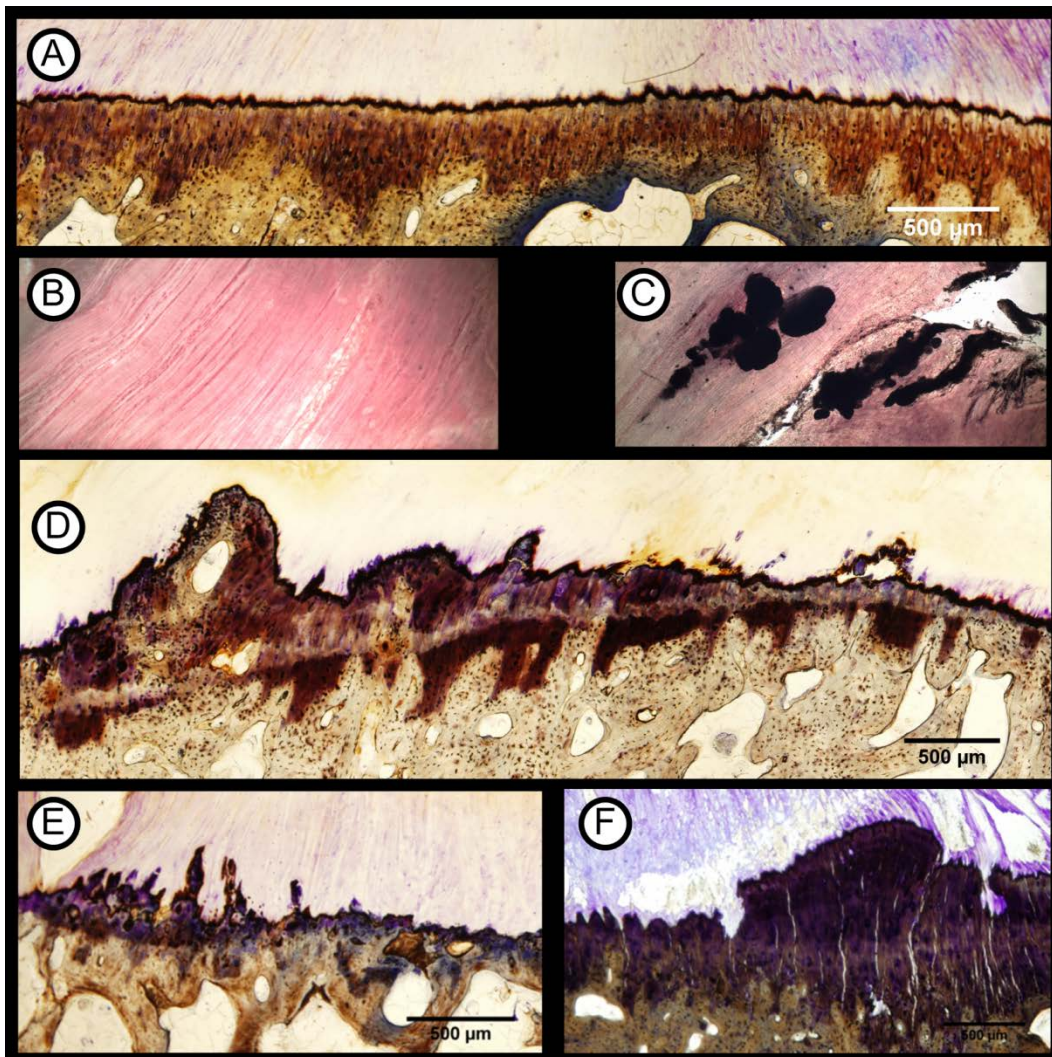


Figure 5-2: Pathophysiology in meniscal entheses due to osteoarthritis. Healthy entheses have a smooth, intact tidemark (A) and are free from calcium deposits within the ligamentous portion (B). Osteoarthritic meniscal entheses exhibited degenerative signs similar to other entheses such as calcium deposits within the ligamentous zone (C), double tidemark formation (D), osteophyte formation, and microcracks/fissuring (E).

5.3.2 μ CT

Table 5.2: μ CT results. The cortical thickness was significantly greater in arthritic medial anterior entheses. Bone mineral density decreased in arthritic lateral anterior entheses. * - represents significant difference ($p < 0.05$) between healthy and OA tissue for a specific enthesis. Mean ($\pm 95\%$ CI)

		Thickness (μm)	Bone Mineral Density (mgHA/cm^3)
LA	Healthy	404.42 (± 82.60)	1056.60 (± 15.05)
	OA	576.19 (± 140.29)	894.20 (± 181.037)
LP	Healthy	400.71 (± 74.01)*	1072.60 (± 66.86)
	OA	666.33 (± 213.31)	1076.13 (± 18.01)
MA	Healthy	295.36 (± 13.20)*	1065.53 (± 52.22)*
	OA	430.40 (± 21.43)	947.80 (± 58.88)
MP	Healthy	295.36 (± 13.20)*	1036.41 (± 42.30)
	OA	672.92 (± 97.38)	1002.45 (± 173.21)

Meniscal insertions in patients with end stage osteoarthritis had significantly thicker zones of mineralization ($586.46 \mu\text{m} \pm 82.22$) relative to healthy tissue ($367 \mu\text{m} \pm 35.49$) ($p = 0.0001$).

Bone mineral density was significantly lower for osteoarthritic samples ($980.15 \text{ mgHA}/\text{cm}^3 \pm 67.89$) compared to healthy ($1057.78 \text{ mgHA}/\text{cm}^3 \pm 21.98$) ($p = 0.044$). When comparisons were made between healthy and osteoarthritic samples at specific entheses several relative differences were found. Thickness of the mineralized zone of osteoarthritic medial anterior meniscal insertions was significantly larger relative to healthy tissue ($p = 0.0002$) (Table 5.2).

Additionally, the mineralized cortical shell of osteoarthritic insertions was significantly thicker for both lateral posterior insertions ($p = 0.041$) and medial posterior insertions ($p = 0.027$) when compared to the respective healthy samples. Bone mineral density of the lateral anterior meniscal

insertion was significantly greater in patients with end stage osteoarthritis ($p = 0.042$) (Table 5.3).

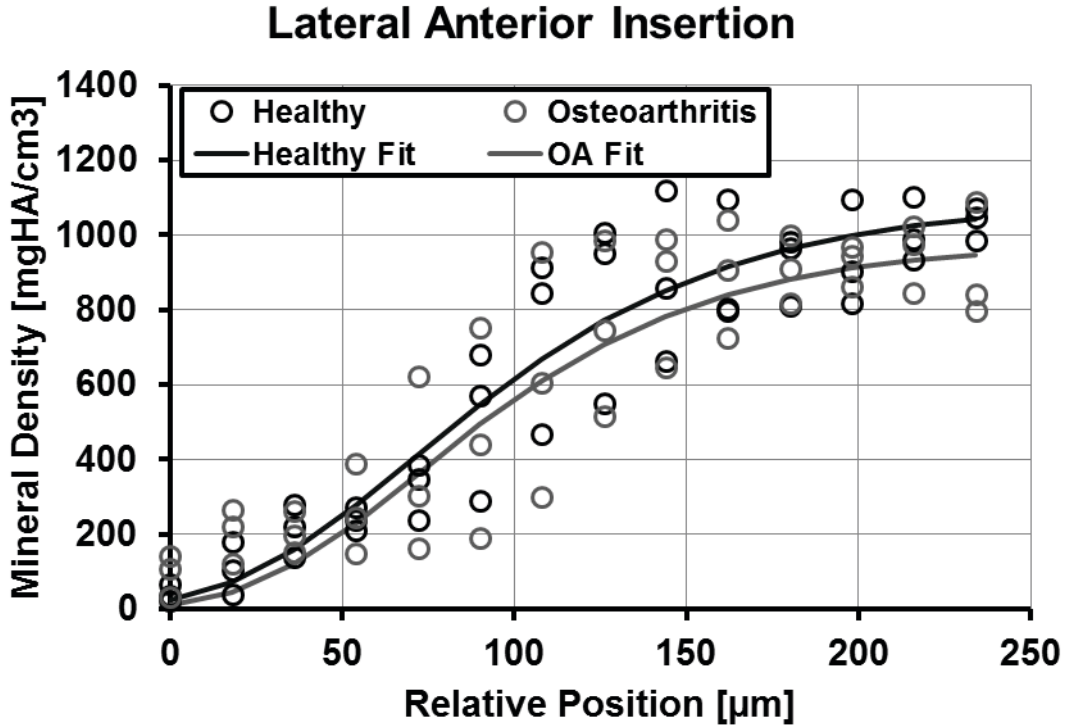


Figure 5-3: Results of fitting the sigmoidal Gompertz function to the mineral density as a function of relative position across the entheses.

The sigmoidal function used to describe mineral density as a function of position provided a good fit to the data as it failed to reject the null hypothesis that the mean of the standard variance is zero (Figure 5-3). In general, the rate of increase in mineralization was greater for arthritic tissue, as indicated by the C coefficient (Table 5.3). The medial anterior exhibited the greatest discrepancy in mineralization rate between healthy and OA tissue (Table 5.3).

Table 5.3: Fitting coefficients for sigmoidal mineral density function. A - represents the peak mineral density. B – represents a horizontal shift in the function, indicative of an initially gradual increase in mineral content. C – represents mineral density growth rate.

	Lateral Anterior		Lateral Posterior		Medial Anterior		Medial Posterior	
	Healthy	OA	Healthy	OA	Healthy	OA	Healthy	OA
A	1089.800	979.794	1118.060	1215.117	983.471	966.264	1068.378	1099.154
B	-3.827	-4.458	-5.243	-5.118	-2.264	-2.554	-4.170	-5.117
C	-0.0190	-0.0208	-0.0187	-0.0199	-0.0164	-0.0191	-0.0182	-0.0174

5.3.3 Indentation

Mechanical evaluation of viscoelastic properties of the entheses revealed a significant decrease in instantaneous and equilibrium elastic moduli in osteoarthritic tissue (Figures 5-4 & 5-5). Specifically, the lateral anterior ($p = 0.0008$) and medial anterior ($p < 0.0001$) entheses were most affected by OA. Furthermore, this degeneration appeared to be primarily localized to the fibrocartilaginous zones (Figures 5-4 & 5-5). In the lateral anterior this was solely in the mineralized tissue, wherein there was the instantaneous and equilibrium elastic modulus was decreased by half. For the medial anterior there was an even greater discrepancy as the instantaneous elastic moduli was up to three times higher in healthy tissue for both mineralized and unmineralized regions (Figure 5-4). For the equilibrium modulus the relative difference between tissues was the same, however, it was only for the mineralized tissue (Figure 5-5).

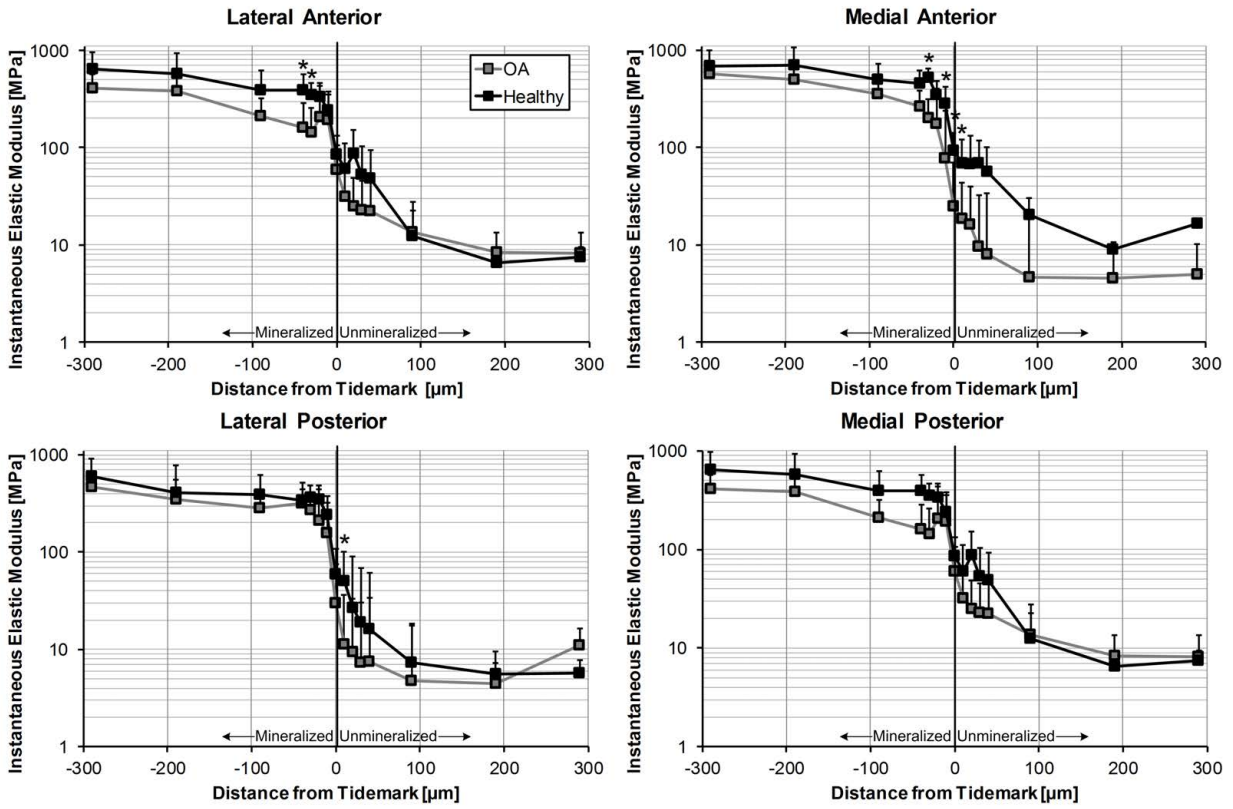


Figure 5-4: Instantaneous elastic modulus as function of relative distance from the tidemark. Several locations within the fibrocartilaginous zones were significantly more compliant in the arthritic lateral anterior, medial anterior, and medial posterior entheses. * - represents significant difference ($p < 0.05$) between healthy and OA tissue for a specific location.

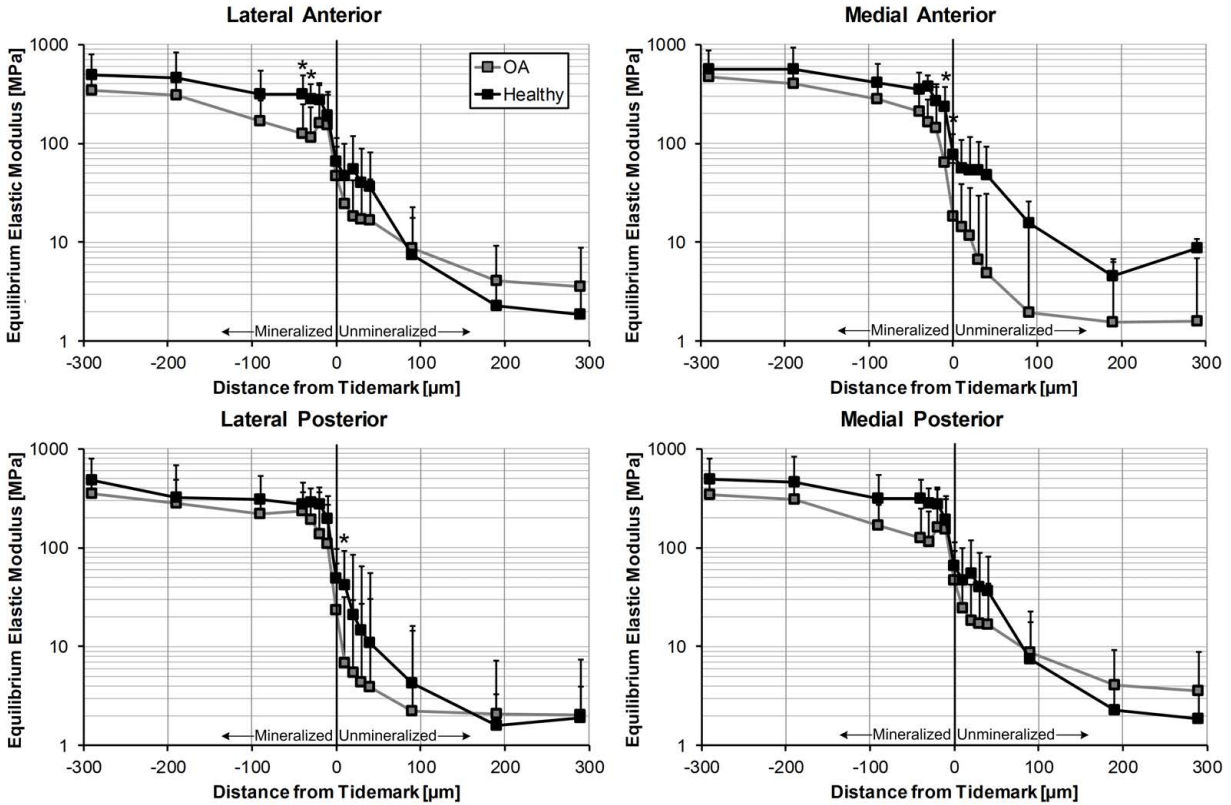


Figure 5-5: Equilibrium elastic modulus as function of relative distance from the tidemark. Several locations within the fibrocartilaginous zones were significantly more compliant in the arthritic lateral anterior, medial anterior, and medial posterior entheses. * - represents significant difference ($p < 0.05$) between healthy and OA tissue for a specific location.

5.4 Discussion

To our knowledge this is the first study to examine pathophysiology of the meniscal entheses. Qualitatively, the entheses exhibited morphological changes including, a breakdown of TM organization, double TM formation, clefts and microcracks/fissures, osteophytes, and calcium deposition within the soft-tissue, all of which disrupt functional homeostasis. Quantitatively, the arthritic tissue was found to have significant increases in GAG thickness in the mineralized fibrocartilage, cortical shell thickness, peak and growth rate of mineral density, and mechanical compliance. As there is limited data specifically on the meniscal entheses these findings must be considered in the context of other enthesopathies.

Histologic examination of patients with patellar tendinosis reveals an accrument of GAGs at the tissue interface³¹. Similarly, internal obturator tendons removed from osteoarthritic hip joints have significantly more GAGs as well as calcium deposits³². These findings implicate swelling of the enthesis that may be an adaptation to increased loading, however, this would also result in disruption of the fibrous matrix and effective load transmission. Calcium deposition also plays an integral role in OA pathology as mineral aggregation has been shown in the articular cartilage, meniscus, and synovial fluid^{24,32,33}. In our study, calcium deposits were observed within the ligamentous zone, potentially disrupting fiber organization and undermining mechanical efficacy. The presence of such deposits is also linked with stimulation of inflammatory and catabolic responses in articular cartilage, thereby contributing to intrinsic degradation³³.

Tidemark integrity is also thought to be crucial for maintaining enthesis functionality³⁴⁻³⁶. Previous evaluation of TM integrity has remained strictly qualitative; however, the metrics introduced here facilitated quantitative comparisons between healthy and arthritic tissue at each enthesis. In general, OA entheses exhibited higher variance and mean amplitude, suggesting a less organized TM. Specifically, the MA had a significantly greater amount of disorganization, potentially leading to detrimental bone formation extending into the soft-tissue including to osteophyte formation^{11,12}. These enthesophytes, distinct from the calcium deposits, commonly appear in the Achilles tendon in athletes, however, their direct ramifications are unclear as patients can be asymptomatic⁷. In articular cartilage, osteophyte detection is associated with disruption of the adjacent articulating surfaces thereby exacerbating adverse joint mechanics³⁷.

Frequently, changes in the TM and osteophyte detection are indicative of accompanying bone related OA pathogenesis including thickening of the periarticular bone²³. The μ CT analyses performed reveals similar changes in the cortical shell, inclusive of both the calcified fibrocartilage and the subchondral bone. Particularly, the medial anterior entheses and the medial and lateral posterior entheses demonstrated a significant increase in thickness of the cortical shell. This increase in thickness may occur as a result of increased stresses in the region due to load bearing and a decrease in overall bone mass³⁸. Changes in cortical thickness have been known to alter cartilage mechanics and may similarly and cortical shell thickening may similarly result in altered mechanics of the entheses²³. It is difficult to assess whether or not the progression of OA results in ultimate thickening of the cortical shell because the initiation point of disease in the tested specimens is unknown. It has been suggested that if OA was initiated as a result of trauma the cortical thickening may be a response of the enthesis to meniscal damage³⁹. Furthermore, thickening of the cortical shell occurs simultaneously with a decrease in average bone mineral density⁴⁰. Overall bone mineral density has been shown to decrease as the rate of bone remodeling increases leading to incomplete mineralization³⁷. Similarly, there was a significant decrease in mineral density in osteoarthritic samples, specifically the medial anterior.

The gradation of mineral content when traversing the TM is of particular interest as it has been shown to influence entheses mechanics^{41,42}. Existing literature suggests a linear increase in mineral content; however, this would appear an oversimplification as the mineralization appears nonlinear during its growth and asymptotic at its extremes⁴². We instead chose a sigmoidal function that could account for no mineralization in the soft-tissue and the nonlinear growth and gradual maturation of mineral density once deep enough into the calcified tissue. There are

apparent differences in fitting coefficients between attachment sites and healthy and OA tissue. The B & C coefficients of the sigmoidal function are indicative of a more gradual start to mineralization and progressive increase in mineral density, respectively. Between healthy attachment sites it is evident that the MA enthesis begins to mineralize sooner however the rate of mineralization is more gradual across the interface. The early initial mineralization of the MA enthesis may be attributable to the thinner cortical zone of the insertion^{1,6}. OA appears to slightly increase the rate of mineralization across the interface, particularly in the MA enthesis. This could have profound effects on stress dissipation across the enthesis as, above a particular percolation threshold, mineralization dictates fiber stiffening⁴¹.

To examine if the morphological and mineralization structural pathologies influence enthesis functionality, a nanoindenter was used to map the viscoelastic material properties across the interface. This modality facilitated testing physiologically relevant loading mechanisms as the FC zones are believed to be predominantly subjected to compression and shearing in that they serve as a stretching-brake¹¹. Therefore it is likely imperative to preserve FC functionality in order to maintain meniscus mechanics. Importantly, the OA entheses were significantly more compliant than healthy. As stated prior, changes in bone remodeling and mineralization dictate mechanics. Additionally, degeneration of hydrophilic GAG content results in a loss of resistance to compression. With the various changes exhibited it follows that there would be a demonstrable change in material properties. These changes were observed primarily in both the calcified and uncalcified fibrocartilage regions. Importantly, these zones are known to be comprised of primarily type II collagen which is severely and irreversibly degraded in early and

late stage OA due to an increase in matrix metalloproteinase-13^{18,43}. Additionally, the lower bone mineral density in the medial anterior entheses correlates with the increased compliance.

An important consideration of this study is the use of end-stage OA tissue. While this most likely provided the most contrast with healthy tissue, the stage at which initial entheses breakdown occurred remains unknown. However, in this initial examination of meniscal entheses it is apparent there are deleterious modifications to their structure and function which may be detrimental to meniscus performance. In particular, the medial anterior entheses repeatedly exhibited signs of degeneration using several independent metrics. This presents an intriguing pattern as current literature places an emphasis on the medial posterior entheses due to the clinical incidence of failure⁹. The work presented here, however, implicates occult changes in entheses functionality. Continued examination of the meniscal entheses and their role in OA pathogenesis may provide new opportunities for arresting OA propagation.

5.5 References

1. Benjamin, M., Evans, E., Rao, R. & Findlay, J. Quantitative differences in the histology of the attachment zones of the meniscal horns in the knee joint of man. *Journal of Anatomy* **177**, 127–134 (1991).
2. Makris, E. a, Hadidi, P. & Athanasiou, K. a The knee meniscus: structure-function, pathophysiology, current repair techniques, and prospects for regeneration. *Biomaterials* **32**, 7411–31 (2011).
3. Messner, K. & Gao, J. The menisci of the knee joint. Anatomical and functional characteristics, and a rationale for clinical treatment. *Journal of anatomy* **193** (Pt 2, 161–78 (1998).
4. Setton, L. a, Guilak, F., Hsu, E. W. & Vail, T. P. Biomechanical factors in tissue engineered meniscal repair. *Clinical orthopaedics and related research* S254–72 (1999).
5. Villegas, D. F. & Donahue, T. L. H. Collagen morphology in human meniscal attachments: a SEM study. *Connective tissue research* **51**, 327–36 (2010).
6. Villegas, D. F., Hansen, T. A., Liu, D. F. & Donahue, T. L. H. A quantitative study of the microstructure and biochemistry of the medial meniscal horn attachments. *Annals of biomedical engineering* **36**, 123–31 (2008).
7. Shaw, H. M. & Benjamin, M. Structure-function relationships of entheses in relation to mechanical load and exercise. *Scandinavian journal of medicine & science in sports* **17**, 303–15 (2007).
8. Haut Donahue, T. L., Hull, M. L., Rashid, M. M. & Jacobs, C. R. How the stiffness of meniscal attachments and meniscal material properties affect tibio-femoral contact pressure computed using a validated finite element model of the human knee joint. *Journal of Biomechanics* **36**, 19–34 (2003).
9. Jones, A. O., Houang, M. T. W., Low, R. S. & Wood, D. G. Medial meniscus posterior root attachment injury and degeneration: MRI findings. *Australasian radiology* **50**, 306–13 (2006).
10. Yao, J., Funkenbusch, P. D., Snibbe, J., Maloney, M. & Lerner, A. L. Sensitivities of medial meniscal motion and deformation to material properties of articular cartilage, meniscus and meniscal attachments using design of experiments methods. *Journal of biomechanical engineering* **128**, 399–408 (2006).
11. Benjamin, M. *et al.* Where tendons and ligaments meet bone: attachment sites ('entheses') in relation to exercise and/or mechanical load. *Journal of anatomy* **208**, 471–90 (2006).

12. Rufai, A., Ralphs, J. R. & Benjamin, M. Structure and histopathology of the insertional region of the human Achilles tendon. *Journal of orthopaedic research : official publication of the Orthopaedic Research Society* **13**, 585–93 (1995).
13. Berthiaume, M.-J. *et al.* Meniscal tear and extrusion are strongly associated with progression of symptomatic knee osteoarthritis as assessed by quantitative magnetic resonance imaging. *Annals of the rheumatic diseases* **64**, 556–63 (2005).
14. Costa, C. & Morrison, W. Medial meniscus extrusion on knee MRI: is extent associated with severity of degeneration or type of tear? *American Journal of* **183**, 17–23 (2004).
15. Stehling, C. *et al.* Loading of the knee during 3.0T MRI is associated with significantly increased medial meniscus extrusion in mild and moderate osteoarthritis. *European journal of radiology* (2011).
16. Adams, J., McAlindon, T., Dimasi, M., Carey, J. & Eustace, S. Contribution of meniscal extrusion and cartilage loss to joint space narrowing in osteoarthritis. *Clinical Radiology* **54**, 502–506 (1999).
17. Petersen, W. & Tillmann, B. Collagenous fibril texture of the human knee joint menisci. *Anatomy and embryology* **197**, 317–24 (1998).
18. Gao, J., Oqvist, G. & Messner, K. The attachments of the rabbit medial meniscus. A morphological investigation using image analysis and immunohistochemistry. *Journal of Anatomy* **185**, 663–667 (1994).
19. Abraham, A. C., Moyer, J. T., Villegas, D. F., Odegard, G. M. & Haut Donahue, T. L. Hyperelastic properties of human meniscal attachments. *Journal of biomechanics* **44**, 413–8 (2011).
20. Hauch, K. N., Villegas, D. F. & Haut Donahue, T. L. Geometry, time-dependent and failure properties of human meniscal attachments. *Journal of biomechanics* **43**, 463–8 (2010).
21. Yao, J., Lancianese, S. L., Hovinga, K. R., Lee, J. & Lerner, A. L. Magnetic resonance image analysis of meniscal translation and tibio-menisco-femoral contact in deep knee flexion. *Journal of orthopaedic research : official publication of the Orthopaedic Research Society* **26**, 673–84 (2008).
22. Goldring, S. R. Role of Bone in Osteoarthritis Pathogenesis. *Osteoarthritis* **93**, 25–35 (2009).
23. Goldring, M. B. & Goldring, S. R. Articular cartilage and subchondral bone in the pathogenesis of osteoarthritis. *Annals of the New York Academy of Sciences* **1192**, 230–7 (2010).

24. Sun, Y. *et al.* Calcium deposition in osteoarthritic meniscus and meniscal cell culture. *Arthritis research & therapy* **12**, R56 (2010).
25. Morrow, D. A., Donahue, T. H., Odegard, G. M. & Kaufman, K. R. A method for assessing the fit of a constitutive material model to experimental stress-strain data. *Computer methods in biomechanics and biomedical engineering* **13**, 247–56 (2010).
26. Oyen, M. L. Spherical Indentation Creep Following Ramp Loading. *Journal of Materials Research* **20**, 2094–2100 (2005).
27. Oyen, M. L. Nanoindentation of Biological and Biomimetic Materials. *Experimental Techniques* (2011).
28. Rho, J., II, M. R. & Tsui, T. Elastic properties of microstructural components of human bone tissue as measured by nanoindentation. *Journal of biomedical* **45**, 48–54 (1999).
29. Hauch, K. N., Oyen, M. L., Odegard, G. M. & Haut Donahue, T. L. Nanoindentation of the insertional zones of human meniscal attachments into underlying bone. *Journal of the mechanical behavior of biomedical materials* **2**, 339–47 (2009).
30. Hu, K., Radhakrishnan, P., Patel, R. V. & Mao, J. J. Regional structural and viscoelastic properties of fibrocartilage upon dynamic nanoindentation of the articular condyle. *Journal of structural biology* **136**, 46–52 (2001).
31. Khan, K. M. *et al.* Patellar tendinosis (jumper’s knee): findings at histopathologic examination, US, and MR imaging. Victorian Institute of Sport Tendon Study Group. *Radiology* **200**, 821–7 (1996).
32. Meknas, K. *et al.* Could tendinosis be involved in osteoarthritis? *Scandinavian journal of medicine & science in sports* (2011).
33. Liu, Y. Z., Jackson, A. P. & Cosgrove, S. D. Contribution of calcium-containing crystals to cartilage degradation and synovial inflammation in osteoarthritis. *Osteoarthritis and cartilage / OARS, Osteoarthritis Research Society* **17**, 1333–40 (2009).
34. Kumar, P., Oka, M., Nakamura, T., Yamamuro, T. & Delecrin, J. Mechanical strength of osteochondral junction. *Nihon Seikeigeka Gakkai zasshi* **65**, 1070–7 (1991).
35. Redler, I., Mow, V. C., Zimny, M. L. & Mansell, J. The ultrastructure and biomechanical significance of the tidemark of articular cartilage. *Clinical orthopaedics and related research* 357–62 (1975).
36. Smith, L. R., Fowler-Gerace, L. H. & Lieber, R. L. Muscle extracellular matrix applies a transverse stress on fibers with axial strain. *Journal of biomechanics* **44**, 1618–20 (2011).

37. Burr, D. B. Anatomy and physiology of the mineralized tissues: role in the pathogenesis of osteoarthritis. *Osteoarthritis and cartilage / OARS, Osteoarthritis Research Society* **12 Suppl A**, S20–30 (2004).
38. Goldring, S. R. Alterations in periarticular bone and cross talk between subchondral bone and articular cartilage in osteoarthritis. *Therapeutic advances in musculoskeletal disease* **4**, 249–58 (2012).
39. Pastoureau, P., Leduc, S., Chomel, A. & De Ceuninck, F. Quantitative assessment of articular cartilage and subchondral bone histology in the meniscectomized guinea pig model of osteoarthritis. *Osteoarthritis and cartilage / OARS, Osteoarthritis Research Society* **11**, 412–23 (2003).
40. Grynblas, M. D., Alpert, B., Katz, I., Lieberman, I. & Pritzker, K. P. Subchondral bone in osteoarthritis. *Calcified tissue international* **49**, 20–6 (1991).
41. Genin, G. M. *et al.* Functional grading of mineral and collagen in the attachment of tendon to bone. *Biophysical journal* **97**, 976–85 (2009).
42. Wopenka, B., Kent, A. & Pasteris, J. The tendon-to-bone transition of the rotator cuff: a preliminary Raman spectroscopic study documenting the gradual mineralization across the insertion in rat tissue. *Appl Spectroscopy* **62**, 1285–1294 (2008).
43. Goldring, M. B. *et al.* Roles of inflammatory and anabolic cytokines in cartilage metabolism: signals and multiple effectors converge upon MMP-13 regulation in osteoarthritis. *European cells & materials* **21**, 202–20 (2011).

CHAPTER 6: CONCLUSIONS AND FUTURE WORK

This work provided an improved material model for each of the four meniscal entheses which can be leveraged to improve numerical modeling of whole joint behavior. From these efforts and knowing that the load bearing tissues of the body are mechano-responsive and identifying that the fibrous portion of the entheses are mechanically unique then led to the desire to observe relative differences between them. Employing the use of a novel pressure microsensor the relative change in internal pressure of the entheses due to physiological and pathological loading was documented. These data confirmed that there are significant differences in mechanical environment that each enthesis must endure. Furthermore, it was found that transecting the anterior cruciate ligament radically changed the internal pressure of the lateral and medial posterior sites. Thus implicating that not only are there profound changes in cartilage and meniscus loading but also in the meniscal entheses. Reaffirming that each attachment site bears a unique environment and understanding that the entire enthesis organ (from the fibrous connective tissue to the subchondral bone) can dictate meniscus mechanics necessitates examining the structure and function across the entire interface. Furthermore, documenting the native structure and function is timely as meniscal replacements are being realized via tissue engineered constructs, however, little attention is given to entheses. It may become critical to couple engineered menisci and entheses in order to truly circumvent joint degradation. Therefore, the collagen fiber orientation, the interdigitation architecture and the material properties through the attachment site were examined. Similar patterns as before were exhibited with the medial posterior being the most compliant, which corresponds to clinical findings in which this site has the highest rate of failure. Additionally, these data and evaluation metrics can

be used in future development of tissue engineered entheses. Lastly, after characterizing the native and structure and function it was then logical to observe if OA pathogenesis, which is inclusive of meniscal extrusion, has an effect on the entheses. In fact, there were several apparent effects on the attachment sites, including changes in mineralization and tissue compliance, particularly in the anterior entheses. This is a dramatic shift in focus as the literature typically focuses on the medial posterior due to its high rate of failure, but the data presented here implicates that the anterior sites may be slowly degrading over time and possibly contributing to OA propagation. Continued examination of the meniscal entheses and their role in OA pathogenesis may provide new opportunities for arresting OA propagation.

Given these findings there are several different investigations that may be undertaken in the future. First, while interdigitation architecture has been recorded, its true mechanical purpose remains unknown. From an engineering perspective this jagged interface should increase the surface area over which the force is transmitted into the subchondral bone, thereby reducing stresses. Finite element modeling techniques could be used to examine interfacial tissue with and without interdigitated fixation to determine the effect it has at a local level and then also at a more global level in a whole joint model. Second, only anterior cruciate transection and a longitudinal meniscal tear were explored using the pressure sensors; however, there remain several other clinically relevant failure mechanisms within the joint which could be investigated. Furthermore, the sensors could be used to evaluate the effect various meniscal repair strategies, in place of or in addition to the gold standard of pressure film on the articular surface. Third, possessing a thorough description of the structure and function of the native attachment sites provides a basis for designing a tissue engineered replacement that could be used for mating meniscal replacements with the tibial plateau. Lastly, knowing that entheses are involved at some

stage in OA pathogenesis it now becomes imperative to understand if this precedes other changes within the joint space. Additionally, it would be worthwhile to understand the mechanisms behind this degradation. This could be accomplished with quantitative polymerase chain reaction to examine if any catabolic cytokines are up-regulated within the entheses. This may yield an early target for arresting OA development, potentially via some targeted drug modality.

Appendix A: GOODNESS OF FIT FOR CONSTITUTIVE MODELS

Evaluation of goodness of fit can be measured using the coefficient of determination (R^2); however, this metric can be misleading in the context of non-linear data. This arises due to the process in which least-squares optimization routines attempt minimize the sum of the squares of the residuals (SS_{err} , the difference between the model and data), as demonstrated by

$$\min_b SS_{err} \Rightarrow \min_b \sum_i (y_i - X_i b)^2$$

where the columns of X_i are the number of terms in the model. Looking at the relationship between the coefficient of determination and SS_{err}

$$R^2 = 1 - \frac{SS_{tot}}{SS_{err}}$$

It is evident that decreasing SS_{err} by merely using additional terms can only improve R^2 . Therefore, it is not meaningful in the context of nonlinear data, such as the models evaluated in chapter 2.

Therefore, in accordance with Morrow et al., 2010, several metrics can be leveraged to evaluate goodness of fit for non-linear constitutive models. First, a statistical test can be performed as an initial screening of ability of the model to predict the experimental data. By assuming that the mean of the standardized variance between the model and data is 0, a hypothesis can be tested such that

$$H_0: \bar{s}_{var} = 0$$

If the test fails to reject the null hypothesis then it follows that the model is a good predictor for the data, however, it is not necessarily a truly quantitative metric when comparing between models. Only this metric was used in Chapter 2 and the resultant p -value was used to determine the best model, which could be a bit misleading.

To support the procedure used in Chapter 2 the root mean square error is also reported here in order to show a quantitative difference between the accuracy of the models.

Table A.1: Fitting coefficients and the root mean square error for each model evaluated.

	Ogden			Mooney-Rivlin			Neo-Hookean	
	μ_1	α_1	RMSE	C_1	C_2	RMSE	C_1	RMSE
MA	0.1081	3.1915	0.212	0.1904	-0.1227	0.209	0.1003	0.219
MP	0.436	4.931	0.835	2.2485	-1.9525	0.831	0.8621	0.921
LA	0.1114	6.1978	0.094	1.1192	-1.0787	0.084	0.3171	0.166
LP	0.0982	4.3606	0.09	0.3808	-0.3136	0.088	0.1389	0.089
	Average		0.307	Average		0.303	Average	0.349

It is apparent that both the Ogden and Mooney-Rivlin models outperform the Neo-Hookean, however there is little difference between them. Hence, the Mooney-Rivlin model was selected as it is computationally less expensive.

Appendix B: VISCOELASTIC FRAMEWORK FOR INDENTATION

For the indentation analyses performed in chapters 4&5 material properties were examined within the framework of Hertzian contact [Lee and Radok 1960]. Displacement-time history is described by integrating over the ramp and hold phase using an explicit creep compliance function $J(t)$ and loading profile, $P(u)$, over the entire ramp and loading phase as generalized by

$$h^n(t) = k_G \int_0^t J(t-u) \frac{dP(u)}{du} du \quad (1)$$

where n is the power law tip geometry factor ($n = 3/2$ for spherical) and k_G are geometrical constants. Assuming linear viscoelastic behavior, a Prony series is used to describe material creep where

$$J(t) = C_0 + \sum_{i=1}^k C_k \exp(-t/\tau_k) \quad (2)$$

Experimental data can then be fit to the explicit solution of the integral using (1) and (2) and assuming a constant loading rate, yielding

$$h^{3/2}(t) = A_0 - \sum_{i=1}^j A_k \exp(-t/\tau_k) \quad (3)$$

where $j = 2$ provided a quality fit to experimental data. Explicit creep function parameters are then determined using

$$C_0 = \frac{8A_0\sqrt{R}}{3P_{max}} \quad (4)$$

$$C_k = \frac{8A_k\sqrt{R}}{3P_{max}(RCF_k)} \quad (5)$$

where RCF is the ramp correction factor for creep accrued during the loading phase as described by

$$RCF_k = \frac{\tau_k}{t_R} [\exp(t_R/\tau_k) - 1] \quad (6)$$

and t_R is the length of the ramp phase. Creep compliance coefficients are then utilized to compute instantaneous, G_0 , and equilibrium shear modulus, G_∞

$$G_0 = \frac{1}{2(C_0 - \sum_{i=1}^j C_k)} \quad (7)$$

$$G_\infty = \frac{1}{2C_0} \quad (8)$$

Shear modulus computed from an assumption of incompressibility can then be converted to a shear modulus with a constant and compressible assumption for Poisson's ratio.

$$G_{0,\infty}^v = 2G_{0,\infty}(1 - \nu) \tag{9}$$

Lastly, shear modulus is converted to elastic modulus using

$$E_{0,\infty} = 2G_{0,\infty}^v(1 + \nu) \tag{10}$$

Oyen, M.L., *Nanoindentation of Biological and Biomimetic Materials. Experimental Techniques 2011; Online*

Appendix C: VISCOELASTIC TIME CONSTANTS

From the viscoelastic material model used for the indentation experiments in chapters 4 & 5 a Prony series with two time constants (τ_1 & τ_2) was found to provide a quality fit to the data. Here the time constants are reported from that process for both the healthy and osteoarthritic samples.

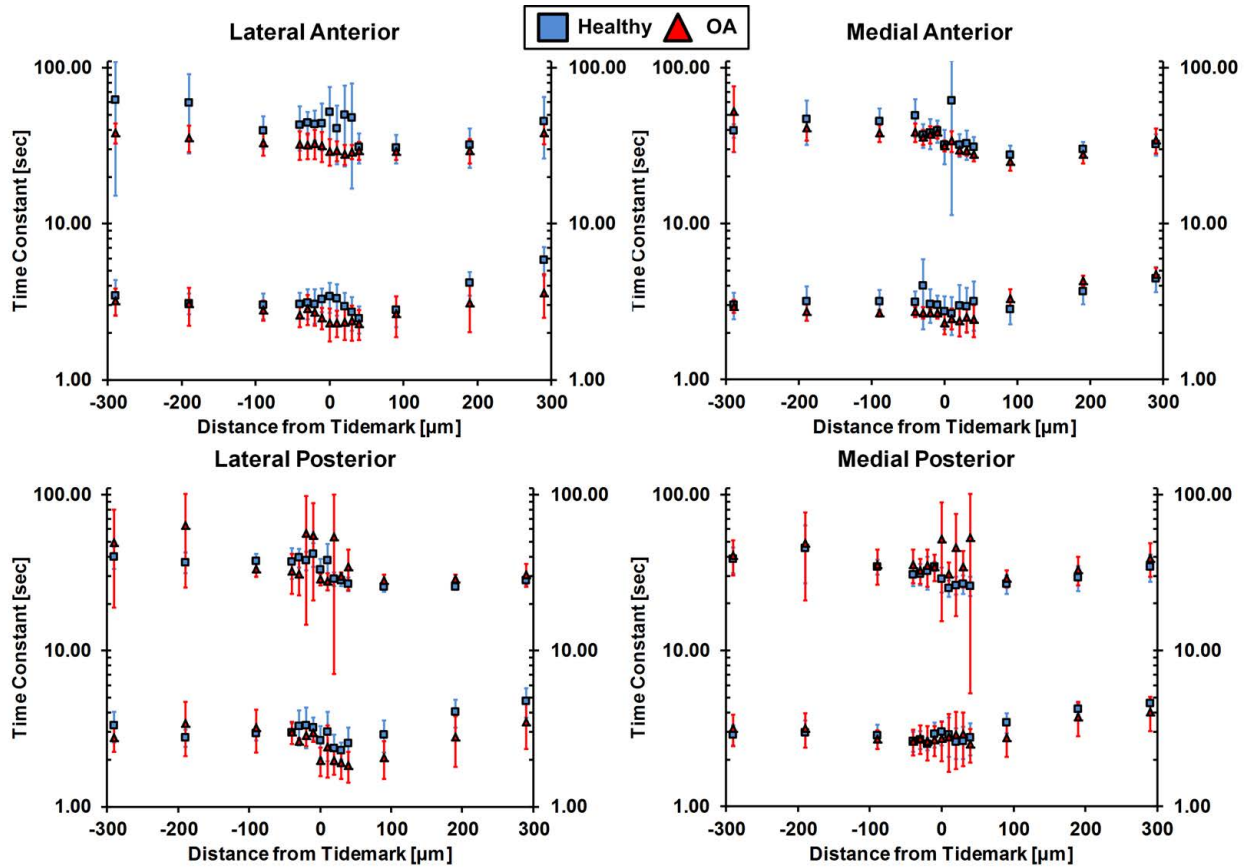


Figure C-1: Viscoelastic time constants. $\tau_1 \in [1, 10]$, $\tau_2 \in [10, 100]$. Mean \pm 95% Confidence Interval